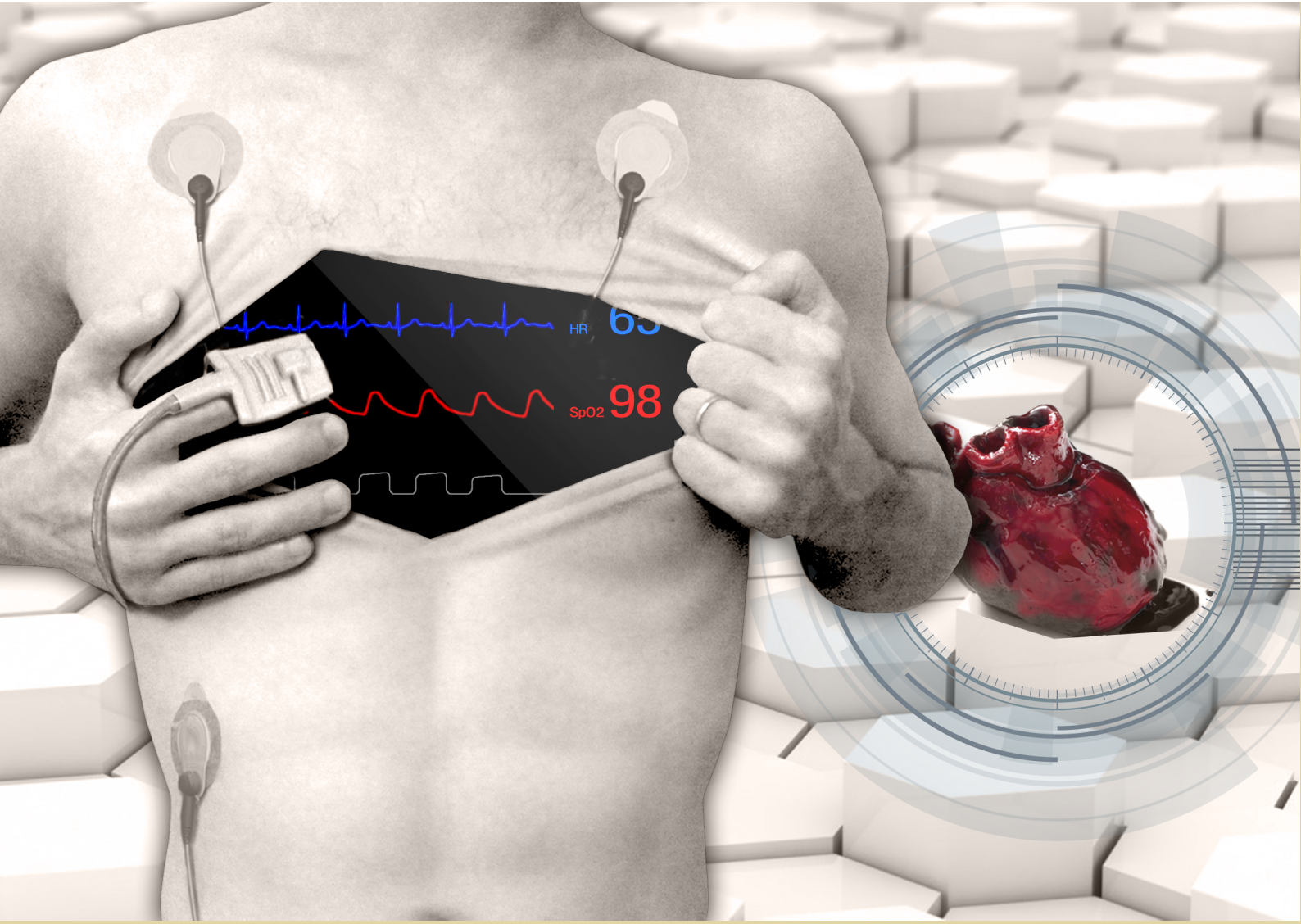

Ricardo Jorge dos Santos Couceiro

CARDIOVASCULAR PERFORMANCE ASSESSMENT FOR P-HEALTH APPLICATIONS

Tese de doutoramento do Programa de Doutoramento em Ciências e Tecnologias da Informação, orientada pelo Professor Doutor Paulo Fernado Pereira de Carvalho e pelo Professor Doutor Rui Pedro Pinto de Carvalho e Paiva, e apresentada ao Departamento de Engenharia Informática da Faculadade de Ciências e Tecnologia da Universidade de Coimbra

Setembro 2014

· U C ·

Universidade de Coimbra

CARDIOVASCULAR PERFORMANCE ASSESSMENT FOR P-HEALTH APPLICATIONS

Ricardo Jorge dos Santos Couceiro

• U  C •

PhD Thesis

Doctoral Program in Information Science and Technology

Thesis advisor

Professor Doutor Paulo Fernando Pereira de Carvalho

Thesis co-advisor

Professor Doutor Rui Pedro Pinto de Carvalho e Paiva

Department of Informatics Engineering
Faculty of Sciences and Technology
University of Coimbra

September 2014

ACKNOWLEDGMENTS

First I would like to express my gratitude to my thesis advisors, Prof. Paulo de Carvalho and Prof. Rui Pedro Paiva, who supported me with their guidance, knowledge and most of all, their encouraging words and presence.

I am also grateful to Prof. Jorge Henriques and Dr. Jens Muhlsteff for their knowledge, support and innumerous advises during the latest years.

I take this opportunity to thanks to HeartCycle, iCIS and HeartSafe projects for supporting my research work.

I am also thankful to my colleagues at the Centre of Informatics and Systems (CISUC), and specially Dr. Bruno Leitão, with whom I was able to share joys, sorrows and most of all a great friendship.

I am also grateful to my parents and sister, who supported and advised me during all these years.

Finally and foremost, it would not be possible to conclude the writing of this thesis without the support, comprehension, encouragement, extraordinary patience and love of my beloved wife Gizelly, who has always been on my side at every single moment.

LIST OF PUBLICATIONS

ARTICLES INCLUDED ON THE THESIS RESULTING FROM THE DOCTORAL RESEARCH PROGRAM

1. Detection of motion artifact patterns in photoplethysmographic signals based on time and period domain analysis
   R. Couceiro, P. Carvalho, R. P. Paiva and J. Henriques and J. Muehlsteff
   Physiological Measurement, accepted for publication in 5 August 2014.
2. Assessment of Cardiovascular Function from Multi-Gaussian Fitting of Finger Photoplethysmogram
   R. Couceiro, P. Carvalho, R. P. Paiva, J. Henriques, I. Quintal, M. Antunes, J. Muehlsteff, C. Eickholt, C. Brinkmeyer, M. Kelm and C. Meyer
   Submitted for publication in *Physiological Measurement*, 2015.
3. Real Time Prediction of Neurally Mediated Syncope
   R. Couceiro, P. Carvalho, R. P. Paiva, J. Muehlsteff, J. Henriques, C. Eickholt, C. Brinkmeyer, M. Kelm, C. Meyer
   IEEE Journal of Biomedical and Health Informatics (J-BHI), accepted for publication in 25 February 2015.

OTHER PUBLICATIONS RESULTING FROM THE DOCTORAL RESEARCH PROGRAM

1. Neurally Mediated Syncope Prediction Based on Changes of Cardiovascular Performance Surrogates: Algorithms comparison
   R. Couceiro, P. Carvalho, R. P. Paiva, J. Muehlsteff, J. Henriques, C. Eickholt, C. Brinkmeyer, M. Kelm, C. Meyer
   7th International Conference on BioMedical Engineering and Informatics (BMEI), Dalian, 2014.
2. A novel multi-parametric algorithm for faint prediction integrating indices of cardiac inotropy and vascular tone
   R. Couceiro, P. Carvalho, R. P. Paiva, J. Muehlsteff, J. Henriques, C. Eickholt, C. Brinkmeyer, M. Kelm, C. Meyer
   36th Annual International Conference of the IEEE Engineering in Medicine and Biology Society (EMBC), 2014
3. Detection of motion artifacts in photoplethysmographic signals: Algorithms comparison
   R. Couceiro, P. Carvalho, R. Paiva, J. Henriques, I. Quintal, and J. Muehlsteff
   The International Conference on Health Informatics, ed: Springer International Publishing, 2014, pp. 327-330.

4. Characterization of surrogate parameters for blood pressure regulation in neurally-mediated syncope
   R. Couceiro, P. Carvalho, R. Paiva, J. Muehlsteff, J. Henriques, V. Schulze
   35th Annual International Conference of the IEEE Engineering in Medicine and Biology Society (EMBC), 2013
5. Detection of motion artifacts in photoplethysmographic signals based on time and period domain analysis
   R. Couceiro, P. Carvalho, R. Paiva, J. Henriques, J. Muehlsteff.
   34th Annual International Conference of the IEEE Engineering in Medicine and Biology Society (EMBC), 2012
6. Multi-Gaussian fitting for the assessment of left ventricular ejection time from the Photoplethysmogram
   R. Couceiro, P. Carvalho, R. Paiva, J. Henriques, M. Antunes, I. Quintal*, et al.*
   34th Annual International Conference of the IEEE Engineering in Medicine and Biology Society (EMBC), 2012
7. Beat-to-beat cardiac output inference using heart sounds
   R. Couceiro, P. Carvalho, R. Paiva, J. Henriques, M. Antunes, I. Quintal, et al.
   33th Annual International Conference of the IEEE Engineering in Medicine and Biology Society (EMBC), 2011
8. Wearable Sensors in Syncope Managment
   C. Meyer, C. Brinkmeyer, M. Kelm, J. Muehlsteff, R. Couceiro, P. Carvalho
   Medical Science Monitor, accepted for publication in 3 September 2014.
9. Beat-to-beat systolic time-interval measurement from heart sounds and ECG.
   R. P. Paiva, P. Carvalho, R. Couceiro, J. Henriques, M. Antunes, I. Quintal and J. Muehlsteff
   Physiological measurement 33(2): 177, 2012.

ABSTRACT

Cardiovascular diseases (CVDs) are currently the leading cause of death in the world and are responsible for over 17 million deaths per year. The mortality of CVDs is increasing, mainly driven by the increase of the population in low and middle income countries, which house about 85% of the world's population. In high-income countries, the access to better diagnostic and therapeutic technologies, as well as healthier life stiles, reverses this tendency and CVD mortality is decreasing. In combination with the increase in the populations' life expectancy, people are affected or die as a result of CVD at older ages, contributing to the rise in the health care expenditures all over the world. A condition largely contributing to this matter is syncope, which has an economic impact equivalent to conditions such as asthma, HIV, and chronic obstructive pulmonary disease. More commonly known as fainting, syncope is associated with high rate of falls and hospitalization and is responsible for reducing lifestyle quality, especially in the elderly.

To face this socioeconomic burden caused by CVDs, the health care paradigm is shifting from a reactive hospital-centered to a preventive individual-centered care, with special emphasis in earlier diagnosis and better prevention and management strategies. Therefore, the development of new methodologies for monitoring the cardiovascular function, capable of being applied in low-cost, non-invasive and portable systems, are essential to prevent and control the evolving epidemic of CVDs.

Despite the recent technological advances, the current standard techniques for the assessment of cardiovascular function, such as the cardiac magnetic resonance and echocardiography, still exhibit several limitations in what concerns to their application in personal health environments. Therefore, the use of widely available and cost-effective modalities such as the electrocardiogram and photoplethysmogram, for the non-invasive, continuous and long-term assessment of the cardiovascular function may be the key to provide a better prevention and management strategies of CVDs. More specifically, the extraction of cardiovascular parameters from these modalities may be crucial in the prediction of syncope events and prevention of falls.

The key contribution of the present thesis is the development of new algorithms for the continuous, non-invasive and robust assessment of cardiovascular function, based on the analysis of the electrocardiogram and photoplethysmogram. Since the photoplethysmogram is easily influenced by noise and motion artifacts, which can be a serious obstacle in the extraction of cardiovascular parameters, it is essential to detect which sections of the photoplethysmogram are liable for further analysis. Therefore, we propose a new method for the detection of motion artifacts, based on the extraction and analysis of time and period domain features. Consequently, we propose a new algorithm for the assessment of the left ventricular ejection time, which is associated with the cardiac function, among other parameters related with blood pressure and vascular tone changes. Finally, we propose a new algorithm for the prediction of syncope events (more specifically, neurally mediated syncope), based on the evaluation of changes in the previously extracted cardiovascular parameters.

The proposed methods were validated in three databases collected in the Department of Informatics Engineering of the University of Coimbra, in the Hospital Center of University of Coimbra and in the Department of Electrophysiology of the University Heart Center, University Hospital Eppendorf, Hamburg, Germany.

RESUMO

As doenças cardiovasculares (CVDs) são atualmente a principal causa de morte no mundo e são responsáveis por mais de 7 milhões de mortes todos os anos. A mortalidade decorrente das CVDs tem vindo aumentar, principalmente devido ao crescimento da população nos países de baixo e médio rendimento, que alojam cerca de 85% da população mundial. Nos países de elevado rendimento, o acesso a melhores tecnologias de diagnostico e melhores terapêuticas, bem como estilos de vida mais saudáveis, inverteram esta tendência e a mortalidade resultante das CVDs está a decrescer. Este facto, aliado ao aumento da esperança média de vida das populações, leva a que as pessoas sejam afectadas ou morram devido a CVDs em idades mais avançadas, contribuindo para o aumento dos gastos com a saúde em todo o mundo. Uma condição que contribui largamente para este problema é a síncope, que têm um impacto económico equivalente a doenças como a asma, HIV e doença pulmonar obstrutiva crónica. Mais conhecida como "desmaio", a síncope está associada a uma frequência elevada de quedas e de hospitalizações, e é responsável por uma menor a qualidade de vida, especialmente em populações mais idosas.

Para enfrentar os encargos socioeconómicos derivados das CVDs, o paradigma da saúde tem vindo a mudar de reativo e centralizado nos hospitais para preventivo e centrado em cada individuo, com um foco especial no diagnostico precoce e em melhores estratégias de prevenção e gestão das CVDs. Assim, o desenvolvimento de novas metodologias para monitorização da função cardiovascular, capazes de serem aplicadas em sistemas de baixo custo, não invasivos e portáteis, são essenciais para a prevenção e controlo desta crescente epidemia que são as CVDs.

Apesar dos recentes avanços tecnológicos, as técnicas padrão atuais para a avaliação da função cardiovascular, como a ressonância magnética cardíaca e ecocardiografia, ainda apresentam várias limitações no que diz respeito à sua aplicação em ambientes de saúde personalizada. Assim, a utilização de modalidades amplamente disponíveis e de baixo custo, como o eletrocardiograma e o fotopletismograma, para a avaliação não-invasiva, contínua e de longo prazo da função cardiovascular pode ser a chave para melhores estratégias de prevenção e gestão de doenças cardiovasculares. Mais concretamente, a extração de parâmetros cardiovasculares a partir destas modalidades pode ser crucial na predição de síncopes e prevenção de quedas.

A principal contribuição da presente tese consiste no desenvolvimento de novos algoritmos para a avaliação continua, não invasiva e robusta da função cardiovascular, com base na análise do eletrocardiograma e do fotopletismograma. Visto que o fotopletismograma é facilmente afectado por ruído e artefactos de movimento, o que representa um obstáculo para a extração de parâmetros cardiovasculares, é fundamental detectar quais as secções do fotopletismograma passiveis de serem posteriormente analisadas. Assim, propomos um novo método para detecção de artefactos de movimento baseado na extração e análise de características do domínio temporal e de período. Consequentemente, propomos um novo algoritmo para a estimação do tempo de ejecção do ventrículo

esquerdo, o qual está associado com a função cardíaca, bem como outros parâmetros relacionados com alterações de pressão sanguínea e de tónus vascular. Finalmente, propomos um novo algoritmo para a predição de síncopes (mais especificamente, síncope neuromediada) baseada na avaliação dos parâmetros previamente extraídos.

Os métodos propostos foram validados em três bases de dados, coligidas no Departamento de Engenharia Informática da Universidade de Coimbra, no Centro Hospitalar da Universidade de Coimbra e no departamento de Eletrofisiologia do Centro Universitário do Coração, Hospital Universitário de Eppendorf, Hamburgo, Alemanha.

CONTENTS

CHAPTER 2.
PHYSIOLOGICAL BACKGROUND

CHAPTER 3.
NON-INVASIVE ASSESSMENT OF CARDIOVASCULAR FUNCTION: REVIEW

CHAPTER 4.
DETECTION OF MOTION ARTIFACT PATTERNS IN PHOTOPLETHYSMOGRAPHIC SIGNALS BASED ON TIME AND PERIOD DOMAIN ANALYSIS

CHAPTER 5.
ASSESSMENT OF CARDIOVASCULAR FUNCTION FROM MULTI-GAUSSIAN FITTING OF FINGER PHOTOPLETHYSMOGRAM

CHAPTER 6.
REAL TIME PREDICTION OF NEURALLY MEDIATED SYNCOPE

LIST OF TABLES

CHAPTER 3.
NON-INVASIVE ASSESSMENT OF CARDIOVASCULAR FUNCTION: REVIEW

CHAPTER 4.
DETECTION OF MOTION ARTIFACT PATTERNS IN PHOTOPLETHYSMOGRAPHIC SIGNALS BASED ON TIME AND PERIOD DOMAIN ANALYSIS

CHAPTER 5.
ASSESSMENT OF CARDIOVASCULAR FUNCTION FROM MULTI-GAUSSIAN FITTING OF FINGER PHOTOPLETHYSMOGRAM

CHAPTER 6.
REAL TIME PREDICTION OF NEURALLY MEDIATED SYNCOPE

ACRONYMS

ABPW	Arterial blood pressure waveform
AC	Alternating current
ACC	Accuracy
AI	Augmentation index
ANS	Autonomic nervous system
AOVC	Aortic valve closure
AOVO	Aortic valve opening
AUC	Area under curve
AV	Atrioventricular
AVVC	Atrioventricular valves closure
BMI	Body mass index
BP	Blood pressure
BPV	Blood pressure variability
BRS	Baroreflex sensitivity
BS	Baroreflex segments
BSA	Body surface area
CHD	Coronary heart disease
CI	Cardiac index
CMR	Cardiac magnetic resonance
CNS	Central nervous system
CO	Cardiac output
CVD	Cardiovascular disease
CVP	Central venous pressure
DBP	Diastolic blood pressure
DC	Direct current
DDA	Double differentiation analysis
DPTT	Differential pulse transit time
ECG	Electrocardiogram
ECHO	Echocardiography
EDV	End-diastolic volume
EF	Ejection fraction
ESC	European Society of Cardiology
ESV	End-systolic volume
FPRh	False positive rate per hour
GTN	Glycerol trinitrate

HF	Heart failure
HFr	High frequency
HR	Heart rate
HRV	Heart rate variability
HS	Heart sound
HUTT	Head-up tilt test
ICG	Impedance cardiogram
ISO	International Standards Organization
IVCT	Isovolumic contraction time
IVRT	Isovolumic relaxation time
LFr	Low frequency
LVEF	Left ventricular ejection fraction
LVET	Left ventricular ejection time
MAP	Mean arterial pressure
MC	Myocardial contractility
MG	Multi-Gaussian
MPI	Myocardial performance index
NMIFS	Normalized mutual information feature selection
NMS	Neurally mediated syncope
NTS	Nucleous tractus solitaries
PAT	Pulse arrival time
PCA	Principal component analysis
PCG	Phonocardiogram
PCM	Physical counter maneuver
PDA	Pulse decomposition analysis
PEP	Pre-ejection period
PP	Pulse pressure
PPG	Photoplethysmogram
PPV	Positive predictive value
PPW	Pulse pressure wave
PTT	Pulse transit time
PV	Pressure-volume
PWA	Pulse wave analysis
PWV	Pulse wave velocity
QS_2	Total electromechanical systole interval
RCC	Rank correlation coefficient
RESP	Respiration

RI	Reflection index
ROC	Receiver operating characteristic
RS_2	Electromechanical systole interval
S_1	First heart sound
S_2	Second heart sound
S_3	Third heart sound
S_4	Fourth heart sound
SA	Sinoatrial
SBP	Systolic blood pressure
SE	Sensitivity
SI	Stiffness index
SP	Specificity
STI	Systolic time intervals
SV	Stroke volume
SVM	Support vector machine
SVR	Systemic vascular resistance
TPRI	Total peripheral resistance
TVR	Total vascular resistance
Z_a	Aortic impedance

Chapter 1.
INTRODUCTION

This thesis addresses the problem of the evaluation of the cardiovascular function using non-invasive modalities capable of being applied in personal-Health (p-Health[1]) applications for the use in ambulatory and home care scenarios. From the analysis of the electrocardiogram (ECG) and photoplethysmogram (PPG) it is proposed the extraction of surrogates capable of describing the changes in the cardiovascular system function and ultimately in the prediction of neurally mediated syncope. In this chapter we present the thesis motivation (section 1.1), followed by section 1.2 where the main contributions and their relevance are addressed. Finally the thesis organization is presented in section 1.3.

1.1. MOTIVATION

> *CVD is today the largest single contributor to global mortality and will continue to dominate mortality trends in the future (WHO, 2009e).*

Cardiovascular diseases (CVDs) are currently the leading cause of death in the world accounting for over 17 million deaths per year, being coronary heart disease (CHD) and stroke the main cause of CVD related deaths [1, 2]. In Europe, over 4 million deaths result from CVDs, representing almost half of all deaths (47%) [3]. By 2030, it is projected that the total number of deaths resultant from CVDs will increase to 23-24 million [1, 4], representing about 33% of all deaths within an expected population of 8.2 billion people [4]. This tendency is mainly driven by the increasing rates of CVD mortality in low and middle-income countries, which house 85% of the world's population. In low-income countries, it is projected that deaths caused by CVDs will surpass those caused by infectious diseases such as HIV/AIDS. In high-income countries the CVD mortality is decreasing, as a result of the access to better diagnostic and therapeutic technologies and healthier life styles [3, 4].

In the United States, approximately 80% of all persons aged above 65 years have at least one chronic condition, and 50% have at least two [4]. Furthermore, CVD is the most frequent diagnosed condition and the major cause of death in people older than 65 years of age. According to [4], it is expected that the worldwide population above 65 years old to almost double fold during 2000-2030 (6.9% to 12% of worldwide population). This shift in world's population age is thus expected to contribute to steadily rising in the age at which people are affected or die due to a CVD event, maintaining CVD as the predominant cause of morbidity and mortality. Furthermore, demographic aging will contribute to an increase in CVDs prevalence and consequently to an increase in health expenditures related to its treatment.

---

[1] Personal health (p-health) refers to personalized monitoring of an individual's health, using, for example, wearable and portable medical monitoring systems.

[2] Systemic vascular resistance (SVR) refers to the resistance to blood flow offered by the systemic vasculature. SVR is sometimes referred as total peripheral resistance (TPR).

[3] Total vascular resistance (TVR) refers to the resistance to blood flow offered by the whole (systemic and

The actual conjuncture of the health care system is struggling with major economic costs and CVDs contribute largely for this matter. Only in the European Union (E.U.), it is estimated that the overall CVDs cost is almost €196 billion a year. In 2009, the cost of CVD to the E.U. heath care systems was just over €106 billion, which represents around 9% of the total health care expenditure [3]. From these, 49% represent inpatient hospital care costs and 29% represent the total drug costs corresponding to patients with CVDs [3]. In the United States, the costs related to CVDs alone rise up to $315.4 billion (in 2010) [5], representing about 12% of the total health care expenditures (about $2.6 trillion [6]).

To face the high economic and health burden resulting from CVDs and chronic diseases it is essential to provide better prevention strategies as well as earlier diagnosis and better management of CVDs. Thus, it is fundamental to provide better solutions that meet the economic and social needs of patients and health care systems. This transformation has already began with a shift from hospital-centered to individual-centered health care systems and from reactive care to preventive care [7]. Special concerns are placed on the early detection of risk factors, early diagnosis and early treatment. Moreover, the research focusing on low-cost, non-invasive and portable diagnosis systems, capable of continuously monitoring the cardiovascular function is essential to prevent and control the evolving epidemic of CVDs.

The current standard techniques for assistance in the diagnosis of CVDs demand high human and economic costs for the health care system. These techniques, such as cardiovascular magnetic resonance (CMR) or the invasive cardiac catheterization lack portability, since they can only be performed in the medical facilities, are expensive and require trained personal. Echocardiography (ECHO), the former gold standard in the evaluation of cardiac function, is becoming gradually popular in ambulatory professional care due to the development of increasingly inexpensive and portable devices. However, its application in p-Health environments still bares obstacles such as the inability to continuously record long-term (beat-to-beat) measurements and the requirement of trained personal. Although the traditional sphygmomanometry is low-cost and readily available, it causes discomfort to the patient and does not permit continuous, long-term recordings. Other p-Health systems such as the Portapres and Niccomo have been proposed as an alternative to the traditional hospital-centered approach, reinforcing the importance of continuously monitoring patient's health. However, these proprietary systems are expensive (e.g., Portapres: US $40,000) which make them unavailable for the general practitioners and medical facilities, where low cost and easy-to-use devices are essential [8]. As an alternative, the photoplethysmogram as a mean for the assessment of the cardiovascular and autonomic function is becoming increasingly popular among the scientific community. However, its translation to the ambulatory and p-Health solutions still lacks reliable and accurate methods for the extraction of hemodynamic variables, beyond the determination of heart rate and blood oxygenation (SpO2) trends (e.g., iSpO2 device [9]).

Several studies have been proposed in the literature concerning the importance of haemodynamic parameters in the prevention and management of CVDs. Baroreflex sensitivity (BRS) was considered a good indicator of arrhythmic cardiac events and sudden cardiac death and is an important index for risk stratification (e.g., post-myocardial infarction) [10]. Cardiac output (CO) together with other haemodynamic parameters is important to assess the deterioration of cardiac function, as well as the evaluation of therapeutic interventions in the treatment of CVDs (e.g., acute heart failure)[11, 12]. Left ventricular function surrogates, such as left ventricular ejection fraction (LVEF) have also been shown to be important predictors of survival to myocardial infarction, chronic heart failure (HF) and among people free of overt cardiovascular disease [11]. Furthermore, arterial stiffening is associated with several cardiovascular risk factors, such as hypertension, left ventricular failure [13], severity of coronary artery disease [14] and increased target organ damage [15]. It is commonly associated with aging, hypercholesterolemia, obesity, it is commonly observed in smokers and has been shown to predict future morbidity and mortality [14].

A practical application of these cardiovascular function surrogates is the prediction of syncope and, more specifically, neurally mediated syncope (NMS). More commonly known as fainting or passing out, syncope is a transient loss of consciousness caused by a reduction of blood flow to the brain. Affecting mostly elderly populations (30.6 incidents per 1000 person-years [16]), syncope is associated with a high rate of falls and hospitalizations, and accounts for 1-3% of all emergency department (ED) visits and 1-6% of all hospital admissions in general [16, 17]. Syncope is responsible for reducing the lifestyle quality and is commonly responsible for mental decline and the appearance of medical complications. The socioeconomic and medical impact on our society is translated into an annual cost of $1.7-2.4 billion resulting from the hospitalizations related to syncope. This expenditure is equivalent to conditions such as asthma, HIV and chronic obstructive pulmonary disease [18].

It is evident that the development of algorithms for syncope prediction, capable of anticipating syncope events, is of extreme importance. These algorithms would enable the development of warning systems capable of advising patients to take the appropriate measures such as performing physical counterpressure maneuvers (PCMs) or simply siting or lying down and, therefore, avoiding a fall.

In fact, falls in the elderly people are a great individual and social burden. It is estimated that 32% of the elderly fall every year and half of these people experience recurrent falls [19]. Falls in elderly cost the UK government about £1 billion per year from which a huge contribution comes from institutionalization (41%) and hospitalization costs (50%) [19]. Since the main causes of falls are cardiovascular disorders and syncope, the methods presented in this thesis can give a significant contribution in this subject.

1.2. CONTRIBUTIONS AND RELEVANCE

This thesis focuses on the study and implementation of algorithms for the reliable extraction of cardiovascular function surrogates for p-Health applications. The proposed algorithms are based on the

analysis of non-invasive signals that can be easily affordable, are commonly used in hospital and primary care facilities or can be integrated into wearable systems for personal health applications, such as the ECG and the PPG. The extraction of cardiovascular parameters in a continuous basis (beat-by-beat) is a fundamental requisite of the present thesis, as well as the robustness of the proposed algorithms in uncontrolled environments (e.g., home care settings).

The proneness of the PPG signal to be easily influenced by external factors, such as motion artifacts, can be a serious limitation to the reliable and long-term extraction of cardiovascular parameters, especially in continuous monitoring applications. Therefore, it is essential to develop robust methodologies capable of distinguishing the sections of the PPG signal that have good quality and consequently can be fed to the upstream PPG analysis methodologies. In this thesis we present a new algorithm for detecting the PPG sections corrupted by motion artifacts based on the analysis of changes in the PPG time and period characteristics. The best features were selected using normalized mutual information features selection (NMIFS) method, which were fed into a support vector machine (SVM) classification model. The proposed methodology was tested in a database consisting of fifteen healthy and cardiovascular diseased subjects, and eleven motion sources. The accuracy achieved by the proposed methodology (88.5%) reflects its capacity in detecting PPG sections corrupted by a wide range of motion artifacts, in both subject groups.

A preliminary version of this work was initially presented in the 34th Annual International Conference of the IEEE Engineering in Medicine and Biology Society and published in the proceedings of the conference [20]. After further developments including the cardiovascular diseased patients in the database, a presentation was made in the IFMBE International Conference on Health Informatics, and published in the respective conference proceedings [21]. Finally, a more complete version of this work was accepted for publication in the Physiological Measurement journal.

For the extraction of cardiovascular function surrogates we propose a method based on the decomposition of the PPG pulse into multiple waves using a Multi-Gaussian model formulation. From the analysis of the systolic phase PPG components several left ventricular ejection time estimates were assessed and compared. The proposed method was tested in a database consisting of 68 healthy and cardiovascular diseased subjects, and the results show a better overall performance when compared with the state of the art. Moreover, the parameters associated with vascular tone, such as reflection index (RI) and stiffness index (SI), were also extracted from the analysis of the proposed Multi-Gaussian model and compared with the reference values of blood pressure and total peripheral resistance. The correlation between the extracted and reference parameters was investigated in 21 volunteers exhibiting hemodynamic instability and a high agreement was found between the SI and mean blood pressure (MBP).

The work regarding the assessment of LVET was initially presented in the 34th Annual International Conference of the IEEE Engineering in Medicine and Biology Society and published in the

proceedings of the conference [22]. After further improvements this work was submitted for publication in the Physiological Measurement journal.

Finally, we propose a solution for prediction of neurally mediated syncope (NMS) based on the analysis of the ECG and PPG signals alone. The cardiovascular parameters known to characterize the chronotropic (heart rate - HR), inotropic (left ventricular ejection time - LVET), vascular tone and blood pressure (pulse arrival time - PAT, stiffness index – SI – and reflection index - SI, respectively) changes were assessed and normalized. A threshold-based approach was adopted to generate alarms when the distance of the selected features to the orthostatic reference exceeds a predefined optimal value. The proposed solution was tested in a database composed of 43 patients suspected to be at risk of hemodynamic instability and showed high ability to predict syncope episodes (above 85%) with a low false positive rate per hour (bellow 0.18 h^{-1}) and good prediction time (above 65 seconds).

A preliminary investigation was firstly presented in the 35th Annual International Conference of the IEEE Engineering in Medicine and Biology Society [23]. The work regarding the proposed syncope prediction algorithm was presented in the 36th Annual International Conference of the IEEE Engineering in Medicine and Biology Society [24]. Finally, a more detailed description of this work was accepted for publication in the IEEE Journal of Biomedical and Health Informatics (J-BHI).

1.3. THESIS ORGANIZATION

The reminder of this thesis is outlined as follows:

CHAPTER 2 – PHYSIOLOGICAL BACKGROUND

This chapter describes the physiological context that underlies the proposed methodologies outlined throughout the present thesis. In this chapter, we start by addressing the physiological aspects of the circulation and the various subsystems that support the functioning of the cardiovascular system the autonomic system and corresponding interactions. Finally, we outline the information that can be extracted from the cardiovascular system and its importance in the prognosis and diagnosis of CVDs and ultimately the prediction of neurally mediated syncope.

CHAPTER 3 – NON-INVASIVE ASSESSMENT OF CARDIOVASCULAR FUNCTION: REVIEW.

This chapter outlines the current state of the art methodologies in three main areas: evaluation of cardiovascular function, assessment of baroreflex sensitivity and prediction of neurally mediated syncope. In these sections, we focus on the methodologies for the assessment of cardiac function, based on non-invasive signals such as the electrocardiogram and the photoplethysmogram, the parameter-based approaches for the estimation of blood pressure and other vascular function surrogates and, finally, the algorithms present in the literature used to predict of neurally mediated syncope.

CHAPTER 4 – DETECTION OF MOTION ARTIFACT PATTERNS IN PHOTOPLETHYSMOGRAPHIC SIGNALS BASED ON TIME AND PERIOD DOMAIN ANALYSIS.

This chapter presents a new algorithm for the detection of motion artifacts on the finger photoplethysmogram based on the analysis of the signal time and period domain characteristics.

CHAPTER 5 – ASSESSMENT OF CARDIOVASCULAR FUNCTION FROM MULTI-GAUSSIAN FITTING OF FINGER PHOTOPLETHYSMOGRAM.

A novel approach to assess the left ventricular ejection time is proposed in this chapter, which is based on the analysis of a Multi-Gaussian model fitted to the PPG pulses. Additionally, from the analysis of the proposed model, parameters associated with vascular tone and blood pressure changes are also investigated.

CHAPTER 6 – REAL TIME PREDICTION OF NEURALLY MEDIATED SYNCOPE.

In this chapter we present a novel approach for prediction of syncope based on the evaluation of hemodynamic changes assessed from the analysis of the ECG and PPG signals alone.

CHAPTER 7 – CONCLUSIONS AND FUTURE WORK.

Chapter 7 finalizes this thesis by summarizing the main findings and outlining further research directions.

REFERENCES

[1] L. J. Laslett, P. Alagona, B. A. Clark, J. P. Drozda, F. Saldivar, S. R. Wilson*, et al.*, "The Worldwide Environment of Cardiovascular Disease: Prevalence, Diagnosis, Therapy, and Policy IssuesA Report From the American College of Cardiology," *Journal of the American College of Cardiology,* vol. 60, pp. S1-S49, 2012.

[2] V. Fuster and B. B. Kelly, *Promoting Cardiovascular Health in the Developing World:: A Critical Challenge to Achieve Global Health*: National Academies Press, 2010.

[3] M. Nichols, N. Townsend, R. Luengo-Fernandez, J. Leal, A. Gray, P. Scarborough*, et al.*, "European cardiovascular disease statistics 2012," *European Heart Network, Brussels, European Society of Cardiology, Sophia Antipolis,* 2012.

[4] P. Libby and R. O. Bonow, *Braunwald's Heart Disease: A Textbook of Cardiovascular Medicine, 2-Volume Set*, 8 ed. Philadelphia: Saunders Elsevier, 2007.

[5] A. S. Go, D. Mozaffarian, V. L. Roger, E. J. Benjamin, J. D. Berry, M. J. Blaha*, et al.*, "Heart Disease and Stroke Statistics—2014 Update: A Report From the American Heart Association," *Circulation,* vol. 129, pp. e28-e292, 2014.

[6] Hyattsville, "Health, United States, 2013: With Special Feature on Prescription Drugs.," 2014.

[7] HeartCycle, "Compliance and effectiveness in HF and CHD closed loop management," ed, 2007.

[8] L. L. TAN. Pre-empting Heart Attack and Stroke. *Innovation 7*.

[9] Masimo. (2014, 13-08-2014). *iSpO2 - Track and Trend Your Blood Oxygen & Pulse Rate*. Available: http://www.ispo2.com/

[10] S. H. Hohnloser and T. Klingenheben, "Clinical Utility of Baroreflex Sensitivity Measurements," *Cardiac Electrophysiology Review,* vol. 1, pp. 354-356, 1997.

[11] I. S. Anand, V. G. Florea, and L. Fisher, "Surrogate end points in heart failure," *J Am Coll Cardiol,* vol. 39, pp. 1414-1421, May 1 2002.

[12] M. R. Pinsky, "Probing the Limits of Arterial Pulse Contour Analysis to Predict Preload Responsiveness," *Anesthesia & Analgesia,* vol. 96, pp. 1245-1247, May 1 2003.

[13] M. O'Rourke, "Isolated systolic hypertension, pulse pressure, and arterial stiffness as risk factors for cardiovascular disease," *Current Hypertension Reports,* vol. 1, pp. 204-211, 1999.

[14] B. A. Kingwell and C. D. Gatzka, "Arterial stiffness and prediction of cardiovascular risk," *Journal of Hypertension,* vol. 20, pp. 2337-2340, 2002.

[15] J. A. Chirinos, "Arterial stiffness: basic concepts and measurement techniques," *Journal of cardiovascular translational research,* vol. 5, pp. 243-255, 2012.

[16] N. Colman, K. Nahm, K. S. Ganzeboom, W. K. Shen, J. Reitsma, M. Linzer*, et al.*, "Epidemiology of reflex syncope," *Clin Auton Res,* vol. 14 Suppl 1, pp. 9-17, Oct 2004.

[17] D. M. Lemonick, "Evaluation of Syncope in the Emergency Department," *American Journal of Clinical Medicine,* vol. 7, 2010.

[18] C. Kessler, J. M. Tristano, and R. De Lorenzo, "The Emergency Department Approach to Syncope: Evidence-based Guidelines and Prediction Rules," *Emergency Medicine Clinics of North America,* vol. 28, pp. 487-500, 8// 2010.

[19] M. P. Tan and R. A. Kenny, "Cardiovascular assessment of falls in older people," *Clinical interventions in aging,* vol. 1, p. 57, 2006.

[20] R. Couceiro, P. Carvalho, R. P. Paiva, J. Henriques, and J. Muehlsteff, "Detection of motion artifacts in photoplethysmographic signals based on time and period domain analysis," in *34th IEEE Engineering in Medicine and Biology Society*, San Diego, California, USA, 2012.

[21] R. Couceiro, P. Carvalho, R. P. Paiva, J. Henriques, I. Quintal, and J. Muehlsteff, "Detection of Motion Artifacts in Photoplethysmographic Signals: Algorithms Comparison," in *The International Conference on Health Informatics*. vol. 42, ed: Springer International Publishing, 2014, pp. 327-330.

[22] R. Couceiro, P. Carvalho, R. Paiva, J. Henriques, M. Antunes, I. Quintal*, et al.*, "Multi-Gaussian fitting for the assessment of left ventricular ejection time from the Photoplethysmogram," in *34th Annual Int. Conf. of the IEEE Eng. in Medicine and Biology Society, EMBC 2012*, San Diego, 2012.

[23] R. Couceiro, P. Carvalho, R. P. Paiva, J. Muehlsteff, J. Henriques, V. Schulze*, et al.*, "Characterization of surrogate parameters for blood pressure regulation in neurally-mediated syncope," in *35th Annual Int. Conf. of the IEEE Eng. in Medicine and Biology Society, EMBC 2013*, 2013, pp. 5381-5385.

[24] R. Couceiro, P. Carvalho, R. P. Paiva, J. Muehlsteff, J. Henriques, C. Eickholt*, et al.*, "A novel multi-parametric algorithm for faint prediction integrating indices of cardiac inotropy and vascular tone," in *36th Annual Int. Conf. of the IEEE Eng. in Medicine and Biology Society, EMBC 2014*, 2014.

Chapter 2.
PHYSIOLOGICAL BACKGROUND

In this chapter we address the fundamental aspects concerning the physiological background of the research work presented in this thesis. We start by describing the anatomy and physiology of the cardiovascular and autonomic systems. Afterward, we outline the interactions between those systems and corresponding regulation mechanisms. Finally, we outline the importance of the assessment of cardiovascular function surrogates and their value in the diagnosis and prognosis of CVDs and, more specifically, syncope.

2.1. THE CARDIOVASCULAR SYSTEM

The cardiovascular system is a highly complex system consisting of two primary components for blood distribution, the heart and the blood vessels, and a third component that does not contain blood but lymph, the lymphatic system. The heart can be viewed functionally as two separate pumps that throw blood into the systemic and pulmonary circulation. The pulmonary circulation is primarily concerned with delivering deoxygenated blood (venous blood) to the lungs, where the gas exchanges between the blood and alveoli takes place, and returning the oxygenated blood (arterial blood) to the heart. The role of the systemic circulation is to supply the oxygenated blood to all tissues of the body (except the lungs). This process is illustrated in Figure 1.

The venous blood returning from the systemic circulation enters the right side of the heart through the superior and inferior vena cava to the right atrium and the right ventricle pumps it to the pulmonary circulation through the pulmonary artery. After the gas exchanges, the arterial blood leaving the lungs enters the left atrium through the pulmonary veins and flows to the left ventricle. The left ventricle ejects the arterial blood into the aorta, which then distributes it to all tissues via the arterial system [1].

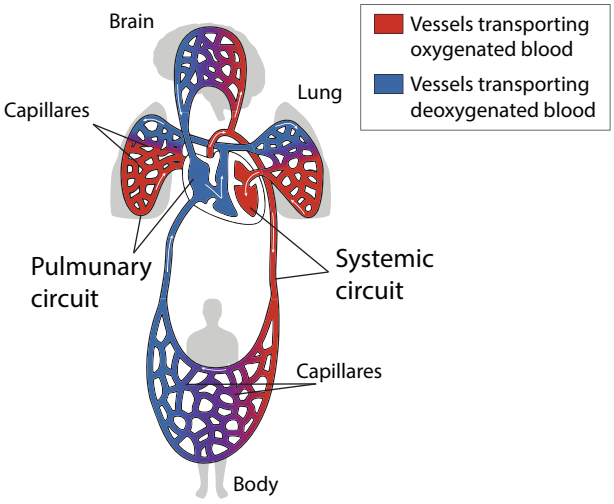

Figure 1 – Schematic representation of the cardiovascular system. The white arrows represent the venous (blue) and arterial (red) blood flow within the pulmonary and systemic circulations. Adapted from [2].

2.1.1. THE HEART

The heart is a hollow, four-chambered, muscular organ composed by the atria (the two upper chambers) and the ventricles (the two lower chambers). The atria receive blood returning to the heart and pump it to the ventricles, which consequently pump the blood into the systemic and pulmonary circulation. One-way valves located at the entrance and exit of both ventricles conduct the blood circulation within the heart (illustrated in Figure 2).

The atrioventricular (AV) valves are located at the entrance of the right and left ventricles (tricuspid and mitral valves, respectively) and are primarily concerned with allowing the blood to flow from the atria to the ventricles.

The semilunar valves are located at the exit of the right and left ventricles (pulmonic and aortic valves, respectively) and the beginning of the great vessels (entrance of the pulmonary artery and ascending aorta) and let the blood flow to the outside of the heart.

The atrioventricular and semilunar valves act (open or close) in response to pressure changes inside and outside the ventricles (atria and great vessels) and play a crucial role in preventing blood regurgitation to the atria and ventricles, respectively.

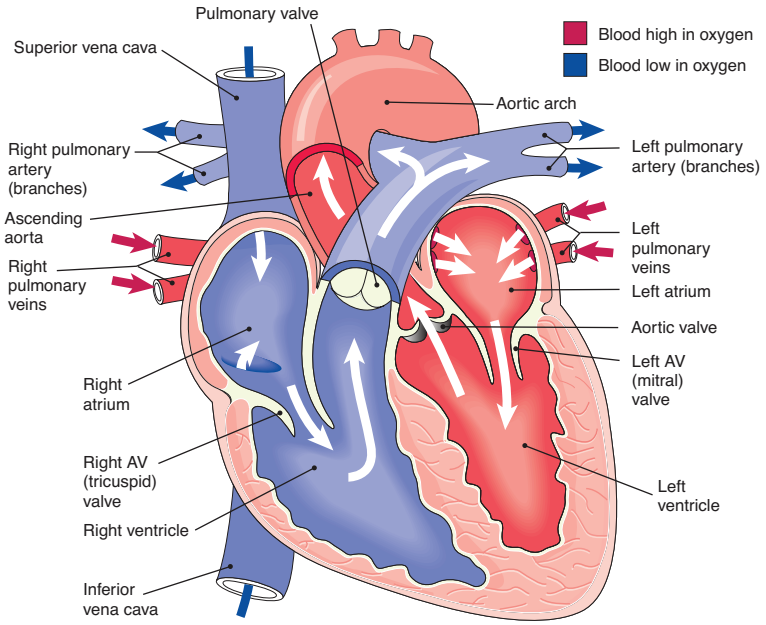

Figure 2 – Illustration of the heart and valves. The white arrows represent the venous (blue) and arterial (red) blood flow inside the heart. Adapted from [3].

THE CARDIAC ELECTRICAL SYSTEM

The cardiac activity has an inherent periodicity, which is controlled by an electrical conducting system composed by specialized fibers that spontaneously generate and rapidly conduct electrical impulses through the heart. These impulses, or action potentials, coordinate the contraction and

relaxation of the cardiac muscle and allow the filling and emptying of the atria and ventricles - this process is called cardiac cycle.

Specialized pacemaker fibers concentrated in the sinoatrial (SA) and atrioventricular (AV) nodes, and the His-Purkinje system play a crucial role in controlling and synchronizing the cardiac activity. The impulses generated in the SA node (normally responsible for controlling heart rate) propagate through the atria causing their simultaneous contraction and consequent blood flow to both ventricles. When reaching the AV node, the impulses are delayed and then relayed to the AV bundle (bundle of His). Travelling down through the right/left bundle branches and the Purkinje fibers, the electrical impulses cause both ventricles to contract almost simultaneously [3, 4].

THE ELECTROCARDIOGRAM

The electrical activity of the heart can be detected at the skin surface and measured as an electrical potential using electrocardiography. The electrocardiogram (ECG – illustrated in Figure 3) represents the different phases of the cardiac muscle electrical activity. The P-wave and QRS complex can be seen as depolarization waves, while the T-wave is know as a repolarization wave. The P-wave represents the depolarization of the atria and occurs before the atrial contraction begins and the QRS complex results from the depolarization of the ventricles, combined with repolarization of the atria. The T-wave is caused by the potentials generated from the recovery of the ventricles from the state of depolarization [4].

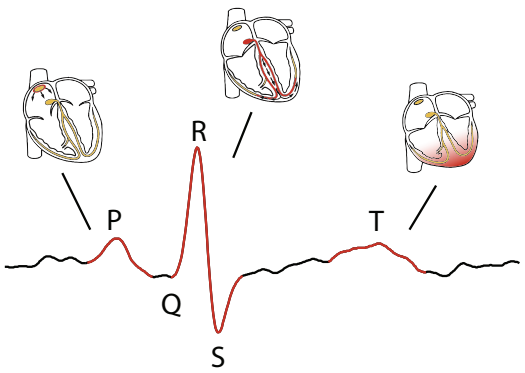

Figure 3 – Representation of the electrocardiogram (ECG) components and the corresponding phases of the cardiac electrical activity.

THE CARDIAC MECHANICAL SYSTEM

The cardiac cycle involves two main stages that are the systole (contraction and ejection) and the diastole (relaxation and filling). The contraction and relaxation of the heart is followed by changes of pressure inside the heart chambers, which cause the heart valves to open and the blood to flow from high to low-pressure areas.

Pressure and volume fluctuations inside the heart are well known and can be described by the Pressure-Volume (PV) loop diagram (presented in Figure 4), which shows the pressure and volume changes inside the left side of the heart. The key concepts of the Pressure-Volume (PV) loop diagram for the left side of the heart are described as follows:

- Point A – After ventricular systole, the left ventricle relaxes and the intra-ventricular pressure drops until it gets lower than the atrial pressure. At this point the AV valves open and the blood flows very rapidly to the ventricle (rapid filling phase).
- Point B – The filling of the ventricles and their rapid contraction result in the raise of the intra-ventricular pressure, which culminates at the closure of the mitral valve. At this point, the pressure exerted in the ventricular walls is called preload and the volume of blood is maximal (end-diastolic volume, EDV).
- Point C – The intra-ventricular pressure continues to rise without changes in ventricular volume (isovolumetric contraction) until it exceeds the pressure within the aorta. At this point, the aortic valve opens and the blood is ejected out of the ventricle (rapid ejection). The ventricular pressure required to open the aortic valve is called afterload.
- Point D – When the intra-ventricular pressure becomes lower than the aortic pressure the aortic valve closes again. At this point, the volume of blood that remains in the ventricle is called end-systolic volume (ESV). The decrease of the intra-ventricular pressure without changes of volume (isovolumetric relaxation) completes the loop and marks the beginning of a new cardiac cycle.

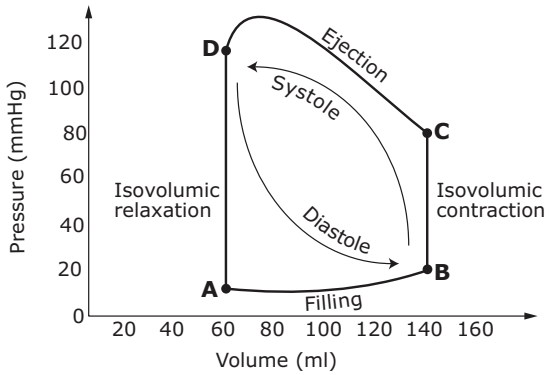

Figure 4 - Pressure-volume loop of the left ventricle (the key concepts are similar for the right side). Adapted from [4].

The Wiggers diagram (Figure 5) illustrates the blood flows and pressures in the left side of the heart, and their temporal correlation with the electrical (ECG) and mechanical (PCG) events, over one cardiac cycle.

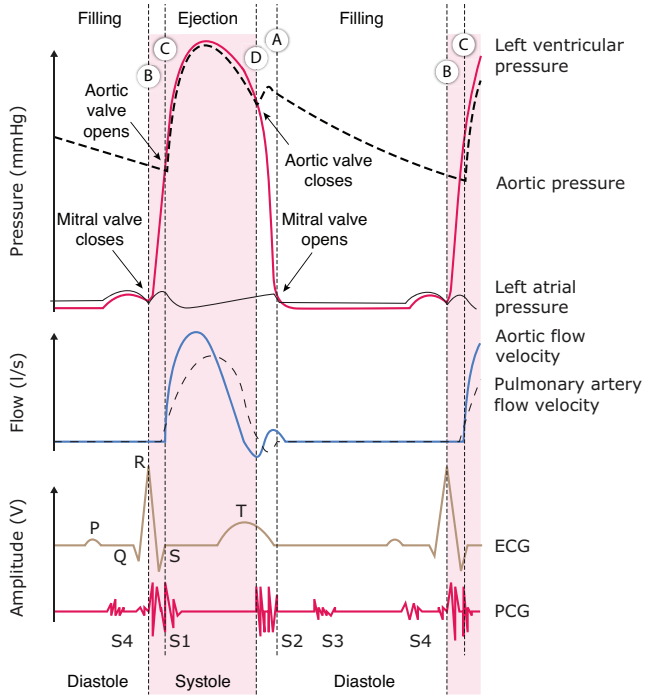

Figure 5 – Wiggers diagram describing the relationship between blood pressures and flows inside the left ventricle and corresponding events in the cardiac electrical and mechanical systems. Adapted from [4].

2.1.2. BLOOD VESSLES

The blood vessels are an integrant part of the circulatory system, whose main goal is to serve the body tissues with blood in order to maintain an appropriate environment for the survival and function of the cells. This is accomplished by transporting blood within a complex and sophisticated network of vessels that carries nutrients and oxygen to the body tissues, retrieves metabolic waste products and conducts hormones between various parts of the body [5].

The vascular network comprises two structurally similar networks that serve distinct purposes. The systemic vascular network starts at the exit of the left ventricle (beginning of the aorta) and branches into smaller and smaller arteries (large arteries, small arteries and arterioles). Small arteries and arterioles are called the resistance vessels and are responsible for the regulation of blood pressure. These are highly innervated by autonomic nerves, which determinate their constriction or dilation.

The arterioles branch into the capillaries, which are responsible for slowing down the blood velocity and enabling the exchange of substances between blood and body tissues (drop off of oxygen and nutrients and take away of wastes and carbon dioxide). When capillaries join together they form post-capillary venules, which converge into increasingly larger veins until the final venous vessels are

reached, the superior and inferior vena cava. Together, venules and veins are the site where most of the blood volume is concentrated and, therefore, are considered as the primary capacitance vessels.

In the pulmonary vascular network, the deoxygenated blood that leaves the right ventricle, passes through the pulmonary arteries and travels along the vascular network until it reaches the capillaries where the exchange of oxygen (received) and carbon dioxide (delivered) occurs. The blood then travels back to the heart and enters the left atria through the pulmonary vein.

The achievement of the primary functions of the circulatory system is guaranteed by anatomical arrangement of the vasculature and by control mechanisms that act directly in the vessels. These mechanisms are capable of constricting and dilating blood vessels, regulating the blood pressure and establishing the amount of blood that reaches specific organs and regions within organs.

THE ARTERIAL BLOOD PRESSURE WAVEFORM

The ejection of blood from the left ventricle into the aorta results in a pulse pressure wave (PPW) that is transmitted to the arterial network and reflects the pressure exerted by the blood in the arterial wall. As the main pressure wave (P1 - illustrated in Figure 6) passes the aortic arch, it travels down and reaches two major reflection sites in the arterial pathway that exhibit significant changes in arterial resistance and compliance. The first site, at the juncture between thoracic and abdominal aorta, causes the pressure wave to be reflected upwards leading to the appearance of the first reflection wave (P2 - illustrated in Figure 6), which is commonly known as second or late systolic wave. At the second site, located between the abdominal aorta and common iliac arteries, the main wave is reflected once again, and appears as a second wave reflection (P3 - illustrated in Figure 6) [6]. Between the first and second reflection waves (P2 and P3, respectively), it is commonly seen a small dip called the dicrotic notch. Lower amplitude reflection waves are also usually observed as a result of the reflections and re-reflections in the systemic vascular structure.

The lowest pressure in the aorta, just before the ejection of blood from the left ventricle, is called diastolic blood pressure (DBP), while the highest pressure exerted by blood in the aorta is called systolic blood pressure (SBP). The difference between SBP and DBP in the aorta is the aortic pulse pressure (PP) [1]. In young healthy adults the DBP and SBP are about 80 and 120 mmHg, respectively [5].

The velocity, morphology and amplitude of the pulse pressure wave change along the arterial pathway as a result of changes in resistance and compliance. As the pulse pressure wave travels along the aorta to the peripheral sites, there is a decrease in the compliance, resulting in an increase in the pulse wave velocity (PWV). The typical values of PWV along arterial path are: aorta - 3 to 5 m/s; large arteries - 7 to 10 m/s; small arteries - 15 to 35 m/s [5]. Moreover, it is also observed an increase in PP, which is believed to be also a consequence of the decrease in compliance and the summation of reflection waves with the waves travelling towards the peripheral sites. The mean aortic (or arterial)

pressure (MAP) also drops when travelling down distributing arteries owing to their relative low resistance [1]. The morphology of the pulse pressure wave recorded at the radial artery is illustrated in Figure 6.

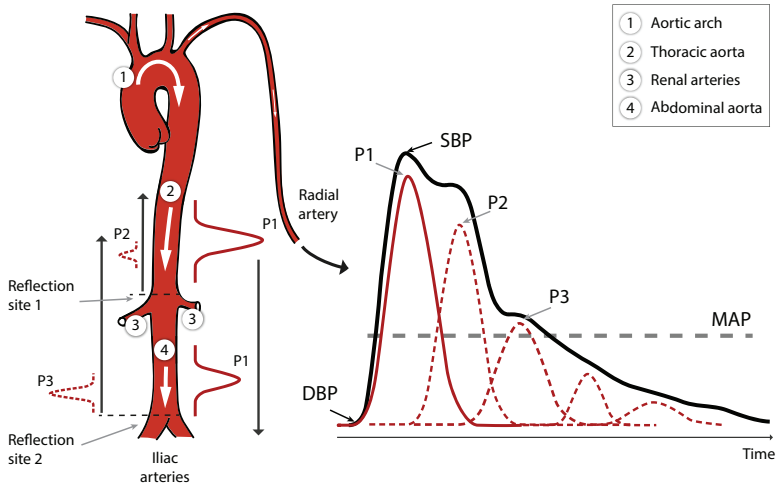

Figure 6 – Morphology of the pulse pressure wave at the radial artery. On the left, a sketch of the arterial system from the aorta/arm to the iliac arteries. On the right, a pulse pressure wave decomposed in the corresponding forward pulse (P1) and pulses reflected at the first (P2) and second (P3) reflection sites [6].

At a normal resting heart rate (HR), the MAP is less then arithmetic average of SBP and DBP and can be assessed by:

$$\mathrm{MAP} = \mathrm{DBP} + {}^{1}/_{3}\,(\mathrm{SBP\text{-}DBP}) \qquad (1)$$

At higher rates, the shape of the pulse pressure wave changes as the period of diastole shortens more than the systolic one, causing an approximation of the MAP to the arithmetic average of the SBP and the DBP. The MAP is also determined by other factors, such as the cardiac output (CO), the systemic vascular resistance (SVR[2]) and central venous pressure (CVP). The relationship between flow, pressure and resistance is described by equation (2).

$$\mathrm{MAP} = (\mathrm{CO} \cdot \mathrm{SVR}) + \mathrm{CVP} \qquad (2)$$

The CO is determined by the HR and stroke volume (SV), which is the volume of blood that leaves the heart in each beat, and is defined by:

$$\mathrm{CO} = \mathrm{HR} \cdot \mathrm{SV} \qquad (3)$$

Therefore, the changes in the SV accompanied by changes in CO alter the MAP and the PP. However, if HR decreases and the value of CO remains unaltered, only changes in pulse pressure are observed [1].

[2] Systemic vascular resistance (SVR) refers to the resistance to blood flow offered by the systemic vasculature. SVR is sometimes referred as total peripheral resistance (TPR).

THE PHOTOPLETHYSMOGRAM

The changes of blood volume in the microvascular bed of tissues can be detected using a non-invasive optical measurement technique called photoplethysmography. In its most common form (transmission mode), a light source (with red or a near infrared wavelength) is used to illuminate the finger (or ear lobe) and a photo-detector is used to measure the light intensity on the other side. The blood flowing across the tissue increases the optical density and path length across the tissue, which decreases the light intensity captured at the photo-detector. By convention, the photoplethysmogram is inverted in order to correlate positively with blood volume changes [7].

The photoplethysmogram (presented in Figure 7) has two main components, which are often called the alternating current (AC) and direct current (DC) components. The AC component is related to the pulsatile nature of the heart and therefore its fundamental frequency is dependent on the HR. This component is superimposed onto a slow changing DC component exhibiting low-frequency oscillations, which are related to changes in capillary density and venous blood volume changes. These fluctuations are induced by several factors, such as respiration, thermoregulation, local auto-regulation and episodic sympathetic outflow [7, 8].

Photoplethysmography is commonly seen in the clinical settings of the anesthesia, critical care and emergency medicine, where pulse oximeters are widely used to infer arterial oxygen saturation (SaO_2) [7, 8].

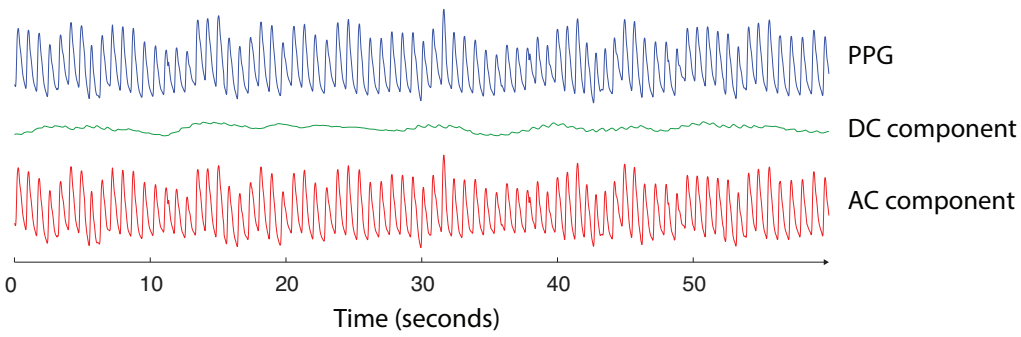

Figure 7 – Representation of the photoplethysmogram and main AC and DC components.

2.2. THE AUTONOMIC NERVOUS SYSTEM

The autonomic nervous system (ANS) plays an important role in controlling internal organs and acts in many involuntary human body actions. In the cardiovascular system, the ANS regulates the heart rate, the contractility of the muscle, constriction/dilatation of blood vessels and total blood volume. All these control mechanisms serve to control the arterial pressure, i.e., to steer the pressure toward some "normal" set point.

The major participant in the autonomic regulation of the cardiovascular function is the Central Nervous System (CNS), which transmits impulses to the peripheral organs and vice-versa. The central nervous system receives afferent input from peripheral and brain sensors. Afferent fibbers enter the medulla oblongata at the nucleus tractus solitaries (NTS), which inhibits and excites sympathetic and vagal neurons, respectively. The sensory information from NTS is also redirected to the hypothalamus. Additionally the medulla receives input from the hypothalamus and higher brain centers [1].

Efferent nerve fibers are connected to the heart and blood vessels. Sympathetic activation of blood vessels and heart causes the constriction of blood vessels, the increase of heart rate and conduction velocity within the heart, and the increase of contractility. Parasympathetic activation, transmitted through the vagus nerve has the opposite effect (decrease) in the heart rate and velocity of conduction, and contractility. Although the parasympathetic activation has little or no direct effect on blood vessels, the inhibitory effects of the vagal nerves in the sympathetic neurons indirectly causes vasodilatation in peripheral vessels [1].

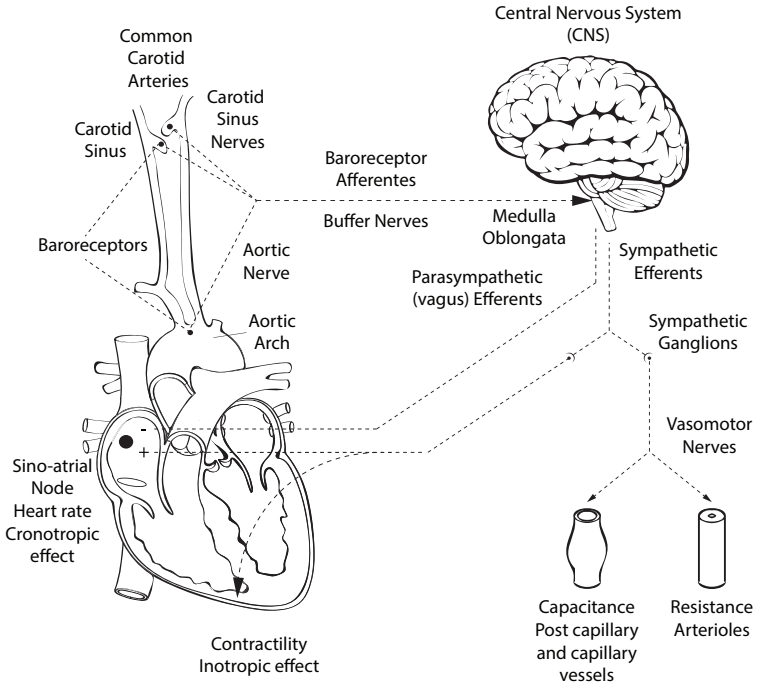

Figure 8 – Representation of the baroreflex feedback system. Adapted from [9].

The baroreceptors are tension-sensitive nerve fiber endings that monitor changes in blood pressure and transmit the corresponding autonomic information to the CNS. The sensors are strategically located in various places in the circulatory system and it is believed that those located in the aortic arch and in the carotid sinus are the most important ones [1]. Changes in blood pressure produce a correspondent change in the frequency of nerve activity, which is transmitted to the CNS. The CNS interprets this

information and generates a response that acts over the cardiovascular function through the efferent pathways to adjust arterial blood pressure [1].

The baroreflex (or baroreceptor reflex) is a negative feedback mechanism responsible for controlling mainly the short-term blood pressure [10]. Changes in blood pressure are sensed by baroreceptors that transmit these changes to the CNS through the afferent nerves, leading to the activation/inhibition of the sympathetic and parasympathetic CNS efferents. These efferent nerves are directly connected to the SA node and, therefore, the heart rate is the result of these antagonistic actions of parasympathetic and sympathetic regulation [10]. The sympathetic nerves are also responsible for controlling the heart muscle contractility, vasoconstriction/vasodilatation and venous blood volume (see Figure 8).

The assessment of the baroreflex function (baroreflex sensitivity - BRS) can be performed from the relationship between the variations in the blood pressure (e.g., SBP or MAP) and RR interval series. In the steady state, the baroreflex is characterized by a sigmoid function and is composed by a linear part and two plateaus (illustrated in Figure 9 - top and bottom). The linear part is characterized by the pronounced effect of the blood pressure changes over the RR, while in the plateaus the RR response is diminished. In these plateaus, the blood pressure changes are a response for changes in the peripheral vasculature resistance and contractility [10].

The BRS can be evaluated as the slope of line tangent to the linear part of the sigmoid, at the operating point, that is, the mean baseline MAP and RR values [10]. As shown in Figure 9, both operating point (big circle) and slope of the linear part of the sigmoidal curve vary with the condition of the analyzed subject. In subjects with depressed BRS, such as the severely hypertensive individuals, it is observed a decrease in the RR intervals range and in the slope of the sigmoid linear portion, when compared to normotensive subjects.

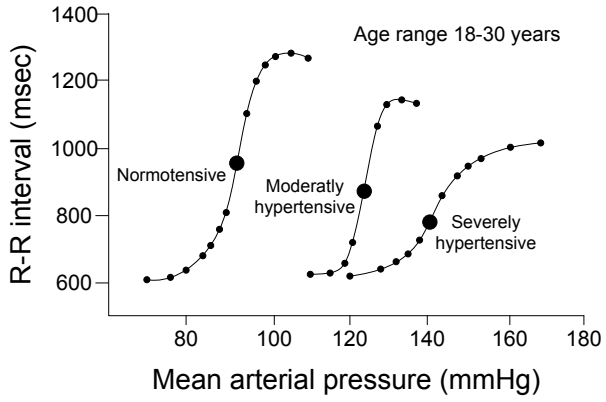

Figure 9 - Representation of the steady-state relationship between R-R interval and mean arterial pressure (MAP) in normotensive, moderately and severely hypertensive subjects. The big circle located at the linear part of the sigmoidal curve represents the operating point. Adapted from [10].

2.3. MULTI-SYSTEM INTERACTIONS AND REGULATION MECHANISMS

The main function of the cardiovascular system is to maintain the arterial blood pressure required for the transport and exchange of blood to body tissues. Blood pressure is directly determined by the arterial blood volume and the arterial compliance, which are in turn primarily affected by the cardiac output (CO) and systemic vascular resistance (SVR) [4]. Cardiac output (CO) is, by definition, the volume of blood ejected by the heart over a certain period of time (commonly per minute), which is therefore affected by the heart rate (HR) and the stroke volume (SV).

The electrical system is responsible for controlling the heart rate as well as synchronizing the cardiac mechanical system. The mechanical system is regulated by three factors controlling the stroke volume: preload, afterload and myocardial contractility. Since the preload and the afterload are dependent on both cardiac and vascular factors, they are functionally interacting with both vascular and cardiac systems. They also determine and are determined by CO. On the other hand, HR and myocardial contractility are strictly cardiac factors.

The respiratory system is responsible for variations in the venous blood flow, central venous pressure and venous return, caused by the periodic changes in the intra-thoracic pressure due to breathing cycle [1, 5].

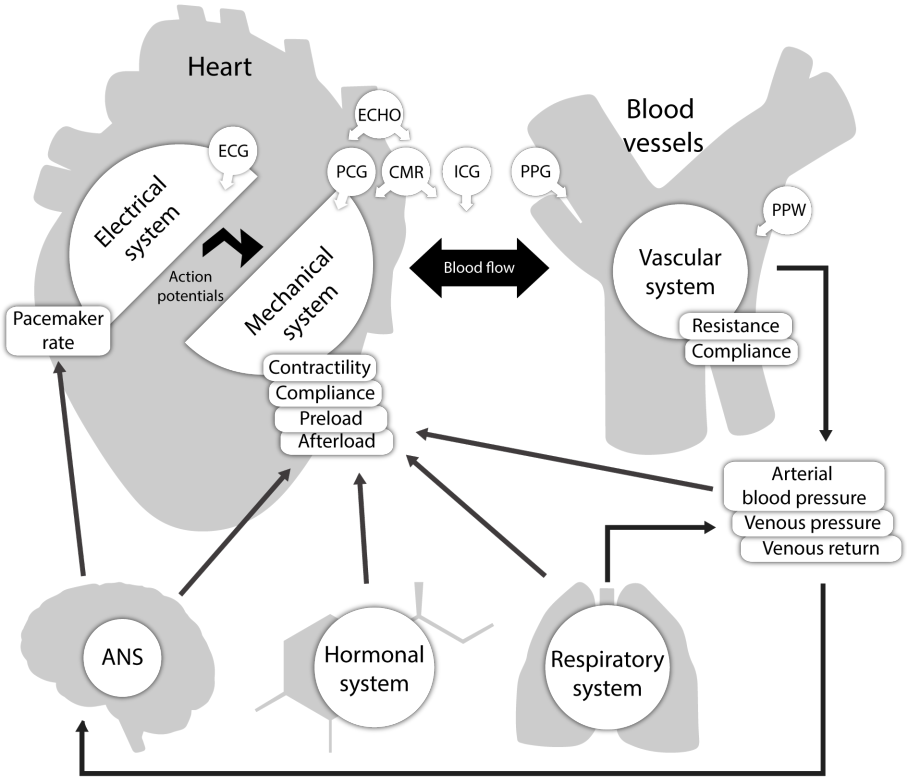

Figure 10 – Schematic representation of interactions between the subsystems involved in cardiac activity. ECG (electrocardiography), PCG (phonocardiography), ECHO (echocardiography), CMR (cardiac magnetic resonance), ICG (impedance cardiography), PPG (photoplethysmography) and PPW (pulse pressure wave).

The ANS regulates the chronotropy (HR), inotropy (myocardial contractility), and dromotropy (velocity of conduction within the heart) through the release of norepinephrine and produces vasodilatation in specific organs through the release of acetylcholine [1].

The hormonal system primary function is to control respiratory activity through the peripheral and central chemoreceptors. These sensors respond to changes in O_2/CO_2 concentrations and pH in blood. The activation of chemoreceptors generally leads to the activation of the sympathetic nervous system to the vasculature causing an increase of arterial pressure [1].

In Figure 10 we illustrate the interactions between the various sub-systems of the cardiovascular system, as well as their interactions with the regulatory mechanisms. Additionally, the non-invasive techniques that can be used to extract knowledge from the cardiovascular system interactions are also presented.

2.4. THE IMPORTANCE OF CARDIOVASCULAR FUNCTION SURROGATES AND NEURALLY MEDIATED SYNCOPE

Several studies have been presented in the literature concerning the importance of hemodynamic and haemodymic parameters, being the evaluation of the cardiac function one of the most important in the prognosis and diagnosis of CVDs. Furthermore, the evaluation of the vascular function is also of major importance, since it is associated with many blood pressure related cardiovascular complications. Indeed, blood pressure variability has also been reported as an important parameter in the prognosis and diagnosis of many CVDs. Additionally, autonomic nervous markers such as heart rate variability and baroreflex sensitivity were also pointed as important in CVD risk assessment [11-13].

The most commonly used method for the evaluation of cardiac function is echocardiography, from which many parameters can be extracted. Good examples, are the baseline of the left ventricle dimensions and the ejection fraction (EF) which has been shown to be one of the most powerful predictors of survival after acute MI, in chronic HF and among people free of overt CVDs [14]. Alternatively to EF, the systolic time intervals (STIs: PEP – Pre-ejection period and LVET – Left ventricular ejection time) became very important in the later years, since they can be more easily assessed in a non-invasive and continuous (beat-to-beat) basis, in contexts where mobility is required (p-health systems). The first area where STIs have been clinically evaluated was suspended chronic myocardial disease [15]. Using the systolic time intervals, Weissler [16] proposed a contractility index defined by PEP/LVET, which was shown to be highly correlated with angiographic EF in several conditions, such as myocarditis, cardiomyopathy and coronary artery disease with angina pectoris [15]. Furthermore, STIs have been also proven to be important in the evaluation of cardiac function of individuals with myocardial infarction (acute and chronic), pulmonary disease, aortic valve disease and chronic coronary artery disease. However, in the later case, the correlation of the contractility index with angiographic EF was shown to be lower [15], with PEP/LVET suggesting better cardiac performance than EF in this situations [17]. LVET alone is commonly associated with stroke volume

and has been indicated as a valuable prognostic parameter related to hypovolemia [18], an important predictor of mortality in patients with cardiac amyloidosis [19] and robust and independent predictor of light chain amyloidosis mortality [20].

Complementary to contractility indexes, cardiac output (and consequently SV) is also a fundamental measure of cardiac function. This measure reflects the capacity of the cardiac muscle to supply sufficient blood volume in order to maintain an "adequate" organ perfusion through the body [21, 22]. Although there are no normal values for CO [22], the evaluation of CO trends along with other hemodynamic parameters were proven to be of great importance in the diagnosis and management of CVDs. For example, the decrease in CO over time may be associated with the deterioration of the cardiac function and the onset or progression of heart failure [21]. Furthermore, CO is the primary standard in the evaluation of the need for therapeutic interventions and cardiovascular responsiveness to those interventions [23] (e.g., vasoactive and intravenous drugs) in the treatment of CVDs such as acute HF [14].

In what concerns to evaluation of the vascular function, arterial stiffness assumes a major role in the development of many CVDs. Arterial stiffening is associated with the increase in afterload, which consequently rises cardiac workload and reduces coronary perfusion. Arterial stiffening is commonly associated with elderly population and with atherosclerosis [24], and is responsible for the rise in systolic blood pressure, isolated systolic hypertension and the majority of cardiovascular events in elderly, with special emphasis to left ventricular failure [25]. Furthermore, arterial stiffness is associated with severity of coronary artery disease and carotid artery disease and is considered to be important in risk assessment in older people [24, 26]. Examples of surrogates that can be extracted from the PPG and PPW for the evaluation the vascular function are the augmentation index (AI), stiffness index (SI) and reflection index (RI). These parameters have been associated with arterial stiffening, PWV in large arteries and PP [6, 8, 27-31].

Another important parameter for the assessment of cardiovascular risk is blood pressure variability (BPV). Increased blood pressure variability has been shown to be related with the risk of fatal cardiovascular events, as well as the risk of all-cause death [32].

In what concerns to the evaluation of the autonomic nervous system modulation, HRV and BRS have been reported to have major importance in the prognosis and management of cardiovascular diseases. HRV was shown to have an important prognostic value in the development of cardiovascular complications, sudden cardiac death and all-cause death [33]. Additionally, the low baroreflex sensitivity has been associated with an increased risk for arrhythmic events [11] and high risk of death [12], and particularly sudden death [13] in post-myocardial infarction individuals. Although BRS is not correlated with EF, depressed values of both measures have been associated with higher risk of mortality [11, 12].

2.4.1. NEURALLY MEDIATED SYNCOPE

Syncope is a sudden transient loss of consciousness and postural tone resulting from the cessation of cerebral blood flow and is characterized by a rapid onset, short duration (10 seconds) and spontaneous complete recovery [24, 34]. It can be classified in four main types depending on its causes: vascular, cardiac, neurologic/cerebrovascular and metabolic/miscellaneous [24]. The vascular causes of syncope can be further categorized into anatomical, orthostatic and reflex-mediated [24]. Syncope resulting from vascular causes, and particularly orthostatic and reflex-mediated causes, is the most common form of syncope, accounting for at least one third of all causes [24], where reflex-mediated syncope (or reflex syncope) alone is responsible for 21% of all syncope episodes [34].

Reflex syncope includes neurally mediated syncope (NMS), situational and carotid sinus syncope. Although there are many syndromes of reflex syncope, they all share the same mechanism, composed by a trigger (the afferent pathway) and a response (the efferent pathway), which consists of an increased vagal tone and sympathetic withdrawal, leading to bradycardia, vasodilation, and consequently hypotension and syncope. The main differences between the causes of reflex syncope rely on the their specific triggers [24].

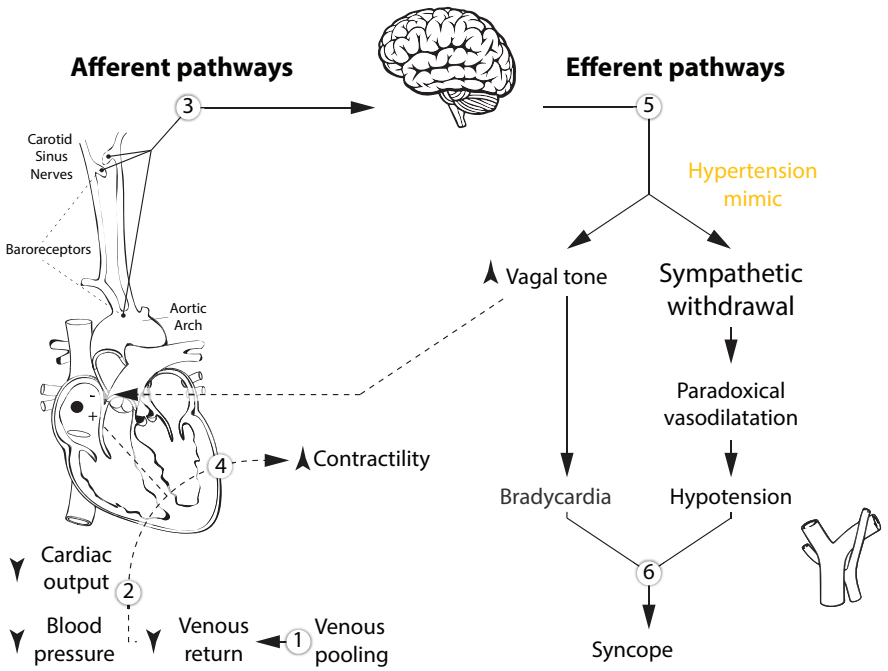

Figure 11 – Reflex mechanisms underlying the development of neurally mediated syncope (NMS).

Neurally mediated syncope (NMS), also known as neurocardiogenic, vasodepressor and vasovagal syncope, belongs to the reflex-mediated syncope group and can be characterized as an abrupt drop in blood pressure (with or without bradycardia) resulting from the abnormal functioning of the blood pressure regulation mechanisms [24]. Investigators believe that NMS is a result of a paradoxical reflex triggered by a decrease of venous return (reduction in preload) caused by an abrupt and excessive

amount of venous blood pooling. The reduction in the CO and blood pressure is sensed by the arterial baroreceptors, which activate the afferent pathway and in combination with a reduced preload leads to more vigorously contractions of the volume-depleted ventricle and to an excessive stimulation of the ventricular mechanoreceptors. The result is a "paradoxical" withdrawal in sympathetic tone and an increase in vagal tone, which leads to a blood pressure decrease and finally syncope [24, 35]. The reflex mechanisms underlying the manifestation of syncope are illustrated in Figure 11.

The effects of the deregulation of the blood pressure regulation mechanisms on the cardiovascular system make evident the importance of monitoring the hemodynamic and haemodynamic changes undergoing in the cardiovascular system. Thus, the extraction of surrogates that characterize these reflex mechanisms, such as changes in heart rate, contractility, vascular tone and blood pressure, are determinant in the diagnosis and prediction of NMS.

2.5. CONCLUDING REMARKS

In the current chapter we outlined the main physiological aspects that govern the research work presented in the current thesis. First, we described the anatomy and physiology of the cardiovascular system, by describing the cardiac and vascular systems and the primary modalities used to assess hemodynamic parameters. Additionally, we introduced the autonomic nervous system and the mechanisms used to regulate blood pressure. Finally, we presented how the various systems interact with each other to regulate blood pressure and how the extraction of parameters from the analysis of non-invasive modalities can be useful in the diagnosis and prognosis of cardiovascular diseases and, specially, on the prediction of neurally mediated syncope.

REFERENCES

[1] R. Klabunde, *Cardiovascular Physiology Concepts*: Lippincott Williams & Wilkins, 2004.

[2] O. College, "Heart Anatomy," O. CNX, Ed., ed. 19 de Junho de 2013 http://cnx.org/contents/6394ffc1-5482-4aa6-9233-23ad34848fa0@3@3.

[3] J. R. Weber and J. Kelley, *Health Assessment in Nursing Third edition* vol. Nursing assessment of the adult - Heart and neck vessels assessment: Lippincott Williams and Wilkins, 2006.

[4] C. Ahlström, "Nonlinear phonocardiographic Signal Processing," Institutionen för medicinsk teknik, 2008.

[5] A. C. Guyton and J. E. Hall, *Textbook of medical physiology*, 11th edition ed.: Elsevier, 2005.

[6] M. Baruch, D. Warburton, S. Bredin, A. Cote, D. Gerdt, and C. Adkins, "Pulse Decomposition Analysis of the digital arterial pulse during hemorrhage simulation," *Nonlinear Biomedical Physics,* vol. 5, p. 1, 2011.

[7] A. Reisner, P. A. Shaltis, D. McCombie, and H. H. Asada, "Utility of the Photoplethysmogram in Circulatory Monitoring," *Anesthesiology,* vol. 108, pp. 950-958 10.1097/ALN.0b013e31816c89e1, 2008.

[8] J. Allen, "Photoplethysmography and its application in clinical physiological measurement," *Physiological Measurement,* vol. 28, p. R1, 2007.

[9] J. T. Ottesen, "Modelling of the baroreflex-feedback mechanism with time-delay," *J Math Biol,* vol. 36, pp. 41-63, 1997.

[10] S. Gouveia, "Contributions to the analysis of short-term cardiovascular coupling," PhD on Applied Mathematics, Faculdade de Ciências, Universidade do Porto, Porto, 2009.

[11] T. G. Farrell, O. Odemuyiwa, Y. Bashir, T. R. Cripps, M. Malik, D. E. Ward*, et al.*, "Prognostic value of baroreflex sensitivity testing after acute myocardial infarction," *British Heart Journal,* vol. 67, pp. 129-137, February 1 1992.

[12] M. La Rovere, G. Specchia, A. Mortara, and P. Schwartz, "Baroreflex sensitivity, clinical correlates, and cardiovascular mortality among patients with a first myocardial infarction. A prospective study," *Circulation,* vol. 78, pp. 816-824, October 1 1988.

[13] S. Hohnloser, T. Klingenheben, A. van de Loo, E. Hablawetz, H. Just, and P. Schwartz, "Reflex versus tonic vagal activity as a prognostic parameter in patients with sustained ventricular tachycardia or ventricular fibrillation," *Circulation,* vol. 89, pp. 1068-1073, March 1 1994.

[14] I. S. Anand, V. G. Florea, and L. Fisher, "Surrogate end points in heart failure," *J Am Coll Cardiol,* vol. 39, pp. 1414-1421, May 1 2002.

[15] R. Lewis, S. Rittogers, W. Froester, and H. Boudoulas, "A critical review of the systolic time intervals," *Circulation,* vol. 56, pp. 146-158, August 1 1977.

[16] A. M. Weissler, W. S. Harris, and C. D. Schoenfield, "Systolic Time Intervals in Heart Failure in Man," *Circulation,* vol. 37, pp. 149-159, February 1 1968.

[17] D. Rater, D. Pugh, and W. Gray, "Practical Significance of Systolic Time Intervals in Coronary Artery Disease," *Chest,* vol. 64, pp. 186-188, August 1973.

[18] T. Geeraerts, P. Albaladejo, A. D. Declère, J. Duranteau, J.-P. Sales, and D. Benhamou, "Decrease in Left Ventricular Ejection Time on Digital Arterial Waveform during Simulated Hypovolemia in Normal Humans," *The Journal of Trauma and Acute Care Surgery,* vol. 56, pp. 845-849, 2004.

[19] D. Bellavia, P. A. Pellikka, T. P. Abraham, G. Al-Zahrani, A. Dispenzieri, J. Oh*, et al.*, ""Hypersynchronization" by Tissue Velocity Imaging in Patients with Cardiac Amyloidosis," *Heart,* May 12, 2008 2008.

[20] R. Q. Migrino, R. K. Mareedu, D. Eastwood, M. Bowers, L. Harmann, and P. Hari, "Left Ventricular Ejection Time on Echocardiography Predicts Long-Term Mortality in Light Chain Amyloidosis," *Journal of the American Society of Echocardiography,* vol. 22, pp. 1396-1402, 2009.

[21] A. N. De Maria and A. Raisinghani, "Comparative Overview of Cardiac Output Measurement Methods: Has Impedance Cardiography Come of Age?," *Congestive Heart Failure,* vol. 6, pp. 60-73, 2000.

[22] M. Pinsky and D. Payen, "Functional hemodynamic monitoring," *Critical Care,* vol. 9, pp. 566 - 572, 2005.

[23] M. R. Pinsky, "Probing the Limits of Arterial Pulse Contour Analysis to Predict Preload Responsiveness," *Anesthesia & Analgesia,* vol. 96, pp. 1245-1247, May 1 2003.

[24] P. Libby and R. O. Bonow, *Braunwald's Heart Disease: A Textbook of Cardiovascular Medicine, 2-Volume Set*, 8 ed. Philadelphia: Saunders Elsevier, 2007.

[25] M. O'Rourke, "Isolated systolic hypertension, pulse pressure, and arterial stiffness as risk factors for cardiovascular disease," *Current Hypertension Reports,* vol. 1, pp. 204-211, 1999.

[26] B. A. Kingwell and C. D. Gatzka, "Arterial stiffness and prediction of cardiovascular risk," *Journal of Hypertension,* vol. 20, pp. 2337-2340, 2002.

[27] M. F. O'Rourke, A. Pauca, and X. J. Jiang, "Pulse wave analysis," *British Journal of Clinical Pharmacology,* vol. 51, pp. 507-522, 2001.

[28] S. C. Millasseau, R. P. Kelly, J. M. Ritter, and P. J. Chowienczyk, "Determination of age-related increases in large artery stiffness by digital pulse contour analysis," *Clin Sci (Lond),* vol. 103, pp. 371-7, Oct 2002.

[29] S. S. DeLoach and R. R. Townsend, "Vascular Stiffness: Its Measurement and Significance for Epidemiologic and Outcome Studies," *Clinical Journal of the American Society of Nephrology,* vol. 3, pp. 184-192, 2008.

[30] P. J. Chowienczyk, R. P. Kelly, H. MacCallum, S. C. Millasseau, T. L. G. Andersson, R. G. Gosling*, et al.*, "Photoplethysmographic assessment of pulse wave reflection: Blunted response to endothelium-dependent beta2-adrenergic vasodilation in type II diabetes mellitus," *J Am Coll Cardiol,* vol. 34, pp. 2007-2014, December 1 1999.

[31] A. Laucevicius, L. Ryliskyte, Z. Petruioniene, MildaKovaite, and N. Misonis, "First Experience With Salbutamol - Induced Changes In The Photoplethysmographic Digital Volume Pulse," presented at the Seminars in Cardiology, 2002.

[32] G. Mancia, M. Bombelli, R. Facchetti, F. Madotto, G. Corrao, F. Q. Trevano*, et al.*, "Long-Term Prognostic Value of Blood Pressure Variability in the General Population: Results of the Pressioni Arteriose Monitorate e Loro Associazioni Study," *Hypertension,* vol. 49, pp. 1265-1270, June 1 2007.

[33] G. R. H. Sandercock and D. A. Brodie, *The role of heart rate variability in prognosis for different modes of death in chronic heart failure* vol. 29, 2006.

[34] A. Moya, R. Sutton, F. Ammirati, J. J. Blanc, M. Brignole, J. B. Dahm*, et al.*, "Guidelines for the diagnosis and management of syncope (version 2009)," *Eur Heart J,* vol. 30, pp. 2631-71, Nov 2009.

[35] B. P. Grubb, "Pathophysiology and differential diagnosis of neurocardiogenic syncope," *The American Journal of Cardiology,* vol. 84, pp. 3-9, 1999.

Chapter 3.
NON-INVASIVE ASSESSMENT OF CARDIOVASCULAR FUNCTION: REVIEW

In this chapter we will review the state of the art on three main research areas: 1) Evaluation of the cardiovascular function; 2) Assessment of baroreflex sensitivity and; 3) Prediction of neurally mediated syncope. We start by discussing the available methodologies for the evaluation of the cardiovascular function, from the assessment of blood pressure and vascular function surrogates to the evaluation of the cardiac performance. We then outline the principal methods in the quantification of the baroreflex sensitivity. This chapter closes with the presentation of algorithms proposed for the prediction of neurally mediated syncope and the main conclusions.

3.1. EVALUATION OF THE CARDIOVASCULAR FUNCTION

In the next sections, we will focus on methods present in the literature that allow the assessment of the cardiac function, which we will designate as cardiac function surrogates, and parameters that focus on the assessment of blood pressure and vascular function surrogates.

3.1.1. CARDIAC FUNCTION SURROGATES

The current gold standard on the assessment of cardiac function is cardiac magnetic resonance (CMR), which provides the evaluation of functional and morphological characteristics with high spatial and temporal resolution along with high contrast between blood and tissues [1]. However, its expensiveness and the need for a stable clinical environment and trained personal make it inadequate in p-health contexts.

Encouraged by the technological advances and the development of inexpensive and portable handheld devices, echocardiography (ECHO - the former gold standard) has become increasingly popular in primary, home care and ambulatory scenarios. ECHO can provide valuable information about the function and structure of the heart, allowing the estimation of measurements such as the velocity of pressure rise, the velocity of ejection, the extent of ejection and the ejection fraction. However, the requirement of trained personal and the inability to record long-term measurements are still major disadvantages in its translation into p-health scenarios. Alternatively, the assessment of systolic time intervals using non-invasive and portable devices gained much importance in this kind of clinical contexts.

Another important measurement of cardiac function that can be extracted using ECHO is stroke volume (SV) and consequently cardiac output ($\mathrm{CO} = \mathrm{HR} \times \mathrm{SV}$), since it provides information about the capability of the heart to eject blood into the system circulation. The SV is determined by the preload, contractility and afterload. The former is in turn determined by the systemic vascular resistance (SVR), i.e., the resistance to the blood flow in the arterial system.

The myocardial contractility, which can be estimated by the ejection fraction using ECHO, refers to the amount of work exerted by the heart muscle to eject blood to the circulatory system, at given levels of preload and afterload and is defined by the amount of pressure variation that the ventricle can generate over time [2].

Several techniques for monitoring CO are currently available, ranging from invasive (e.g., pulmonary artery catheterization and the direct Fick method) to minimally-invasive approaches (e.g., transpulmonary thermodilution, oesophageal doppler monitoring), and non-invasive approaches (e.g., pulse waveform analysis, echocardiography, impedance cardiography and photoplethysmography).

One of the most recognized techniques (pulse wave analysis - PWA) for the non/minimally-invasive assessment of the SV/CO is based on the analysis of the arterial blood pressure waveform (ABPW) obtained at a peripheral artery (invasively or non-invasively) or finger (non-invasively). Based on this technique several methods have been proposed (e.g., pulse counter analyses, model flow method and pulse power analysis), sharing the principle that SV/CO can be estimated from the analysis of the relationship between blood pressure (BP), arterial compliance and systemic vascular resistance (SVR) [3].

Wesseling et al. [4] proposed a systolic pulse contour analysis method where SV is assessed using a Windkessel model, which relates SV to the systolic portion of the arterial blood pressure waveform and the aortic impedance (Z_A). Since no simple direct methods exist to establish the appropriate value for Z_A, many approaches have been followed to estimate Z_A, using a linear combination of HR, MAP and age multiplied by an individual calibration factor in [4], multiple linear regression including pulse pressure (PP), HR and MAP in [5], or a pressure wave profile index multiplied by a dimensional factor in [6]. Other approaches such as the model flow method [7], pulse power analysis [8] or long time interval analysis of the peripheral pressure waveform [9] have also been proposed for SV assessment. Commercially available systems using the aforementioned methods differ on the need for external calibration (e.g., LiDCO^{TM} and PiCCO systems), the requirement of demographic/biometric characteristics (Flo Trac/Vigileo^{TM} system) or not requiring external data at all (Nextfin and MostCare systems) [3]. A disadvantage of these methods is the dependence of the CO estimates on the accuracy of the measured ABPW, which can be influenced by factors such as intense vasoconstriction and the measuring site [3, 10].

Another model for the evaluation of SV was proposed by Finkelstein et al. [11] where a linear combination of left ventricular ejection time (LVET), body surface area (BSA), heart rate and age is used to estimate SV. Since SV is also determined by other factors such as contractility, preload and afterload, we proposed on [12] a non-linear extension of the Finkelstein model including surrogates of these parameters. In the proposed non-linear models, the pre-ejection period (PEP) and the contractility index ($\mathrm{CI} = \mathrm{PEP}/\mathrm{LVET}$), assessed from the analysis of the phonocardiogram (PCG), were included as surrogates for MAP, afterload and myocardial contractility. It was concluded that the non-linear models

and especially the inclusion of PEP in the models improved significantly the estimation of SV. Moreover, the inclusion of the CI assessed from the PCG resulted in the degradation of the SV measurement as a result of the merged uncertainty in the estimation of PEP and LVET.

Methods based on the analysis of the PPG waveform have also been proposed by Wang et al. [13, 14] to assess CO. By selecting different models of the cardiovascular system (Windkessel model [13], tube model [14]) both authors used surrogate measures of MAP and total vascular resistance (TVR[3]) in their models. The ratio between systolic and diastolic components of the curve over the cardiac cycle (IPA) was used as a TVR surrogate in both methods while a parameter derived from frequency domain analysis of the PPG waveform (NHA) in [13] and pulse arrival time (PAT) in [14] were used as surrogates for MAP. Additionally, two calibration procedures are needed to assess absolute values of CO in [14]. More recently, Lee at al. [15] proposed a multivariate regression model using frequency and morphological parameters (among others) derived from PPG for the assessment of CO/SV (and SVR).

Another modality commonly used for assessing SV is the impedance cardiography (ICG), which continuously measures changes in impedance associated with variations in continuous blood flow and volume in the ascending aorta. Using the ICG, many equations relating SV to maximal impedance change ($dZ(t)_{max}/dt$) and LVET have been presented in the literature [16-19]. More recently Qiu-Jin et al. [20] deducted a novel impedance change equation, which is based on a parallel impedance model and the Ohm's law.

SYSTOLIC TIME INTERVALS

An alternative non-invasive approach for assessing global cardiac function is the use of systolic time intervals (STIs – PEP and LVET). The pre-ejection period (PEP) is defined as the time interval from the beginning of the ventricular electrical depolarization (Q-wave[4]) to the opening of the aortic valve, whereas left ventricular ejection time (LVET) refers to the time interval from opening to the closure of the aortic valve, and is defined as the time interval in which the blood is ejected from the left ventricle (see Figure 1). While subjects with a healthy heart reveal a short PEP and a long LVET [21], in cardiac dysfunctions it is observed a prolongation in the PEP and shortening in LVET. Based on this knowledge, Weissler [22] proposed the PEP/LVET ratio index as a measure of LV function, which is less heart rate dependent than its individual components.

[3] Total vascular resistance (TVR) refers to the resistance to blood flow offered by the whole (systemic and pulmonary) vasculature.

[4] Alternatively to the Q-wave, the onset of PEP is often defined by the R-wave, avoiding the uncertainty inherent to the identification of the Q-wave.

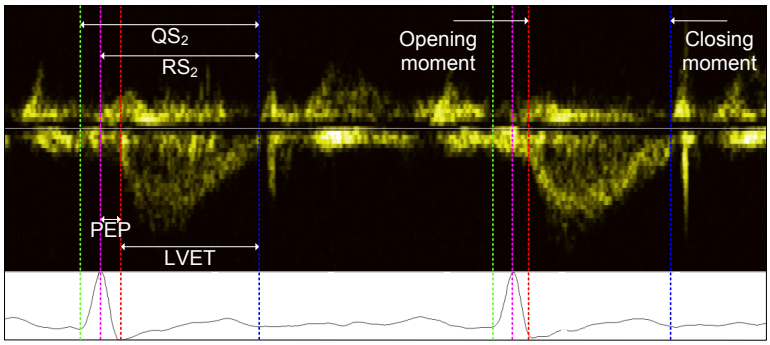

Figure 1 - Annotations of aortic valve timings using Doppler mode echocardiography.

In an attempt to expand the use of STIs, Mancini et al. [23] and Tei et al. [24] proposed another measure for the assessment of the left ventricular function, the myocardial performance index (MPI). This measure is defined as the sum of isovolumic contraction time (IVCT) and isovolumic relaxation time (IVRT) divided by ejection time, i.e., (IVCT+IVRT)/LVET, and allows the characterization of both systolic and diastolic function in a single index. However, as pointed out in [25] and [26], the MPI index must be used with great caution when evaluating severe diastolic dysfunctions, since it can be masked by complex systolic/diastolic interrelationships and bidirectional changes of the IVRT.

STIs can be determined using invasive, as well, as non-invasive techniques in in-hospital settings. For example, the gold standard is echocardiography, which is non-invasive and allows a reliable determination of STIs using Doppler or M-mode analysis. However, the use of echocardiography in p-health settings, where mobility is fundamental, is not viable, which motivated several authors to propose alternative methods for STI measurement. Thus, methods based on the ICG waveform [16, 27-35] and more recently on the PPG [36, 37] and PCG [38-40] waveform have been proposed to assess these parameters.

Although the ICG waveform analysis is the reference for portable devices in the determination of STIs, there is still some controversy on how to determine the ICG characteristic points that capture the opening (B-point) and closure of the aortic valve (X-point) [31, 32]. Kubicek et al. [16] proposed a method where LVET is defined from the zero-crossing preceding the maximum peak of dZ/dt to the negative peak of dZ/dt in the region of the second heart sound. In a later revision [27], the B-point was defined from the zero crossing point to the 15% response point of dZ_{max}/dt, in [30] Ono et al. defined the B-point (B_{ONO}) as the intersection of the zero-line and the regression line calculated from the portion (40% to 80%) of the curve preceding dZ_{max}/dt. The X-point is defined as the nadir of the dZ/dt downward deflection in [30-32] (X_0) (see Figure 2). In [33, 34] the characteristic points B, C and X are detected as local extremes and zero-crossings in different scales of the signal, which is decomposed using wavelet transform. More recently, Carvalho et al. [35] defined the B and X points as local minima in the ICG 3rd derivative, using B_{ONO} and X_0 as references.

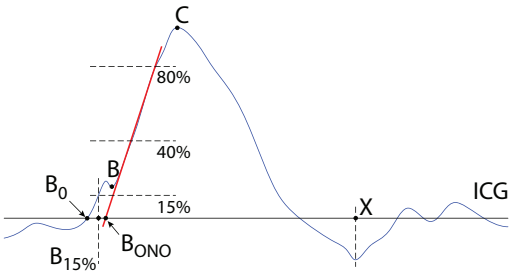

Figure 2 – Schematic representation of the main approaches for the determination of the B and X points in the ICG.

Chan et al. [36] proposed a method for the determination of LVET based on the analysis of successive derivatives (up to fourth) of the PPG. In this study, several characteristic points are extracted in each derivative based on well-defined waveform features (e.g., amplitude, slope and curvature). Using these characteristic points, three estimations of LVET are extracted which are then used to assess a final LVET estimation based on a rule-based decision logic approach. More recently [37], we proposed a new method for the estimation of LVET based on the analysis of the systolic model of the decomposed PPG pulse. The PPG pulse is decomposed into multiple Gaussian functions corresponding to the systolic and diastolic phases of the PPG pulse, and the LVET is assessed from the 3rd derivative of the functions corresponding to the systolic phase. The analysis of the systolic model rather than the whole PPG pulse was motivated by the need of reducing the influence of noise and pulse wave reflections in the estimation of LVET.

Carvalho et al. [38] and Paiva et al. [39, 40] proposed a method based on the analysis of the PCG for the assessment of the PEP and the LVET. Carvalho et al. [38] assumed that the heart sound S_1 is characterized by two well-defined high frequency components, corresponding to the closing of the atrio-ventricular valves, and to the opening of the aortic valve. Based on this assumption, the author proposed a method based on the analysis of the instantaneous frequency and energy of S_1 to assess the aortic valve opening time instant. Paiva et al. [39, 40] followed a Bayesian approach for PEP estimation based on the analysis of the instantaneous amplitude (IA) of the S_1. Assuming that the closure of the atrioventricular valves (AVVC) are well defined by a peak in IA, the opening of the aortic valve (AOVO) is detected in the IA signal resorting to typical time intervals between AVVC and AOVO. The closure of the aortic valve was defined as the onset of the second heart sound (S_2), captured by a high-frequency signature [41].

3.1.2. CARDIOVASCULAR SYSTEM MODELS AND NON-INVASIVE BLOOD PRESSURE ASSESSMENT

The estimation of blood pressures and flows has been widely investigated since the first cardiovascular model was formally developed and published by the German physiologist Otto Frank in 1899. Since then, many models of the cardiovascular system have been presented in the literature, ranging from lumped parameter models (e.g., [42-46]), to distributed networks where the blood flow in a distributed compliant network is governed by fluid dynamic equations (e.g., [47]), or to finite element

techniques that consider the spatial orientations, structures and mechanical properties of muscle fibers (e.g., [48]). The objectives of the proposed models also varied significantly, ranging from the simulation of the dynamics of the heart (e.g., [49, 50]) to the whole cardiovascular system (e.g., [42, 46, 51]). Nevertheless, a common goal is shared by most of the proposed studies, that is the qualitative simulation of the cardiovascular dynamics. In the presented simulations, blood pressures and flows are evaluated based on well-founded physiological knowledge, rather than a quantitative analysis of the estimated trends and values against the measured ones.

Recent methods for the assessment of non-invasive and cuff-less BP focus on the analysis of the pulse wave travelling from the heart to peripheral sites and on the electromechanical timings of the heart. In what concerns to the analysis of the pulse wave, the main approaches rely on the estimation of pulse wave velocity (PWV) or, inversely, pulse transit time (PTT), that is, the time taken by the pulse wave to travel between two distinct arterial sites. However, these approaches do not account for changes in the vascular structure properties, which result in a constant need of external calibration procedures. This issue gains emphasis when considering the BP estimation during transient events (e.g., physical exercise, administration of vaso-active drugs and posture changes). Other approaches focus on the estimation of the amplitude of arterial volume pulse wave either as an independent surrogate or combined with PTT, on the electromechanical[5] systole interval (RS_2) as a surrogate for BP and on the evaluation of the arrival time and amplitude of the pulse wave components.

BLOOD PRESSURE AND VASCULAR FUNCTION SURROGATES

The problem of non-invasive and cuffless blood pressure (BP) measurement has been the focus of numerous studies and publications in the past decades. Firstly proposed by Penaz in 1970 [52], the volume clamp method is certainly the most recognized in this field, which is based on keeping the finger vessels in a constant "vascular unloading" state using a inflatable finger cuff and in the signal acquisition using a built-in PPG sensor. However, the original apparatus carried several disadvantages and its translation to a commercial device only happened in 1980 with the presentation of the Finapres™ by Wesseling and colleagues [53, 54]. Since then several alternatives systems have been presented (e.g., the Task Force Monitor). Despite the technological advances, these systems are still bulky and expensive, their usage is in some cases complex and can cause discomfort, and also require frequent calibrations [55].

An alternative to the volume clamp method for the non-invasive BP assessment is the use of surrogates extracted from the analysis of the pulse wave traveling from the heart to a peripheral site. In this field, one of the most recognized and promising surrogates is the pulse wave velocity (PWV) or,

[5] The exact definition of the electromechanical systole is the time span between the ECG's Q-wave and the onset of the S_2 sound (closing of the aortic valve). However, from a practical engineering viewpoint, the RS_2 is usually simpler and more accurate to compute, since the uncertainty in identifying the Q-wave is much higher compared to the uncertainty in determining the R-wave.

inversely, the pulse transit time (PTT) [56-76]. Moreover, the amplitude of the arterial volume pulse wave has been also considered as a surrogate for BP, and is often combined with PTT [69, 77-79]. Other methods focus on the assessment of the time from the R-peak to the 2nd Heart Sound (S_2) [80-82]. Recently, in [83, 84] the relationship between the characteristics of the pulse components has also been proposed as a surrogate for BP.

The "true" PTT is defined as the time interval taken by the pulse wave to travel a certain distance along a homogeneous arterial segment. Thus, to measure PTT, the pulse wave has to be recorded accurately in two locations of the analyzed arterial segment [58, 72]. However, the placement of two sensors at a small distance apart is often difficult and uncomfortable, leading to alternative approaches. The most common approach to assess PTT is based on the simultaneous detection of the ECG R-peak and the beginning of the pulse wave inflection measured at a peripheral site (see Figure 3). However, the measured time difference results in an approximation of PTT, often called as PAT (Pulse Arrival Time) and its relation to the (true) PTT measure is described by:

$$\mathrm{PAT} = \mathrm{PEP} + \mathrm{PTT} \tag{4}$$

where PEP[6] (Pre-Ejection Period) is the time from the Q-peak wave to the opening of the aortic valve, and is not related to the pulse propagation.

Alternatively to the PAT measurement [56, 58-73, 75], other approaches have been followed to extract BP surrogates. In [73, 74, 76, 85], the PTT is estimated by subtracting the extracted PEP (e.g., using ICG-based methods) from the PAT measurement, while in [86] the influence of PEP is avoided by normalizing PAT with the pulse rate. Other approaches resort on the subtraction of two PAT measures (DPTT – differential pulse transit time) from distinct arterial pathways [57, 76] (see Figure 3) or in the same arterial pathway [87-89]. Furthermore, some authors also suggested PAT and PTT measures considering different characteristic points in the pulse wave (e.g., the systolic biggest inflection of the ascending curve or the peak of the pulse wave) [58, 62-65, 68, 69, 74, 90] and different methods for their identification (e.g., Hilbert–Huang transform [91] and time delay methods [92]).

[6] The exact definition of Pre-Ejection Period is the time span from the onset of the ventricular electrical depolarization (Q-wave) to the onset of the aortic valve opening. However, from a practical engineering viewpoint, the R-wave is often assumed as the beginning of the systolic electrical activity since the uncertainty in its identification is much lower compared to the determination of the Q-wave.

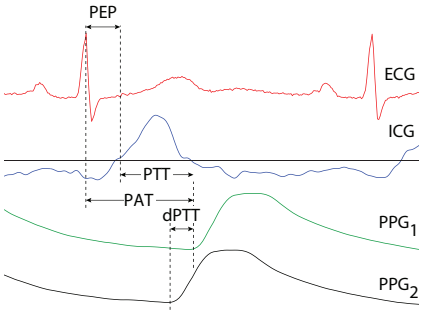

Figure 3 – Representation of PEP, PAT, PTT and DPTT. The PPG_1 and PPG_2 representations refer to different arterial segments.

Empirically, the changes in PWV or, inversely, PTT, are usually followed by changes in BP, which are translated into an inverse correlation between BP and PTT/PAT measurements. However, the PTT and PAT only reflect part of a complex system integration that induces BP changes. Therefore, assuming a linear relationship between PTT and BP can lead to contrasting results, ranging from very low (ρ=-0.1) to very strong (ρ=-0.99) correlations, depending on the measuring conditions, physiological context and adopted approaches [93].

To account for the non-linear relationship between PTT and BP, Isebree Moens and Korteweg proposed the Moens-Korteweg equation, which relates the velocity of the pulse wave and the elastic and geometric properties of a short elastic vessel. This equation is often employed to BP surrogates, such as PTT, and is given by:

$$\mathrm{PWV} = \frac{\mathrm{distance}}{\mathrm{PTT}} = \sqrt{\frac{\mathrm{Eh}}{\rho 2\mathrm{r}}} \qquad (5)$$

where *E* is the Young elasticity modulus of the wall, ρ is the blood density, *h is* the wall thickness and r is the vessel radius. Indeed, it is assumed that ρ, r and *h* undergo small or insignificant changes, and the main variations are expected to come from the elasticity modulus. Hughes [94] provided the link between PWV and BP by presenting the following equation:

$$\mathrm{E} = \mathrm{E}_0 \mathrm{e}^{\alpha \mathrm{P}} \qquad (6)$$

where $\alpha \approx 0.017 \mathrm{mmHg}^{-1}$ and *P* is the mean arterial pressure (MAP). By combining equation (5) and the linearization of equation (6) ($\mathrm{E} \sim \mathrm{E}_o(1 + \alpha \mathrm{P})$) one gets the quadratic dependency that relates PTT with MAP:

$$\mathrm{P} = \mathrm{A}(1/\mathrm{PTT})^2 + \mathrm{B} \qquad (7)$$

From the Moens-Korteweg equation, Bramwell and Hill [95] derived another expression, the Bramwell-Hill equation, which relates the velocity of the pulse wave to the vessel compliance/distensibility and is given by:

$$\mathrm{PWV} = \sqrt{\frac{\mathrm{A}}{\rho \mathrm{C_A}}} = \sqrt{\frac{\mathrm{V}.\Delta \mathrm{P}}{\rho.\Delta \mathrm{V}}} \quad (8)$$

with A the lumen area, $\mathrm{C_A} = \Delta \mathrm{A}/\Delta \mathrm{P}$ the compliance area and ρ the blood density. Modeling the pressure-volume relationship with a sigmoidal curve (e.g., [96, 97]) yields the link between BP and PWV. Shaltis et al. [96] proposed the following equation for the aforementioned relationship:

$$\mathrm{V} = \frac{\mathrm{a}}{1 + \mathrm{e}^{-\mathrm{bP}}} \quad (9)$$

where a and b are fitting parameters. Substituting equation (9) into (8) and rearranging the equation with Taylor expansions, Yan and Zhang [98] obtained:

$$\mathrm{PWV} = \sqrt{\frac{\mathrm{e}^{\mathrm{bP}} + 1}{\rho \mathrm{b}}} \approx \frac{1}{\sqrt{\rho \mathrm{b}}} \frac{\sqrt{2}}{(1 - \frac{\mathrm{bP}}{4})} \equiv \frac{1}{\mathrm{cP\text{-}c}/4} \leftrightarrow \mathrm{PTT} = \mathrm{L}(\mathrm{cP\text{-}c}/4) \quad (10)$$

where L is the distance the pulse travels and c is a constant determined by experimental data fitting.

From the Moens-Korteweg and Bramwell-Hill equations, several authors derived calibration functions to relate BP and PWV (or PTT), differing on the number of unknown parameters, number and non-linearity of the terms and additional parameters. Chen et al. [60] proposes a two term calibration function considering the initial (during calibration) BP and PTT measurements, along with an unknown parameter and the PTT change, while Poon et al. [67] presented two dependent functions for the calibration of SBP and DBP, considering SBP, DBP and PTT initial measurements along with a patient specific coefficient and a weighted PTT. Gesche et al. [99] proposed a calibration function with two non-linear terms and a correction factor to model the relation between PWV and BP. The dynamics of the cardiovascular and regulation systems is also taken into account, by including PTT and two compensation terms (PTTV and VPTT) in [100], and a zero-crossing factor in [101]. From these equations, it is possible to derive the unknown parameters by fitting PTT to BP (measured with another device) through a calibration step. However, the continuous changes in the vascular properties, such as the diameter of blood vessels, are not hold in these models, which implies an intermittent re-calibration of the model parameters in long term measurements [75, 102]. An alternative calibration procedure, which doesn't rely on the use of external devices, was proposed by Poon et al. [103] and McCombie et al. [104], which is based on the mapping of PTT changes related to changes in hydrostatic pressure provoked by the lifting of the hand above the level of the heart.

Although several approaches have been proposed in the literature using Moens-Korteweg equation [56, 59, 60, 67, 105] or Bramwell and Hill equation [96, 98, 106, 107] there is still some controversy on

which parameter (PTT, PAT, DPTT) best describes variations in BP. This issue has been addressed in several studies considering the influence of PEP and PTT during transient events such as physical exercise [72, 76, 105, 108], posture change [73, 109] and administration of vaso-active drugs [85].

Muehlsteff et al. [105] showed that during intermittent short-term physical exercises the variations in PEP were almost identical to the variations in PAT and were consistent to the variations in BP. This conclusion was later confirmed by Deb et al. [72] and more recently by Wong et al. [108], who evaluated the changes of PEP, PTT and PAT in pre/post exercise conditions, and Proença et al. [76], who studied the ability of DPTT [72, 76], PTT (subtracting PEP)[76] and PAT to reflect changes in BP, under various contexts of physical exercise. Both authors concluded that BP is most consistently correlated to PAT, than DPTT and finally PTT. Moreover, Proença et al. [76] showed that to capture the small variations in BP ($\Delta BP \approx 10$ mmHg) using the Moens-Korteweg equation, it is necessary to accuratly estimate PTT (8-16ms), which is not possible due to the contribution of PEP measurement accuracy (9.8 ± 21.37 ms).

Contrarily to the aforementioned conclusions, Muehlsteff et al. [73] showed that calibration functions (e.g., Moens-Korteweg equation) based on PAT measures are not suited for inferring BP changes in contexts of posture change. The author demonstrated that the PAT measurement is strongly affected by posture changes at almost constant values of systolic blood pressure (SBP) and diastolic blood pressure (DBP). Changes in PAT are believed to be primarily caused by the sensitivity of PEP and LVET due to fluid shifts inside the body, which in turn affect cardiac preload and filling.

Payne et al. [85] studied the effect of vaso-active drugs in the determination of BP through PAT and PTT measurements. In the proposed study, the author showed that PAT is significantly better correlated with SBP than it is with either DBP and MAP and its relation with SBP is relatively unaffected by different drugs in the overall studied population. Contrarily, PTT was more strongly correlated with DBP and MAP. Although the correlation PTT-DBP and PTT-MAP appeared to be poorly influenced by drug administration, the PTT-SBP correlation was differently affected depending on the administrated drug. In conclusion, the author suggested that the use of PAT as a purely vascular function surrogate should be avoided, not rejecting the potential of PAT in the assessment of BP variability and rapid pressure change. In a study using anesthetized dogs, Zhang et al. [110] concluded that PAT is not a reliable substitute for PTT even at the adopted ideal circumstances.

Other approaches presented in the literature investigate how photoplethysmogram (PPG) components, i.e., baseline and amplitude (PA) can be combined with PTT [69] or even used separately to estimate BP (e.g., [77, 78, 111]). It is believed that the PPG AC component reflects changes in the blood resistance and compliance in the vasculature, while the DC component is an indicator of changes in blood volume [77]. Chua et al. [69] proposed a method where SBP and DBP are defined by linear functions depending on current and past PAT and PA estimations, while Shaltis et al. [78] proposed a method for estimating of MAP based on a non-linear function of the current PA estimations. Nitzan et

al. [111] studied the very low fluctuations in blood volume pulse peak, pulse amplitude and pulse period to assess SBP and DBP. Jeong et al. [77] estimated SBP and DBP based on the amplitude, foot and peak of the pulse wave extracted from AC and DC components of the PPG.

Additionally to the PTT-based approaches, another potentially relevant measure, the RS_2, has also been reported in the literature for BP estimation [80-82]. The RS_2 is defined by the time interval between the R-peak wave of the ECG and the peak of the 2nd heart sound S2 in the PCG. Zhang et al. [80] proposed a method for the estimation of BP based on RS_2 during dynamical physical exercise. The proposed surrogate presented a close inverse correlation with SBP, which is believed to be related with the change in the rate of ejection. Zhang et al. [81] proposed a modified mathematical model of the cardiovascular system to simulate the relationship between SBP and RS_2. In this study, it was demonstrated that RS_2 is inversely correlated with systolic blood pressure under the effects of changing peripheral resistance, heart rate and contractility. Following the approach presented in [80], Wong et al. [82] used the parameter RS_2 to estimate SBP and DBP in normal and abnormal subjects during resting condition.

Recently, Baruch at al. [83] proposed a novel (pulse decomposion analysis - PDA) model based on the analysis of the arterial blood pressure waveform. Using the equation proposed by Moens-Korteweg, the authors relate the aortic DBP, SBP and PP with the pressures at each arterial path, which are in turn described by the time of arrival and amplitude of the pulse componentes at the peripheral site. Using this model, the author proposed two indices for the assessment of PP and SBP, that are P2P1 (the amplitude ratio of the first reflection wave and the main pulse) and T13 (the time span between the main pulse and the 2nd reflection wave). These indices were proven to be strongly correlated with aortic SBP and PP (measured by cardiac cathetherization), respectively [83, 84].

VASCULAR FUNCTION SURROGATES

In addition to BP, the pulse wave has also been intensively studied in order to extract valuable information describing the elastic properties of the arteries. Commonly used terms to describe these properties include arterial stiffness, compliance, elasticity (or elastic modulus), distensibility and vascular impedance. Studies employing these surrogates indicate that increased arterial stiffness is associated with increased cardiovascular risk, including hypertension and severity of coronary artery disease [112] and increased target organ damage [113]. Increased arterial stiffness is also associated with aging, hypercholesterolemia, obesity, and it is commonly observed in smokers. Other diseases such as diabetes mellitus and kidney disease were also related with increased arterial stiffness [113]. Additionally, arterial stiffness has been shown to predict future morbidity and mortality [112].

One of the simplest surrogates of arterial stiffness is PP, but depending on the measuring site and techniques, this surrogate alone was shown to lack in accuracy [114]. Additionally, the pulse wave velocity measured from the carotid to the femoral artery has also been proposed as a risk predictor for cardiovascular events [114].

From the analysis of the photoplethysmogram, three main indices have been proposed in literature, which are the augmentation index (AI), the stiffness index (SI) and the reflection index (RI), illustrated in Figure 4. In [115], the SI is defined as the time delay between the direct and reflection waves ($SI = T_{DIAS}\text{-}T_{MAX}$), while in [115, 116] the RI is determined by the ratio between the height of the diastolic wave to the maximum pulse height ($RI = P_{DIAS}/P_{MAX}$). Millesseau et al. [117] proposed the correction of SI with relation to the subject height *h* ($SI_{MIL} = h/(T_{DIAS}\text{-}T_{MAX})$), and suggested that this index increases with age. The SI is associated with the velocity of a pulse wave in large arteries [118], large artery stiffness [119] and also has been shown to correlate with PP [83]. The RI has been associated with small artery stiffness [118] and changes in vascular tone [115, 120].

The augmentation index was defined by Takazawa et al. [121] as the ratio between the late and early systolic components ($AI_{TAK} = P_C/P_B$) derived from the PPG second derivative, while Rubins et al. [122] proposed two definitions of AI depending on the PPG morphology (type A: $AI_{RUB} = 1\text{-}P_1/P_{MAX}$ and type C: $AI_{RUB} = 1\text{-}P_2/P_{MAX}$). The augmentation index (AI) is commonly associated with aging and arterial stiffening [54, 83, 123].

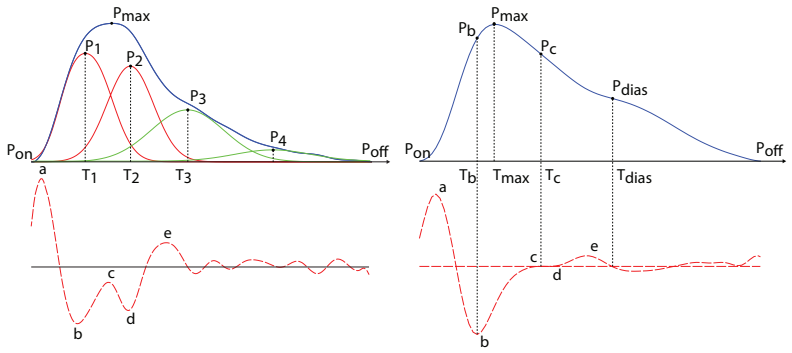

Figure 4 –Representation of the characteristic points of the PPG pulse. Left: PPG pulse and respective components (P1, P2, P3 and P4). Right: PPG pulse and characteristic points extracted from DDA.

From the analysis of the PPG 2nd derivative (DDA – double differentiation analysis), Takazawa et al. [121] proposed the identification of five consecutive waves, located at the systolic (*a*, *b*, *c* and *d* waves) and at the diastolic (*e* wave) phases of the PPG pulse and demonstrated that their relationship with the *a* wave provides valuable information about the cardiovascular system. Examples of these relationships are the *b*/*a* ratio, which was associated with increased arterial stiffness and aging, the *c*/*a*, *d*/*a* and *e*/*a* ratio, which is related with decreased arterial stiffness, and the (*b*-*c*-*d*-*e*)/a ratio, which was shown to increase with age.

Another important property of the peripheral vascular network is the ability to reduce or increase the radius of the vessels, known as vasoconstriction and vasodilation. This property affects the resistance of the blood flow in the peripheral circulation and is defined as systemic vascular resistance (SVR). Methods proposed in literature for the assessment of SVR consist in the determination of the pulse

width (length of the PPG pulse at half height) [124], the inflection point area ratio (IPA = A_{dias}/A_{sys}), which is the ratio between the area of the diastolic and systolic phases [13], the area difference ratio (ADR) and the decay constant time (VRC) calculated using a piecewise linear interpolation criterion [125]. The ADR parameter (illustrated in Figure 5), was calculated as the difference between the area of the triangle formed by P_{dias}-P_{off}-T_{dias} (A_t) and the area under the curve of the pulse *Y(t)*, but above the horizontal line T_{dias}-P_{off} (A_p) divided by A_t, and was defined as:

$$ADR = \frac{A_t - A_p}{A_t} \quad (11)$$

Recently, Jeong et al. [126] evaluated the relationship between the aforementioned parameters (DDA-derived, PAT-derived and others) and BP, during exercise in senior populations. The authors were able to find a strong association between the PAT_{PEAK} (R-wave to PPG peak) and PAT_{R-A} (measured from the R-wave to the *a* wave of the 2nd PPG derivative), and SBP. Moreover, a strong negative correlation was also found between PAT_{MACC} (R-wave to the peak of the PPG 1st derivative) and $PAT_{R-A,}$ and PP.

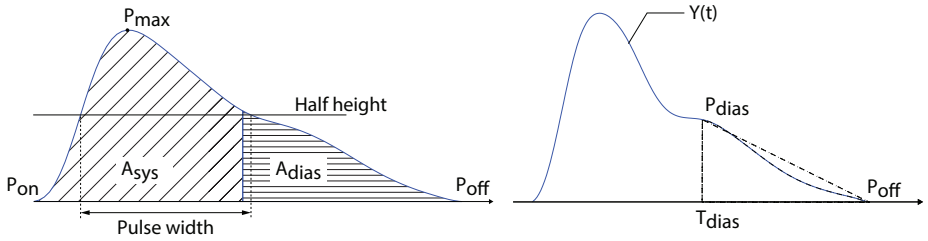

Figure 5 – Illustration of the characteristic points and areas used in the extraction of SVR surrogates. Left: Pulse width and systolic/diastolic areas used in the assessment of IPA. Right: Characteristic points used in the determination of ADR.

3.2. ASSESSMENT OF BAROREFLEX SENSITIVITY

The evaluation of Baroreflex sensitivity (BRS) has been studied since 1969, when the first concept was presented by Smyth et al. [127]. Since then, several methods have been proposed in the literature for BRS quantification resorting to the analysis of the relationship between RR and BP, among other variables (e.g., RESP), using either time [127-132], frequency [133, 134] and model-based [135-145] approaches. However, all these methods resort to the acquisition of a continuous (beat-to-beat) arterial blood pressure waveform, which is often inaccessible in the generality of the clinical and hospital settings. An approach that could be used to improve the applicability of BRS to a wider range of clinical scenarios is based on surrogate measurements of BP (e.g., Pulse Transit Time and Pulse Arrival Time) as an alternative to the inconvenient continuous and direct measurement of BP. However, as far as we know, these kind of approaches have been poorly tackled in the literature [146, 147].

In the time domain based analysis, the sequences technique proposed by Di Rienzo et al. [128, 129] in 1985 and enhanced in 2001, was the first structured method aiming to the quantification of BRS. This technique is based on the regression analysis of short segments called baroreflex segments

("BSs"), consisting in synchronous variations in SBP and RR values and characterized by simultaneous amplitude variations. From 2002 to 2009, improvements in the time domain BRS assessment were presented by Malberg et al. [130] with the dual sequence method, Westerhof et al. [131] with the cross-correlation baroreflex sensitivity ("xBRS") estimate, Gouveia et al. [132] with the events technique and recently Bauer et al. [148] with the bivariate phase-rectified signal averaging. Because the time domain techniques rely on the analysis of short segments of data, it is believed that these methods mainly reflect the parasympathetic modulation of the ANS.

The frequency domain techniques, in contrast with the time domain based techniques, are capable of distinguishing baroreflex activity of different frequencies: low frequencies (LFr: 0.04-0.15 Hz) are associated with sympathetic ANS effects, while high frequencies (HFr: 0.15-0.4 Hz) are associated with vagal/ parasympathetic and respiratory activity. The main techniques in this field were presented by Robbe et al. [133], with the Transfer function method, and by Pagani et al. [134] with the Alpha technique.

Additionally, several studies also focused on the analysis of the HR variability, being the main approaches based on time and frequency domain analysis. Techniques such as the Fourier transform, high order spectra analysis are commonly used to detect the low and high frequency components related with the sympathetic/parasympathetic and ventilatory modulations. Additionally, nonlinear and nonstationary techniques (e.g Lyapunov exponents and wavelet transform) were also used to elucidate the complex short and long term nature of the HR variability [149].

The inability of the frequency and time domain techniques to distinguish between negative and positive feedback, causality between effects, and to account for other external influences, motivated several authors to extend these techniques by assuming a closed loop system, where it is considered a feedforward pathway (where cardiac and arterial effects result in changes of BP) and a feedback pathway (the arterial baroreflex). Some studies contemplate the analysis of the variability of a single measurement (e.g., HR - [135, 136]), while other authors use of several parameters (e.g., HR, BP, RESP - [137-141]) in the characterization of one or both parts (feedback/feedforward) of the CNS regulation.

3.3. PREDICTION OF NEURALLY MEDIATED SYNCOPE

The prediction of neurally mediated syncope (NMS) is a problem that has been the focus of intense research in the later decades and therefore several methods have been proposed in the literature, differing the objectives, methods and used modalities. The most common approach to this problematic is the early prediction of the head-up tilt table test (HUTT) outcome (e.g., [150-155] [156-163]) based on a analysis of HR, BP parameters before and after tilt, i.e., during the supine position and early passive standing position. Another approach is the real time prediction of NMS syncope events (e.g., [164-169]), which focus on the real-time analysis of cardiovascular parameters for the prediction of impending syncope.

Methods for the early prediction of the HUTT outcome are mainly focused on the analysis of the HR and/or SBP variability using either time [150-154, 160, 161] and frequency domain techniques [155, 156] or both [157-159]. The time domain methods focus on the evaluation of temporal changes of HR during the supine and upright positions, using statistical features, such as mean, standard deviation [150, 152, 157, 158], variance and kurtosis [154], or even doing simple comparisons between the HR in both phases [151, 153]. In addition to the analysis of the HR variability, Naschitz et al. [154] also included in the proposed model features based on the PTT parameters. Other methods focused on the analysis of the BP variation alone, with the quantification of the number of SBP reductions during the early up-right position [161], and on a combined analysis of HR and BP changes regarding to the baseline values [160]. The frequency domain methods are mainly based on the evaluation of the characteristics of the low (LFr: 0.04-0.15Hz) and high (HFr: 0.15-0.40Hz) frequency components (e.g., power and area) and on the relationship between the characteristics of those components (the LFr/HFr ratio) as measures of sympathovagal balance [155-159]. Common methods used to identify and analyze these components are the Fourier transform [155] and auto-regressive models [159]. Additionally, methods using indices of myocardial contractility assessed from endocardial acceleration (PEA) [162] and from transthoracic impedance cardiography [163] have also been proposed in the literature. In [170] we also studied the importance of contractility and vascular tone surrogates, in the characterization of the mechanisms underlying the development of NMS. In a thorough evaluation of the early syncope prediction methods, Blanes et al. [171], concluded that the problem of early syncope prediction is far from being solved, and should be handled with caution.

In contrast with the early prediction of syncope, the real-time prediction problem has only been talked in the later years, where the analysis of the HR and BP changes have also been considered [164, 165]. Virag et al [164] proposed a method for real time prediction of impending syncope based on the time and frequency analysis of the HR and SBP signals. The proposed method is based on the evaluation of a cumulative risk function using normalized HR and SBP trends, as well as the HR and SBP LFr powers. Mereu et al. [165] evaluated the prediction ability of HR and BP (SBP, MBP, DBP and PP) trends and the ratio between the dRR (1^{st} derivative of RR) with those trends. Nevertheless, these methods require the continuous monitoring of BP using systems, which still carry several disadvantages (e.g., expensiveness, hard management and recurrent calibration). Motivated by the need of solutions that do not rely on these systems, several authors focused on the analysis of non-invasive and widely available modalities, such as the ECG and PPG. The proposed methods focus on the evaluation of changes of the pulse arrival time (PAT) alone [168], as a surrogate for SBP changes, or along with HR changes [166, 167], inotropic and vascular tones changes [172, 173] and, consequently, prediction of syncope. In Table 1 we present a summary of the results achieved by the methods proposed in the literature for real time prediction of NMS.

Table 1 – Results achieved by the real time prediction methods proposed in literature.

Method	SE (%)	SP (%)	PPV (%)	FPRh (h^{-1})	Pre-Time avg±std (s)	Modalities	# volunteers
Virag et al. [164]	95	93	-	-	128±216	ECG/ABPW	1155
Mereu et al. [165]	86.2	89.1	-	-	44.1±6.6	ECG/ABPW	145
Eickolt et al. [166]	81	85	-	-	203±227s	ECG/PPG	44
Meyer et al. [167]	100	100	100	-	99±108	ECG/PPG	14
Muhlsteff et al. [168]	90.48	83.33	82.61	-	77.71±71.78	ECG/PPG	44
Couceiro et al. [172]	100	92.3	85.7	0.146	217.6±197.4s	ECG/PPG	44
Couceiro et al. [173]	100	84.6	75	0.29	341.75±286.33	ECG/PPG	44

From Table 1 one observes that the method presenting the best results was proposed by Meyer et al. [167], achieving a sensitivity (SE), specificity (SP) and positive predict value (PPV) of 100%. Despite the great results presented by the authors, the use of a small number of patients (14) in the validation of the proposed method suggests that these values should be analyzed with great caution. The second method achieving the highest SE, SP and PPV values was presented by Couceiro et al. [172], which introduces parameters that characterize changes in inotropy (LVET) and vascular tone (SI and RI) in addition to HR and PAT changes. This method was validated in a larger population composed of 44 patients and achieved a SE of 100%, and SP o 92.3% and a PPV of 85.7%. Moreover, the low number of false positives per hour (FPRh: $0.146h^{-1}$) and the high prediction time (217.6s) is a good indicator when considering its translation to p-health applications. More recently, the features proposed in [172] were used to train and test an SVM classification model combined with a "Firing power" regularization method [173]. The proposed model presented a lower performance, which is reflected by the decrease of the SP (84.6%), PPV (75%) and by the increase of the FPRh ($0.29h^{-1}$). Contrarily, its prediction time was the highest among all the methods presented in Table 1. The third method presenting the best performance was proposed by Virag et al. [164]. This method resorts on the analysis of the HR and SBP trends and achieved an SE of 95% and a SP of 93%. Although no values were provided regarding the PPV and FPRh, the validation of the proposed method on a much larger population, composed of 1155 patients, suggests that the presented results are founded on strong statistics, which represents a great advantage when compared to the aforementioned methods. The remaining algorithms proposed by Mereu et al. [165], Eickolt et al. [166] and Muhlsteff et al. [168] presented similar performances regarding the SE and SP metrics (above 80%) but distinct prediction times, ranging from 44.1s (Mereu et al. [165]) to 203s (Eickolt et al. [166]). In sum, these results show that the surrogates associated with contractility and vascular tone changes can provide major enhancements in the prediction of syncope events, which were reflected in the reduction of the number of false alarms and in the increase of the time at which syncope is predicted.

3.4. CONCLUDING REMARKS

In this chapter we introduced the main methods for the evaluation of the cardiovascular function, estimation of baroreflex sensitivity and prediction of neurally mediated syncope, based on the analysis of non-invasive signals such as the electrocardiogram, photoplethysmogram and arterial blood pressure waveform. In the evaluation of the cardiac function, we focused on the methods for the assessment of stroke volume, cardiac output and systolic time intervals. Additionally, the methods currently used for the continuous non-invasive assessment of blood pressure were outlined along with other relevant parameters of vascular function. The main methods used to assess the function of the baroreceptor reflex mechanisms were also tackled in the present chapter. Finally, we outlined the main contributions presented in the literature, focusing on the early and real time prediction of neurally mediated syncope.

The non-invasive evaluation of the cardiovascular function is a vast research area whose complexity greatly depends on the adopted modalities and assessment contexts. The most commonly used modality for the assessment of relevant cardiovascular parameters is the arterial blood pressure waveform, measured by volume-clamp based systems. Despite the technological advances observed in the later years, these proprietary systems still carry disadvantages that limit their usage in p-health and ambulatory environments. Their expensiveness, hard management, the need for recurrent calibrations and the induced discomfort are some of the commonly observed drawbacks. Therefore, the assessment of cardiovascular parameters from widely available bio-signals such as the electrocardiogram and photoplethysmogram can bring a huge step forward in the non-invasive assessment of the cardiovascular function. The systolic time intervals, such as the left ventricular ejection time, were suggested as valuable indices for the non-invasive assessment of the myocardial contractility. Additionally, pulse transit time and pulse arrival time have also been indicated as valuable surrogates for blood pressure. However, these parameters are still covered in deep controversy, and their applicability largely depends on the used methods and modalities, as well as the physiological conditions. Furthermore, the methods employing these parameters still require frequent calibrations for the long-term assessment of non-invasive BP. Other parameters that have been recently unveiled, based on the decomposition of the ABP/PPG showed to be highly associated with systolic and diastolic blood pressure, which can represent a great improvement in the assessment of non-invasive and cuff-less blood pressure monitoring. Additionally, due to the intrinsic nature of the mechanisms that trigger neurally mediated syncope, the application of these cardiovascular parameters to real time prediction systems might contribute to the improvement of the results already proposed in literature.

REFERENCES

[1] G. Korosoglou, S. Giusca, G. Gitsioudis, C. Erbel, and H. A. Katus, "Cardiac magnetic resonance and computed tomography angiography for clinical imaging of stable coronary artery disease. Diagnostic classification and risk stratification," *Frontiers in Physiology,* vol. 5, 2014.

[2] A. Hutton, "Cardiac Output Monitors," ed.

[3] P. E. Marik, "Noninvasive cardiac output monitors: a state-of the-art review," *Journal of cardiothoracic and vascular anesthesia,* vol. 27, pp. 121-134, 2013.

[4] K. H. Wesseling, B. De Werr, J. A. P. Weber, and N. T. Smith, "A simple device for the continuous measurement of cardiac output," *Advances in Cardiovascular Physics,* vol. 5, pp. 16-52, 1983.

[5] G. Antonutto, M. Girardis, D. Tuniz, E. Petri, and C. Capelli, "Assessment of cardiac output from noninvasive determination of arterial pressure profile in subjects at rest," *European Journal of Applied Physiology and Occupational Physiology,* vol. 69, pp. 183-188, 1994.

[6] S. M. Romano and M. Pistolesi, "Assessment of cardiac output from systemic arterial pressure in humans," *Crit Care Med,* vol. 30, pp. 1834-41, Aug 2002.

[7] K. H. Wesseling, J. R. Jansen, J. J. Settels, and J. J. Schreuder, "Computation of aortic flow from pressure in humans using a nonlinear, three-element model," *J Appl Physiol,* vol. 74, pp. 2566-2573, May 1 1993.

[8] A. Rhodes and R. Sunderland, "Arterial Pulse Power Analysis: The LiDCO^{TM} plus System," in *Functional Hemodynamic Monitoring*. vol. 42, M. Pinsky and D. Payen, Eds., ed: Springer Berlin Heidelberg, 2005, pp. 183-192.

[9] Z. Lu and R. Mukkamala, "Continuous cardiac output monitoring in humans by invasive and noninvasive peripheral blood pressure waveform analysis," *J Appl Physiol,* vol. 101, pp. 598-608, August 1 2006.

[10] L. W. J. Bogert, K. H. Wesseling, O. Schraa, E. J. Van Lieshout, B. A. J. M. De Mol, J. Van Goudoever*, et al.*, "Pulse contour cardiac output derived from non-invasive arterial pressure in cardiovascular disease," *Anaesthesia,* vol. 65, pp. 1119-1125, 2010.

[11] S. M. Finkelstein and J. N. Cohn, "Method and apparatus for measuring Cardiac Output," United States of America Patent, 1993.

[12] R. Couceiro, P. Carvalho, R. Paiva, J. Henriques, M. Antunes, I. Quintal*, et al.*, "Beat-to-beat cardiac output inference using heart sounds," in *33th Annual Int. Conf. of the IEEE Eng. in Medicine and Biology Society, EMBC 2011*, 2011, pp. 5657-5661.

[13] L. Wang, E. Pickwell-Macpherson, Y. P. Liang, and Y. T. Zhang, "Noninvasive cardiac output estimation using a novel photoplethysmogram index," in *31st Annual International Conference of the IEEE Engineering in Medicine and Biology Society, 2009. EMBS 2009*, 2009, pp. 1746-1749.

[14] L. Wang, C. C. Poon, and Y. T. Zhang, "The non-invasive and continuous estimation of cardiac output using a photoplethysmogram and electrocardiogram during incremental exercise," *Physiol Meas,* vol. 31, pp. 715-26, May 2010.

[15] Q. Y. Lee, S. J. Redmond, G. S. Chan, P. M. Middleton, E. Steel, P. Malouf*, et al.*, "Estimation of cardiac output and systemic vascular resistance using a multivariate regression model with features selected from the finger photoplethysmogram and routine cardiovascular measurements," *Biomedical engineering online,* vol. 12, p. 19, 2013.

[16] W. G. Kubicek, J. N. Karnegis, R. P. Patterson, D. A. Witsoe, and R. H. Mattson, "Development and evaluation of an impedance cardiac output system," *Aerosp Med,* vol. 37, pp. 1208-12, Dec 1966.

[17] B. B. Sramek, D. M. Rose, A. Miyamoto, and P. Baturic, "Stroke volume equation with a linear base impedance model and its accuracy, as compared to thermodilution and magnetic flowmeter techniques in humans and animals," 1983.

[18] D. P. Bernstein, "A new stroke volume equation for thoracic electrical bioimpedance: theory and rationale," vol. 14, pp. 904-909, 1986.

[19] D. Bernstein and H. Lemmens, "Stroke volume equation for impedance cardiography," *Medical and Biological Engineering and Computing,* vol. 43, pp. 443-450, 2005.

[20] X. Qiu-Jin, W. Zhen, K. Ming-Xing, W. Ping, L. Pei, and J. Jian-Feng, "Thoracic impedance change equation deduced on the basis of parallel impedance model and Ohm's law," *Medical Physics,* vol. 39, pp. 1042-1045, 2012.

[21] F. Van de Werf, J. Piessens, H. Kesteloot, and H. De Geest, "A comparison of systolic time intervals derived from the central aortic pressure and from the external carotid pulse tracing," *Circulation,* vol. 51, pp. 310-316, February 1 1975.

[22] A. M. Weissler, W. S. Harris, and C. D. Schoenfield, "Systolic Time Intervals in Heart Failure in Man," *Circulation,* vol. 37, pp. 149-159, February 1 1968.

[23] C. Tei, L. H. Ling, D. O. Hodge, K. R. Bailey, J. K. Oh, R. J. Rodeheffer*, et al.*, "New index of combined systolic and diastolic myocardial performance: a simple and reproducible measure of cardiac function: a study in normals and dilated cardiomyopathy," *J Cardiol,* vol. 26, pp. 357-66, Dec 1995.

[24] J. Ärnlöv, E. Ingelsson, U. Risérus, B. Andrén, and L. Lind, "Myocardial performance index, a Doppler-derived index of global left ventricular function, predicts congestive heart failure in elderly men," *European Heart Journal,* vol. 25, pp. 2220-2225, December 1 2004.

[25] T. C. Gillebert, N. V. de Veire, M. L. De Buyzere, and J. D. Sutter, "Time intervals and global cardiac function. Use and limitations," *European Heart Journal,* vol. 25, pp. 2185-2186, December 1 2004.

[26] M. Dandel, D. Kemper, H. Lehmkuhl, and R. Hetzer, "Evaluation of left ventricular filling pressures by the Tei index," *J Am Soc Echocardiogr,* vol. 17, p. 709; author reply 710, Jun 2004.

[27] W. G. Kubicek, R. P. Patterson, and D. A. Witsoe, "Impedance cardiography as a noninvasive method of monitoring cardiac function and other parameters of the cardiovascular system," *Annals of the New York Academy of Sciences,* vol. 170, pp. 724-732, 1970.

[28] P. Carvalho, R. P. Paiva, J. Henriques, M. Antunes, I. Quintal, and J. Muehlsteff, "Impedance Cardiogram: evaluation of existing and new characteristic point definitions," presented at the 32nd Annual International Conference of the IEEE Engineering in Medicine and Biology Society, Buenos Aires, Argentina, 2010.

[29] S. Reddy, L. Shyu, B. Hurwitz, J. H. Nagel, and N. Schneiderman, "Improved Reliability of impedance cardiography by new signal processing techniques.," presented at the Engineering in Medicine and Biology Conference, 1988.

[30] T. Ono, M. Miyamura, Y. Yasuda, T. Ito, T. Saito, T. Ishiguro*, et al.*, "Beat-to-Beat Evaluation of Systolic Time Intervals during Bicycle Exercise Using Impedance Cardiography," *The Tohoku Journal of Experimental Medicine,* vol. 203, pp. 17-29, 2004.

[31] D. S. Miles and R. W. Gotshall, "Impedance cardiography: noninvasive assessment of human central hemodynamics at rest and during exercise," *Exerc Sport Sci Rev,* vol. 17, pp. 231-63, 1989.

[32] A. Sherwood, M. T. Allen, J. Fahrenberg, R. M. Kelsey, W. R. Lovallo, and L. J. van Doornen, "Methodological Guidelines for Impedance Cardiography," *Psychophysiology,* vol. 27, pp. 1-23, 1990.

[33] Z. Shuguang, F. Yanhong, Z. Hailong, and T. Min, "Detection of Impedance Cardioaraphy's Characteristic Points Based on Wavelet Transform," in *27th Annual International Conference of the Engineering in Medicine and Biology Society, 2005. IEEE-EMBS 2005*, 2005, pp. 2730-2732.

[34] L.-Y. Shyu, Y.-S. Lin, C.-P. Liu, and W.-C. Hu, "The detection of impedance cardiogram characteristic points using wavelet transform," *Computers in biology and medicine,* vol. 34, pp. 165-175, 2004.

[35] P. Carvalho, R. P. Paiva, J. Henriques, M. Antunes, I. Quintal, and J. Muehlsteff, "Robust Characteristic Points for ICG-Definition and Comparative Analysis," in *BIOSIGNALS*, 2011, pp. 161-168.

[36] G. H. Chan, P. M. Middleton, B. G. Celler, L. Wang, and N. H. Lovell, "Automatic detection of left ventricular ejection time from a finger photoplethysmographic pulse oximetry waveform: comparison with Doppler aortic measurement," *Physiological Measurement,* vol. 28, p. 439, 2007.

[37] R. Couceiro, P. Carvalho, R. Paiva, J. Henriques, M. Antunes, I. Quintal*, et al.*, "Multi-Gaussian fitting for the assessment of left ventricular ejection time from the Photoplethysmogram," in *34th Annual Int. Conf. of the IEEE Eng. in Medicine and Biology Society, EMBC 2012*, San Diego, 2012.

[38] P. Carvalho, R. P. Paiva, R. Couceiro, J. Henriques, I. Quintal, J. Muehlsteff*, et al.*, "Assessing systolic time-intervals from heart sound: a feasibility study," in *31st Annual International Conference of the IEEE Engineering in Medicine and Biology Society, 2009. EMBS 2009*, 2009, pp. 3124-8.

[39] R. P. Paiva, P. Carvalho, X. Aubert, J. Muehlsteff, J. Henriques, and M. Antunes, "Assessing PEP and LVET from heart sounds: algorithms and evaluation," in *31st Annual International Conference of the IEEE Engineering in Medicine and Biology Society, 2009. EMBS 2009*, 2009, pp. 3129-33.

[40] R. Paiva, P. Carvalho, R. Couceiro, J. Henriques, M. Antunes, I. Quintal*, et al.*, "Beat-to-beat systolic time-interval measurement from heart sounds and ECG," *Physiological measurement,* vol. 33, p. 177, 2012.

[41] D. Kumar, P. Carvalho, M. Antunes, J. Henriques, L. Eugenio, R. Schmidt*, et al.*, "Detection of S1 and S2 heart sounds by high frequency signatures," in *28th Annual International Conference of the IEEE Engineering in Medicine and Biology Society, 2006. EMBS '06*, 2006, pp. 1410-6.

[42] T. L. Davis and R. G. Mark, "Teaching physiology through simulation of hemodynamics," presented at the Computers in Cardiology, Chicago, IL , USA, 1990.

[43] R. Beyar and Y. Goldstein, "Model studies of the effects of the thoracic pressure on the circulation," *Annals of Biomedical Engineering,* vol. 15, pp. 373-383, 1987.

[44] M. Ursino and E. Magosso, "Role of short-term cardiovascular regulation in heart period variability: a modeling study," *Am J Physiol Heart Circ Physiol,* vol. 284, pp. H1479-1493, April 1 2003.

[45] T. Heldt, E. B. Shim, R. D. Kamm, and R. G. Mark, "Computational modeling of cardiovascular response to orthostatic stress," *J Appl Physiol,* vol. 92, pp. 1239-1254, March 1 2002.

[46] M. S. Olufsen, J. T. Ottesen, H. T. Tran, L. M. Ellwein, L. A. Lipsitz, and V. Novak, "Blood pressure and blood flow variation during postural change from sitting to standing: model development and validation," *J Appl Physiol,* vol. 99, pp. 1523-1537, October 1 2005.

[47] M. S. Olufsen, C. S. Peskin, W. Y. Kim, E. M. Pedersen, A. Nadim, and J. Larsen, "Numerical Simulation and Experimental Validation of Blood Flow in Arteries with Structured-Tree Outflow Conditions," *Annals of Biomedical Engineering,* vol. 28, pp. 1281-1299, 2000.

[48] J. M. Guccione, K. D. Costa, and A. D. McCulloch, "Finite element stress analysis of left ventricular mechanics in the beating dog heart," *Journal of Biomechanics,* vol. 28, pp. 1167-1177, 1995.

[49] M. Danielsen and J. T. Ottesen, "Describing the Pumping Heart as a Pressure Source," *Journal of Theoretical Biology,* vol. 212, pp. 71-81, 2001.

[50] J. T. Ottesen and M. Danielsen, "Modeling ventricular contraction with heart rate changes," *Journal of Theoretical Biology,* vol. 222, pp. 337-346, 2003.

[51] H. Hardy, R. Collins, and R. Calvert, "A digital computer model of the human circulatory system," *Medical and Biological Engineering and Computing,* vol. 20, pp. 550-564, 1982.

[52] J. Penaz, "Photoelectric measurement of blood pressure, volume and flow in the finger," Dresden, Germany, 1973, pp. 104-104.

[53] B. P. M. Imholz, W. Wieling, G. A. van Montfrans, and K. H. Wesseling, "Fifteen years experience with finger arterial pressure monitoring," *Cardiovascular Research,* vol. 38, pp. 605-616, June 1, 1998 1998.

[54] J. Allen, "Photoplethysmography and its application in clinical physiological measurement," *Physiological Measurement,* vol. 28, p. R1, 2007.

[55] E. Chung, G. Chen, B. Alexander, and M. Cannesson, "Non-invasive continuous blood pressure monitoring: a review of current applications," *Frontiers of Medicine,* vol. 7, pp. 91-101, 2013/03/01 2013.

[56] E. R. Nye, "The effect of blood pressure alteration on the pulse wave velocity," *Br Heart J,* vol. 26, pp. 261-5, Mar 1964.

[57] L. A. Geddes, M. H. Voelz, C. F. Babbs, J. D. Bourland, and W. A. Tacker, "Pulse Transit Time as an Indicator of Arterial Blood Pressure," *Psychophysiology,* vol. 18, pp. 71-74, 1981.

[58] J. D. Lane, L. Greenstadt, D. Shapiro, and E. Rubinstein, "Pulse Transit Time and Blood Pressure: An Intensive Analysis," *Psychophysiology,* vol. 20, pp. 45-49, 1983.

[59] C. Wippermann, D. Schranz, and R. Huth, "Evaluation of the pulse wave arrival time as a marker for blood pressure changes in critically ill infants and children," *Journal of Clinical Monitoring and Computing,* vol. 11, pp. 324-328, 1995.

[60] W. Chen, T. Kobayashi, S. Ichikawa, Y. Takeuchi, and T. Togawa, "Continuous estimation of systolic blood pressure using the pulse arrival time and intermittent calibration," *Medical and Biological Engineering and Computing,* vol. 38, pp. 569-574, 2000.

[61] K. Meigas, R. Kattai, and J. Lass, "Continuous blood pressure monitoring using pulse wave delay," presented at the Proceedings of the 23rd Annual International Conference of the IEEE Engineering in Medicine and Biology Society, Istanbul, Turkey, 2001

[62] P. Fung, G. Dumont, C. Ries, C. Mott, and M. Ansermino, "Continuous noninvasive blood pressure measurement by pulse transit time," in *26th Annual International Conference of the IEEE Engineering in Medicine and Biology Society, 2004. IEMBS '04*, 2004, pp. 738-41.

[63] J. Lass, K. Meigas, D. Karai, R. Kattai, J. Kaik, and M. Rossmann, "Continuous blood pressure monitoring during exercise using pulse wave transit time measurement," in *26th Annual International Conference of the IEEE Engineering in Medicine and Biology Society, 2004. IEMBS '04*, 2004, pp. 2239-42.

[64] J. Naschitz, S. Bezobchuk, R. Mussafia-Priselac, S. Sundick, D. Dreyfuss, I. Khorshidi*, et al.*, "Pulse Transit Time by R-Wave-Gated Infrared Photoplethysmography: Review of the Literature and Personal Experience," *Journal of Clinical Monitoring and Computing,* vol. 18, pp. 333-342, 2004.

[65] Y. M. Wong and Y. T. Zhang, "Effects of exercise on the pulse transit time," in *The 2nd IEEE-EMBS International Summer School and Symposium on Medical Devices and Biosensors (ISSS-MDBS)*, Hong Kong, 2004.

[66] J. Y. Foo, S. J. Wilson, G. R. Williams, M. A. Harris, and D. M. Cooper, "Pulse transit time changes observed with different limb positions," *Physiol Meas,* vol. 26, pp. 1093-102, Dec 2005.

[67] C. C. Poon and Y. T. Zhang, "Cuff-less and noninvasive measurements of arterial blood pressure by pulse transit time," in *27th Annual International Conference of the Engineering in Medicine and Biology Society, 2005. IEEE-EMBS 2005*, 2005, pp. 5877-80.

[68] Y. Wong and Y. Zhang, "The Effects of Exercises on the Relationship between Pulse Transit Time and Arterial Blood Pressure," in *27th Annual International Conference of the Engineering in Medicine and Biology Society, 2005. IEEE-EMBS 2005*, 2005, pp. 5576-8.

[69] C. P. Chua and C. Heneghan, "Continuous blood pressure monitoring using ECG and finger photoplethysmogram," in *28th Annual International Conference of the IEEE Engineering in Medicine and Biology Society, 2006. EMBS '06*, 2006, pp. 5117-20.

[70] Y. Liu and Y. T. Zhang, "Pulse Transit Time and Arterial Blood Pressure at Different Vertical Wrist Positions," in *The international Special Topic Conference on Information Technology in Biomedicine*, Ioannina - Epirus, Greece, 2006.

[71] X. F. Teng and Y. T. Zhang, "An evaluation of a PTT-based method for noninvasive and cuffless estimation of arterial blood pressure," in *28th Annual International Conference of the IEEE Engineering in Medicine and Biology Society, 2006. EMBS '06*, 2006, pp. 6049-52.

[72] S. Deb, C. Nanda, D. Goswami, J. Mukhopadhyay, and S. Chakrabarti, "Cuff-Less Estimation of Blood Pressure Using Pulse Transit Time and Pre-ejection Period," presented at the Proceedings of the 2007 International Conference on Convergence Information Technology, 2007.

[73] J. Muehlsteff, X. A. Aubert, and G. Morren, "Continuous Cuff-less Blood Pressure Monitoring based on the Pulse Arrival Time Approach: The Impact of Posture," in *30th Annual International Conference of the IEEE Engineering in Medicine and Biology Society, 2008. EMBS 2008*, Vancouver, Canada, 2008.

[74] M. Y. M. Wong and Y. T. Zhang, "The Effects of Pre-Ejection Period on the Blood Pressure Estimation Using Pulse Transit Time " in *5th International Workshop on Wearable and Implantable Body Sensor Networks*, Hong Kong, HKSAR, China, 2008.

[75] M. Y. Wong, C. C. Poon, and Y. T. Zhang, "An evaluation of the cuffless blood pressure estimation based on pulse transit time technique: a half year study on normotensive subjects," *Cardiovasc Eng,* vol. 9, pp. 32-8, Mar 2009.

[76] J. Proença, J. Muehlsteff, X. Aubert, and P. Carvalho, "Is Pulse Transit Time a good indicator of Blood Pressure changes during short physical exercise in a young population? ," in *32ndAnnual International Conference of the IEEE Engineering in Medicine and Biology Society, 2010. EMBS 2010*, 2010.

[77] I. Jeong, S. Jun, D. Um, J. Oh, and H. Yoon, "Non-invasive estimation of systolic blood pressure and diastolic blood pressure using photoplethysmograph components," *Yonsei Med J,* vol. 51, pp. 345-53, May 2010.

[78] P. Shaltis, A. Reisner, and H. Asada, "Calibration of the photoplethysmogram to arterial blood pressure: capabilities and limitations for continuous pressure monitoring," in *27th Annual International Conference of the Engineering in Medicine and Biology Society, 2005. IEEE-EMBS 2005*, 2005, pp. 3970-3.

[79] M. Sugawara, K. Niki, H. Furuhata, S. Ohnishi, and S. Suzuki, "Relationship between the pressure and diameter of the carotid artery in humans," *Heart and Vessels,* vol. 15, pp. 49-51, 2000.

[80] X.-Y. Zhang and Y.-T. Zhang, "A novel method for the noninvasive and continuous monitoring of arterial blood pressure on an electronic stethoscope," in *3rd European Medical and Biological Engineering Conference* Prague, Czech Republic 2005.

[81] X. Y. Zhang and Y. T. Zhang, "A model-based study of relationship between timing of second heart sound and systolic blood pressure," in *28th Annual International Conference of the IEEE Engineering in Medicine and Biology Society, 2006. EMBS '06*, 2006, pp. 1387-90.

[82] M. Y. M. Wong, X. Y. Zhang, and Y. T. Zhang, "The Cuffless Arterial Blood Pressure Estimation based on the Timing- Characteristics of Second Heart Sound " in *28th Annual International Conference of the IEEE Engineering in Medicine and Biology Society, 2006. EMBS '06*, New York City, USA, 2006.

[83] M. Baruch, D. Warburton, S. Bredin, A. Cote, D. Gerdt, and C. Adkins, "Pulse Decomposition Analysis of the digital arterial pulse during hemorrhage simulation," *Nonlinear Biomedical Physics,* vol. 5, pp. 1-15, 2011.

[84] M. Baruch, K. Kalantari, D. Gerdt, and C. Adkins, "Validation of the pulse decomposition analysis algorithm using central arterial blood pressure," *BioMedical Engineering OnLine,* vol. 13, p. 96, 2014.

[85] R. A. Payne, C. N. Symeonides, D. J. Webb, and S. R. J. Maxwell, "Pulse transit time measured from the ECG: an unreliable marker of beat-to-beat blood pressure," *J Appl Physiol,* vol. 100, pp. 136-141, January 1 2006.

[86] M. Vettorello, S. Santambrogio, A. Calini, L. Tizzoni, G. Marconi, M. Lippi*, et al.*, "Predicting haemorrhage in pre-hospital traumatic patients: evaluation of the novel heart-to-arm time index," *Acta Anaesthesiologica Scandinavica,* vol. 57, pp. 929-935, 2013.

[87] N. Gaddum, J. Alastruey, P. Beerbaum, P. Chowienczyk, and T. Schaeffter, "A technical assessment of pulse wave velocity algorithms applied to non-invasive arterial waveforms," *Annals of biomedical engineering,* vol. 41, pp. 2617-2629, 2013.

[88] O. Vardoulis, T. G. Papaioannou, and N. Stergiopulos, "Validation of a novel and existing algorithms for the estimation of pulse transit time: advancing the accuracy in pulse wave velocity measurement," *American Journal of Physiology-Heart and Circulatory Physiology,* vol. 304, pp. H1558-H1567, 2013.

[89] G. Zhang, M. Gao, and R. Mukkamala, "Robust, beat-to-beat estimation of the true pulse transit time from central and peripheral blood pressure or flow waveforms using an arterial tube-load model," in *33th Annual Int. Conf. of the IEEE Eng. in Medicine and Biology Society, EMBC 2011*, 2011, pp. 4291-4294.

[90] M. Wong, C. Poon, and Y.-T. Zhang, "An Evaluation of the Cuffless Blood Pressure Estimation Based on Pulse Transit Time Technique: a Half Year Study on Normotensive Subjects," *Cardiovascular Engineering,* vol. 9, pp. 32-38, 2009.

[91] Y. Choi, Q. Zhang, and S. Ko, "Noninvasive cuffless blood pressure estimation using pulse transit time and Hilbert–Huang transform," *Computers & Electrical Engineering,* vol. 39, pp. 103-111, 2013.

[92] S. Veerabhadrappa, A. L. Vyas, and S. Anand, "Estimation of pulse transit time using time delay estimation techniques," in *Biomedical Engineering and Informatics (BMEI), 2011 4th International Conference on*, 2011, pp. 739-743.

[93] C. Douniama, C. U. Sauter, and R. Couronne, "Acquisition of Parameters for Noninvasive Continuous Blood Pressure Estimation – Review of the Literature and Clinical Trial," presented at the World Congress on Medical Physics and Biomedical Engineering, Munich, germany, 2009.

[94] D. J. Hughes, C. F. Babbs, L. A. Geddes, and J. D. Bourland, "Measurements of Young's modulus of elasticity of the canine aorta with ultrasound," *Ultrasonic Imaging,* vol. 1, pp. 356-367, 1979.

[95] J. C. Bramwell and A. V. Hill, "The Velocity of the Pulse Wave in Man," *Proceedings of the Royal Society of London. Series B, Containing Papers of a Biological Character,* vol. 93, pp. 298-306, April 1 1922.

[96] P. Shaltis, A. Reisner, and H. Asada, "A hydrostatic pressure approach to cuffless blood pressure monitoring," in *26th Annual International Conference of the IEEE Engineering in Medicine and Biology Society, 2004. IEMBS '04*, 2004, pp. 2173-6.

[97] H. T. Hosaka, JP), H. T. Sakata, JP), Y. T. Sugo, JP), T. T. Sohma, JP), and H. T. Kasuya, JP), "Pulse-wave propagation time basis blood pressure monitor," United States Patent, 1997.

[98] Y. S. Yan and Y. T. Zhang, "Modeling the Effects of Radial Blood Pressure Change on Pulse Transit Time," in *International Special Topic Conference on Information Technology in Biomedicine*, Ioannina - Epirus, Greece, 2006.

[99] H. Gesche, D. Grosskurth, G. Küchler, and A. Patzak, "Continuous blood pressure measurement by using the pulse transit time: comparison to a cuff-based method," *European journal of applied physiology,* vol. 112, pp. 309-315, 2012.

[100] S. Liu, H. T. Ma, L. Chen, X. Wang, and D. Yuan, "A compensation method for blood pressure estimation by pulse transit time," in *TENCON 2013-2013 IEEE Region 10 Conference (31194)*, 2013, pp. 1-3.

[101] W. Gu, C. C. Poon, M. Sy, H. Leung, Y. Liang, and Y.-T. Zhang, "A h-shirt-based body sensor network for cuffless calibration and estimation of arterial blood pressure," in *Wearable and Implantable Body Sensor Networks, 2009. BSN 2009. Sixth International Workshop on*, 2009, pp. 151-155.

[102] B. McCarthy, C. Vaughan, B. O'Flynn, A. Mathewson, and C. Ó. Mathúna, "An examination of calibration intervals required for accurately tracking blood pressure using pulse transit time algorithms," *Journal of human hypertension,* 2013.

[103] C. C. Poon and Y.-T. Zhang, "Using the changes in hydrostatic pressure and pulse transit time to measure arterial blood pressure," in *29th Annual International Conference of the IEEE Engineering in Medicine and Biology Society, 2007. EMBS 2007*, 2007, pp. 2336-2337.

[104] D. B. McCombie, P. A. Shaltis, A. T. Reisner, and H. H. Asada, "Adaptive hydrostatic blood pressure calibration: Development of a wearable, autonomous pulse wave velocity blood pressure monitor," in *29th Annual International Conference of the IEEE Engineering in Medicine and Biology Society, 2007. EMBS 2007*, 2007, pp. 370-373.

[105] J. Muehlsteff, X. L. Aubert, and M. Schuett, "Cuffless estimation of systolic blood pressure for short effort bicycle tests: the prominent role of the pre-ejection period," in *28th Annual International Conference of the IEEE Engineering in Medicine and Biology Society, 2006. EMBS '06*, 2006, pp. 5088-92.

[106] K. W. Chan, K. Hung, and Y. T. Zhang, "Noninvasive and cuffless measurements of blood pressure for telemedicine," in *23rd Annual International Conference of the IEEE Engineering in Medicine and Biology Society, 2001. IEMBS '01*, Istanbul, Turkey, 2001.

[107] C. C. Y. Poon, Y.-T. Zhang, and Y. Liu, "Modeling of Pulse Transit Time under the Effects of Hydrostatic Pressure for Cuffless Blood Pressure Measurements," in *3rd IEEE/EMBS International Summer School on Medical Devices and Biosensors*, Cambridge, MA, 2006, pp. 65 - 68.

[108] M. Y. M. Wong, E. Pickwell-MacPherson, Y. T. Zhang, and J. C. Cheng, "The effects of pre-ejection period on post-exercise systolic blood pressure estimation using the pulse arrival time technique," *European journal of applied physiology,* vol. 111, pp. 135-144, 2011.

[109] J. Muehlsteff, M. Kelm, and C. Meyer, "Experiences with Pulse Arrival Time as Surrogate for Systolic Blood Pressure," *Biomedical Engineering/Biomedizinische Technik,* 2013.

[110] G. Zhang, M. Gao, D. Xu, N. B. Olivier, and R. Mukkamala, "Pulse arrival time is not an adequate surrogate for pulse transit time as a marker of blood pressure," *Journal of Applied Physiology,* vol. 111, pp. 1681-1686, 2011.

[111] M. Nitzan, A. Babchenko, and B. Khanokh, "Verylow frequency variability in arterial blood pressure and blood volume pulse," *Medical and Biological Engineering and Computing,* vol. 37, pp. 54-58, 1999.

[112] B. A. Kingwell and C. D. Gatzka, "Arterial stiffness and prediction of cardiovascular risk," *Journal of Hypertension,* vol. 20, pp. 2337-2340, 2002.

[113] J. A. Chirinos, "Arterial stiffness: basic concepts and measurement techniques," *Journal of cardiovascular translational research,* vol. 5, pp. 243-255, 2012.

[114] I. S. Mackenzie, I. B. Wilkinson, and J. R. Cockcroft, "Assessment of arterial stiffness in clinical practice," *QJM,* vol. 95, pp. 67-74, February 1 2002.

[115] P. J. Chowienczyk, R. P. Kelly, H. MacCallum, S. C. Millasseau, T. L. G. Andersson, R. G. Gosling*, et al.*, "Photoplethysmographic assessment of pulse wave reflection: Blunted response to endothelium-dependent beta2-adrenergic vasodilation in type II diabetes mellitus," *J Am Coll Cardiol,* vol. 34, pp. 2007-2014, December 1 1999.

[116] J. Padilla, E. Berjano, J. Saiz, L. Facila, P. Diaz, and S. Merce, "Assessment of relationships between blood pressure, pulse wave velocity and digital volume pulse," in *Computers in Cardiology, 2006*, 2006, pp. 893-896.

[117] S. C. Millasseau, J. M. Ritter, K. Takazawa, and P. J. Chowienczyk, "Contour analysis of the photoplethysmographic pulse measured at the finger," *J Hypertens,* vol. 24, pp. 1449-56, Aug 2006.

[118] S. S. DeLoach and R. R. Townsend, "Vascular Stiffness: Its Measurement and Significance for Epidemiologic and Outcome Studies," *Clinical Journal of the American Society of Nephrology,* vol. 3, pp. 184-192, 2008.

[119] S. C. Millasseau, R. P. Kelly, J. M. Ritter, and P. J. Chowienczyk, "Determination of age-related increases in large artery stiffness by digital pulse contour analysis," *Clin Sci (Lond),* vol. 103, pp. 371-7, Oct 2002.

[120] A. Laucevicius, L. Ryliskyte, Z. Petruioniene, MildaKovaite, and N. Misonis, "First Experience With Salbutamol - Induced Changes In The Photoplethysmographic Digital Volume Pulse," presented at the Seminars in Cardiology, 2002.

[121] K. Takazawa, N. Tanaka, M. Fujita, O. Matsuoka, T. Saiki, M. Aikawa*, et al.*, "Assessment of Vasoactive Agents and Vascular Aging by the Second Derivative of Photoplethysmogram Waveform," *Hypertension,* vol. 32, pp. 365-370, August 1, 1998 1998.

[122] U. Rubins, "Finger and ear photoplethysmogram waveform analysis by fitting with Gaussians," *Medical and Biological Engineering and Computing,* vol. 46, pp. 1271-1276, 2008.

[123] M. F. O'Rourke, A. Pauca, and X. J. Jiang, "Pulse wave analysis," *British Journal of Clinical Pharmacology,* vol. 51, pp. 507-522, 2001.

[124] A. Awad, A. Haddadin, H. Tantawy, T. Badr, R. Stout, D. Silverman*, et al.*, "The relationship between the photoplethysmographic waveform and systemic vascular resistance," *Journal of Clinical Monitoring and Computing,* vol. 21, pp. 365-372, 2007.

[125] L.-x. Hou, M. Wei, X. Wang, X.-z. Chen, Y. Feng, and K. Jiang, "A novel non-iterative shape method for estimating the decay time constant of the finger photoplethysmographic pulse," *Journal of Zhejiang University SCIENCE A,* vol. 12, pp. 438-445.

[126] I. Jeong and J. Finkelstein, "Applicability of the second derivative photoplethysmogram for non-invasive blood pressure estimation during exercise," in *Health Care Exchanges (PAHCE), 2013 Pan American*, 2013, pp. 1-5.

[127] H. S. Smyth, P. Sleight, and G. W. Pickering, "Reflex Regulation of Arterial Pressure during Sleep in Man: A Quantitative Method of Assessing Baroreflex Sensitivity," *Circ Res,* vol. 24, pp. 109-121, January 1 1969.

[128] M. Di Rienzo, G. Bertinieri, G. Mancia, and A. Pedotti, "A new method for evaluating the baroreflex role by a joint pattern analysis of pulse interval and systolic blood pressure series.," *Medical and Biological Engineering and Computing,* vol. 23, pp. 313-314, 1985.

[129] M. Di Rienzo, P. Castiglioni, G. Mancia, A. Pedotti, and G. Parati, "Advancements in estimating baroreflex function: Exploring different aspects of autonomic control of the heart through the sequence technique.," *Engineering in Medicine and Biology Magazine, IEEE,* vol. 20, pp. 25-32, 2001.

[130] H. Malberg, N. Wessel, A. Hasart, K.-J. Osterziel, and A. Voss, "Advanced analysis of spontaneous baroreflex sensitivity, blood pressure and heart rate variability in patients with dilated cardiomyopathy," *Clin. Sci.,* vol. 102, pp. 465-473, April 2002.

[131] B. E. Westerhof, J. Gisolf, W. J. Stok, K. H. Wesseling, and J. M. Karemaker, "Time-domain cross-correlation baroreflex sensitivity: performance on the EUROBAVAR data set," *J Hypertens,* vol. 22, pp. 1371-80, Jul 2004.

[132] S. Gouveia, A. P. Rocha, P. Laguna, and P. Lago, "Time domain baroreflex sensitivity assessment by joint analysis of spontaneous SBP and RR series," *Biomedical Signal Processing and Control,* vol. 4, pp. 254-261, 2009.

[133] H. Robbe, L. Mulder, H. Ruddel, W. Langewitz, J. Veldman, and G. Mulder, "Assessment of baroreceptor reflex sensitivity by means of spectral analysis," *Hypertension,* vol. 10, pp. 538-543, November 1 1987.

[134] M. Pagani, V. Somers, R. Furlan, S. Dell'Orto, J. Conway, G. Baselli*, et al.*, "Changes in autonomic regulation induced by physical training in mild hypertension," *Hypertension,* vol. 12, pp. 600-610, December 1, 1988 1988.

[135] M. Hájek, J. Potucek, and V. Brodan, "Mathematical model of heart rate regulation during exercise," *Automatica,* vol. 16, pp. 191-195, 1980.

[136] S. R. Seydnejad and R. I. Kitney, "Time-varying threshold integral pulse frequency modulation," *IEEE Trans Biomed Eng,* vol. 48, pp. 949-62, Sep 2001.

[137] G. Nollo, A. Porta, L. Faes, M. Del Greco, M. Disertori, and F. Ravelli, "Causal linear parametric model for baroreflex gain assessment in patients with recent myocardial infarction," *Am J Physiol Heart Circ Physiol,* vol. 280, pp. H1830-1839, April 1 2001.

[138] A. Porta, G. Baselli, O. Rimoldi, A. Malliani, and M. Pagani, "Assessing baroreflex gain from spontaneous variability in conscious dogs: role of causality and respiration," *Am J Physiol Heart Circ Physiol,* vol. 279, pp. H2558-2567, November 1 2000.

[139] G. Baselli, S. Cerutti, S. Civardi, A. Malliani, and M. Pagani, "Cardiovascular variability signals: towards the identification of a closed-loop model of the neural control mechanisms," *IEEE Trans Biomed Eng,* vol. 35, pp. 1033-46, Dec 1988.

[140] T. J. Mullen, M. L. Appel, R. Mukkamala, J. M. Mathias, and R. J. Cohen, "System identification of closed-loop cardiovascular control: effects of posture and autonomic blockade," *Am J Physiol Heart Circ Physiol,* vol. 272, pp. H448-461, January 1 1997.

[141] R. Barbieri, A. M. Bianchi, J. K. Triedman, L. T. Mainardi, S. Cerutti, and J. P. Saul, "Model dependency of multivariate autoregressive spectral analysis," *IEEE Eng Med Biol Mag,* vol. 16, pp. 74-85, Sep-Oct 1997.

[142] R. Barbieri, G. Parati, and J. P. Saul, "Closed- versus open-loop assessment of heart rate baroreflex," *IEEE Eng Med Biol Mag,* vol. 20, pp. 33-42, Mar-Apr 2001.

[143] M. Ursino, "A mathematical model of the carotid baroregulation in pulsating conditions," *IEEE Trans Biomed Eng,* vol. 46, pp. 382-92, Apr 1999.

[144] M. S. Olufsen, H. T. Tran, J. T. Ottesen, Research Experiences for Undergraduates Program, L. A. Lipsitz, and V. Novak, "Modeling baroreflex regulation of heart rate during orthostatic stress," *Am J Physiol Regul Integr Comp Physiol,* vol. 291, pp. R1355-1368, November 1 2006.

[145] J. T. Ottesen, "Modelling the dynamical baroreflex-feedback control," *Mathematical and Computer Modelling,* vol. 31, pp. 167-173, 2000.

[146] Y. Chee, J. Lee, H. Park, and I. Kim, "Baroreflex Sensitivity with Pulse Arrival Time," presented at the 6th International Special Topic Conference on Information Technology Applications in Biomedicine, Tokyo, Japan, 2007.

[147] Q. Liu, C. Poon, and Y.-T. Zhang, "A novel method to estimate baroreflex sensitivity based on pulse transit time," in *IEEE-EMBS International Conference on Biomedical and Health Informatics (BHI), 2012*, 2012, pp. 432-434.

[148] A. Bauer, A. Morley-Davies, P. Barthel, A. Müller, K. Ulm, M. Malik*, et al.*, "Bivariate phase-rectified signal averaging for assessment of spontaneous baroreflex sensitivity: pilot study of the technology," *Journal of Electrocardiology,* vol. 43, pp. 649-653, 11// 2010.

[149] U. R. Acharya, K. P. Joseph, N. Kannathal, C. M. Lim, and J. S. Suri, "Heart rate variability: a review," *Medical and Biological Engineering and Computing,* vol. 44, pp. 1031-1051, 2006.

[150] N. Lippman, K. M. Stein, and B. B. Lerman, "Failure to decrease parasympathetic tone during upright tilt predicts a positive tilt-table test," *The American journal of cardiology,* vol. 75, pp. 591-595, 1995.

[151] Z. Mallat, E. Vicaut, A. Sangaré, J. Verschueren, G. Fontaine, and R. Frank, "Prediction of head-up tilt test result by analysis of early heart rate variations," *Circulation,* vol. 96, pp. 581-584, 1997.

[152] G. Kochiadakis, P. Lees, E. Kanoupakis, N. Igoumenidis, E. Manios, and P. Vardas, "Spectral analysis of heart rate variability in the analysis of autonomic nervous system activity during tilt-table testing in patients with unexplained syncope," in *Computers in Cardiology 1997*, 1997, pp. 367-369.

[153] M. Sumiyoshi, Y. Nakata, Y. Mineda, T. Tokano, M. Yasuda, Y. Nakazato*, et al.*, "Does an early increase in heart rate during tilting predict the results of passive tilt testing?," *Pacing and Clinical Electrophysiology,* vol. 23, pp. 2046-2051, 2000.

[154] J. E. Naschitz, I. Rosner, M. Rozenbaum, M. Fields, H. Isseroff, J. P. Babich*, et al.*, "Patterns of cardiovascular reactivity in disease diagnosis," *QJM,* vol. 97, pp. 141-151, March 1, 2004 2004.

[155] C. Kouakam, D. Lacroix, N. Zghal, R. Logier, D. Klug, P. Le Franc*, et al.*, "Inadequate sympathovagal balance in response to orthostatism in patients with unexplained syncope and a positive head up tilt test," *Heart,* vol. 82, pp. 312-318, 1999.

[156] G. A. Ruiz, C. MADOERY, F. ARNALDO, C. Menendez, and M. C. Tentori, "Frequency-Domain Analysis of Heart Rate Variability During Positive and Negative Head-Up Tilt Test: Importance of Age," *Pacing and Clinical Electrophysiology,* vol. 23, pp. 325-332, 2000.

[157] C. A. Morillo, G. J. Klein, D. L. Jones, and R. Yee, "Time and frequency domain analyses of heart rate variability during orthostatic stress in patients with neurally mediated syncope," *The American journal of cardiology,* vol. 74, pp. 1258-1262, 1994.

[158] A. Madrid, C. Moro, E. Marin-Huerta, L. Novo, J. Mestre, J. Lage*, et al.*, "[Usefulness of the RR variability in the diagnosis of neurogenic syncope]," *Revista espanola de cardiologia,* vol. 47, pp. 536-543, 1994.

[159] K. Efremov, D. Brisinda, A. Venuti, E. Iantorno, C. Cataldi, F. Fioravanti*, et al.*, "Heart rate variability analysis during head-up tilt test predicts nitroglycerine-induced syncope," *Open Heart,* vol. 1, pp. 1-8, June 1, 2014 2014.

[160] E. Bellard, J.-O. Fortrat, B. Vielle, J.-M. Dupuis, J. Victor, and G. Lefthériotis, "Early predictive indexes of head-up tilt table testing outcomes utilizing heart rate and arterial pressure changes," *The American journal of cardiology,* vol. 88, pp. 903-906, 2001.

[161] M. Pitzalis, F. Massari, P. Guida, M. Iacoviello, F. Mastropasqua, B. Rizzon*, et al.*, "Shortened Head-Up Tilting Test Guided by Systolic Pressure Reductions in Neurocardiogenic Syncope," *Circulation,* vol. 105, pp. 146-148, January 15, 2002 2002.

[162] L. Mangin, A. Kobeissi, D. Lelouche, Y. D'Hérouville, P. Mansier, B. Swynghedauw*, et al.*, "Simultaneous Analysis of Heart Rate Variability and Myocardial Contractility During Head-Up Tilt in Patients with Vasovagal Syncope," *Journal of cardiovascular electrophysiology,* vol. 12, pp. 639-644, 2001.

[163] D. Schang, M. Feuilloy, G. Plantier, J.-O. Fortrat, and P. Nicolas, "Early prediction of unexplained syncope by support vector machines," *Physiological Measurement,* vol. 28, p. 185, 2007.

[164] N. Virag, R. Sutton, R. Vetter, T. Markowitz, and M. Erickson, "Prediction of vasovagal syncope from heart rate and blood pressure trend and variability: Experience in 1,155 patients," *Heart Rhythm,* vol. 4, pp. 1375-1382, 2007.

[165] R. Mereu, G. De Barbieri, T. Perrone, A. Mugellini, A. Di Toro, and L. Bernardi, "Heart rate/blood pressure ratio as predictor of neuromediated syncope," *International Journal of Cardiology,* vol. 167, pp. 1170-1175, 8/20/ 2013.

[166] C. Eickholt, T. Drexel, J. Muehlsteff, A. Ritz, M. Siekiera, K. Kirmanoglou*, et al.*, "Neurally mediated syncope prediction based on heart rate and pulse arrival time," *European Heart Journal,* vol. 34, p. 161, August 1, 2013 2013.

[167] C. Meyer, G. Morren, J. Muehlsteff, C. Heiss, T. Lauer, P. Schauerte*, et al.*, "Predicting neurally mediated syncope based on pulse arrival time: algorithm development and preliminary results," *Journal of cardiovascular electrophysiology,* vol. 22, pp. 1042-1048, 2011.

[168] J. Muehlsteff, T. Correia, R. Couceiro, P. Carvalho, A. Ritz, C. Eickholt*, et al.*, "Detection of hemodynamic adaptations during impending syncope: Implementation of a robust algorithm based on pulse arrival time measurements only," *35th Annual Int. Conf. of the IEEE Eng. in Medicine and Biology Society, EMBC 2013,* vol. 2013, pp. 2291-4, 2013.

[169] J. Muehlsteff, A. Ritz, T. Drexel, C. Eickholt, P. Carvalho, R. Couceiro*, et al.*, "Pulse Arrival Time as surrogate for systolic blood pressure changes during impending neurally mediated syncope," in *34th Annual Int. Conf. of the IEEE Eng. in Medicine and Biology Society, EMBC 2012*, 2012, pp. 4283-4286.

[170] R. Couceiro, P. Carvalho, R. P. Paiva, J. Muehlsteff, J. Henriques, V. Schulze*, et al.*, "Characterization of surrogate parameters for blood pressure regulation in neurally-mediated syncope," in *35th Annual Int. Conf. of the IEEE Eng. in Medicine and Biology Society, EMBC 2013*, 2013, pp. 5381-5385.

[171] F. J. Gimeno-Blanes, J. L. Rojo-Álvarez, A. J. Caamaño, J. Flores-Yepes, and A. García-Alberola, "On the feasibility of tilt test outcome early prediction using ECG and pressure parameters," *EURASIP J. Adv. Sig. Proc.,* vol. 2011, p. 33, 2011.

[172] R. Couceiro, P. Carvalho, R. P. Paiva, J. Muehlsteff, J. Henriques, C. Eickholt, *et al.*, "A novel multi-parametric algorithm for faint prediction integrating indices of cardiac inotropy and vascular tone," in *36th Annual Int. Conf. of the IEEE Eng. in Medicine and Biology Society, EMBC 2014*, 2014.

[173] R. Couceiro, P. Carvalho, R. P. Paiva, J. Muehlsteff, J. Henriques, C. Eickholt, *et al.*, "Neurally Mediated Syncope Prediction Based on Changes of Cardiovascular Performance Surrogates: Algorithms comparison," presented at the 7th International Conference on BioMedical Engineering and Informatics (BMEI), Dalian, China, 2014.

Chapter 4.
DETECTION OF MOTION ARTIFACT PATTERNS IN PHOTOPLETHYSMOGRAPHIC SIGNALS BASED ON TIME AND PERIOD DOMAIN ANALYSIS

This chapter consists of the following article:

Detection of motion artifact patterns in photoplethysmographic signals based on time and period domain analysis

R. Couceiro, P. Carvalho, R. P. Paiva and J. Henriques and J. Muehlsteff

Physiological Measurement, accepted for publication, 2014.

DOI:10.1088/0967-3334/35/12/2369

Journal impact factor in 2013: 1.617

IOP Publishing | Institute of Physics and Engineering in Medicine Physiological Measurement

Physiol. Meas. **00** (2014) 1

Detection of motion artifact patterns in photoplethysmographic signals based on time and period domain analysis

R Couceiro[1] , P Carvalho[1], R P Paiva[1], J Henriques[1] and J Muehlsteff[2]

[1] Center for Informatics and Systems of the University of Coimbra, Polo II, 3030–290 Coimbra, Portugal
[2] Philips Research Laboratories Europe, HTC, 5656AE Eindhoven, The Netherlands

E-mail: rcouceir@dei.uc.pt

Received 26 May 2014
Accepted for publication 5 August 2014
Published

Abstract

The presence of motion artifacts in photoplethysmographic (PPG) signals is one of the major obstacles in the extraction of reliable cardiovascular parameters in continuous monitoring applications. In the current paper we present an algorithm for motion artifact detection based on the analysis of the variations in the time and the period domain characteristics of the PPG signal. The extracted features are ranked using a Normalized Mutual Information Feature Selection algorithm and the best features are used in a Support Vector Machine classification model to distinguish between clean and corrupted sections of the PPG signal. The proposed method has been tested in healthy and cardiovascular diseased volunteers, considering eleven different motion artifact sources. The results achieved by the current algorithm (sensitivity—SE: 84.3%, specificity—SP: 91.5% and accuracy—ACC: 88.5%) show that the current methodology is able to identify both corrupted and clean PPG sections with high accuracy in both healthy (ACC: 87.5%) and cardiovascular diseases (ACC: 89.5%) context.

Keywords: photoplethysmography, motion artifacts; period domain analysis, time domain analysis, feature extraction, feature selection, support vector machine

1. Introduction

Photoplethysmography (PPG) is a non-invasive, low cost tool to continuously monitor blood volume changes in tissue as a function of time. One of the major advances of the PPG-based technology in clinical environments is the pulse oximeter, which has been accepted by the International Standards Organization (ISO) and the European Committee for Standardization as the standard non-invasive measure of oxygen saturation level since 1987 (Shang *et al* 2007). Motivated by unmet needs in low cost, unobtrusive and portable techniques in personal-Health (p-Health), the PPG technique has been object of extensive research in the later decades. Due to technological advances in the field of opto-electronics, clinical instrumentation and digital signal processing, the PPG technique achieved a broader spectrum of potential applications, ranging from the field of clinical physiological monitoring to the vascular assessment, and autonomic function evaluation (Allen 2007). Moreover, this technique has been widely applied in many clinical areas such as anesthesia, surgical recovery and critical care (Allen 2007).

However, the quality of the PPG signals can be easily influenced by properties of the light-emitting diode and photodetector, as well as the pressure exerted on the PPG probe, which may affect the morphology of the PPG waveform (Reisner *et al* 2008). Moreover, the ambient light at the photodetector, poor blood perfusion of the peripheral tissues and motion artifacts (Sukor *et al* 2011) are also common sources of errors. In uncontrolled environments such as home care settings, these potential error sources are more frequent and can become a serious obstacle to the reliable use of PPG derived parameters, especially in continuous monitoring applications. Therefore, it is important to provide signal quality or trust metric that provides the subsequent analysis algorithms with a level of trust in the derived parameters, which reduces the false alarms, allows identifying inaccurate readings and finally increases patient safety.

Although the recent technological advances allowed the minimization of some of these limitations, motion artifact detection and suppression is still a major challenge (Allen 2007, Sukor *et al* 2011) in particular without using additional sensors. Indeed, the field of motion artifact and noise suppression has been subject of intensive research in the last decade. Various approaches have been investigated, where the clean PPG signal is recovered or reconstructed from the corrupted one. A common approach in this field is to use adaptive filtering techniques (Graybeal and Petterson 2004, Lee *et al* 2004, Foo and Wilson 2006, Kunchon *et al* 2009) to reduce noise and motion artifacts. In these approaches, an adaptive filter (e.g. Least Mean Square adaptive filter) is applied as a joint process estimator to cancel noise and motion artifacts and consequently retrieve a clean PPG signal. However, some studies indicate that these techniques introduce phase shifts in the PPG signal, which may compromise its subsequent interpretation (Foo 2006). Additionally, similar findings have been shown for wavelet based transformation techniques.

Another common approach is to use accelerometers as a reference noise signal to cancel out motion artifacts in PPG signals (Gibbs and Asada 2005, Han *et al* 2007, Kim *et al* 2007, Wood and Asada 2007). However, these methods present major drawbacks. Here, an accelerometer needs to be coupled to the PPG sensor in order to retrieve the noise reference and synchronisation of both signals, which makes this approach hardly suitable for current equipment in clinical settings. Additionally, there is not a direct correlation between movements (acceleration data) and motion artifacts in PPG (Yousefi *et al* 2012).

Other authors opted to use time-frequency analysis (Lee and Zhang 2003, Yan *et al* 2005, Reddy *et al* 2008, Raghuram *et al* 2012) and source separation techniques (Kim and Yoo 2006) to recover the clean PPG signal. Reddy *et al* (Reddy and Kumar 2007) proposed a motion artifact reduction method based on Singular Value Decomposition. Later in (Reddy *et al* 2008), the same author applied a beat-by-beat Fourier series analysis to reconstruct a

clean PPG signal. Yan *et al* (2005) applied Smoothed Pseudo Wigner-Ville Distribution for motion artifacts reduction. Raghuram *et al* (2012) proposed the use of an Empirical Mode Decomposition technique combined with the Hilbert-Huang transform to reconstruct clean PPG section from the corrupted PPG signal. Kim *et al* (Kim and Yoo 2006) proposed the combination of a block interleaving and low pass filtering technique approach with an Independent Component Analysis technique to separate the PPG from motion artifacts. These techniques assume that underlying a corrupted PPG signal there is a clean/uncorrupted reference capable of being retrieved, which is not often possible. Additionally, the distortion induced by the reconstruction of a clean PPG signal can significantly bias the extracted measurements (e.g. Left Ventricular Ejection Time—LVET) and induce subsequent wrong diagnosis.

In many applications (hospital as well as home monitoring), an alternative to noise reduction is the robust detection of PPG signal sections corrupted by noise and motion artifacts and exclude them from the subsequent analysis. Techniques such as morphological analysis (Sukor *et al* 2011) and higher-order statistical analysis (Krishnan *et al* 2008) have been proposed in this research field. Sukor *et al* (2011) proposed an algorithm based on the analysis of several morphological characteristics of the PPG pulses to distinguish bad quality pulses from good ones. The author reports that the proposed methodology is able to identify motion artifacts with an accuracy of 83%. Krishnan *et al* (2008) used a sensor fusion approach combining high order statistical features from the time and frequency domain to discriminate corrupted PPG sections. The proposed methodology was able to detect motion artifacts with a probability of 91% and a false alarm probability of 0.06%.

Despite the good results presented in (Sukor *et al* 2011), we believe that motion artifact detection performance can still be increased. It is our goal not only to evaluate the changes in the morphological characteristics of the PPG signal, but also to utilize the idea that clean and corrupted PPG sections have different period characteristics. It is still unknown which time/period characteristics best distinguish clean and corrupted PPG sections and it is expected that these characteristics depend on the target population in clinical practice. Therefore, a study regarding the evaluation of the best features in the time and period domain for artifact discrimination and their application in both healthy and cardiovascular diseased (CVD) populations has yet to be developed.

In this paper, we present a motion artifact detection methodology, which is based only on the analysis of the time and period domain characteristics of the PPG signal from 8 healthy volunteers and 7 CVD patients. In the time domain analysis we evaluate the changes in the main morphological characteristics of the PPG beats. In the period domain analysis, the period characteristics of the PPG signal are assessed and compared using a sliding window approach. Several features are extracted, and the Normalized Mutual Information Feature Selection (NMIFS) algorithm (Estevez *et al* 2009) is used to select the most relevant and least redundant ones. The most discriminative features are used as inputs to a Support Vector Machine (SVM) classification model.

The paper is organized as follows: the proposed methodology is introduced in section 2. The results and respective discussion are presented in section 3. Finally, the conclusions are summarized in section 4.

2. Methods

The proposed methodology for the detection of motion artifacts consists of the following stages (see figure 1): (a) Pre-processing and baseline removal; (b) Segmentation; (c) Feature extraction; (d) Feature selection and (e) Classification.

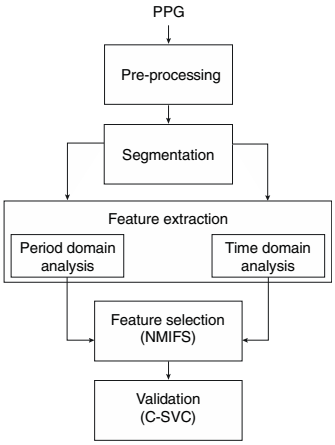

Figure 1. Scheme of the proposed motion artifacts detection methodology.

2.1. Pre-processing

The goal of the pre-processing stage is to remove the frequency components that do not represent the fundamental features of the PPG signal. Based on the algorithm proposed in (Chan *et al* 2007), the high frequency components which are not physiologically related to the PPG waveform were removed using a low-pass Butterworth filter with a 18 Hz cut-off frequency and a 2 s window moving average filter is applied to derive an approximation of the PPG signal baseline, which is subtracted from the original PPG signal.

2.2. Segmentation

The morphology of the PPG pulse is a result of a complex interaction between the left ventricle and the systemic circulation. It is composed of an early main pulse created by the ventricular contraction and various additional pulses caused by pressure pulse reflections in the central arterial tree to the peripheral vasculature. As the main pulse (P1—illustrated in figure 2) arrives at the first reflection site, which is, the junction between the thoracic and abdominal aorta, there is a significant decrease in the artery diameter along with the change in its elasticity causing the main pulse to be reflected. The main pulse continues to travel downwards and reaches the second reflection site, which arises from the juncture between abdominal aorta and common iliac arteries (Baruch *et al* 2011). These reflection sites are commonly known as the renal and iliac reflections sites and give rise to the second (commonly known as second systolic peak) and third reflection waves (P2 and P3, respectively—illustrated in figure 2). Additionally, there are also other minor reflections and re-reflections in the systemic structure that give rise to smaller reflection waves.

Commonly, in healthy individuals, these reflection waves occur during early diastole and a dicrotic notch can be observed between the first and second PPG peaks. Contrarily, in elder individuals and/or individuals with cardiovascular diseases, the vascular properties may lead to a significant increase of the pulse wave velocity up to a factor of three (e.g. due to arterial stiffening), leading to the occurrence of the reflected waves during late systole and preventing the distinction between direct and reflected waves.

The main objective of the segmentation step is to detect the characteristic points correspondent to the onset and offset of the PPG pulses and allowing the posterior extraction of

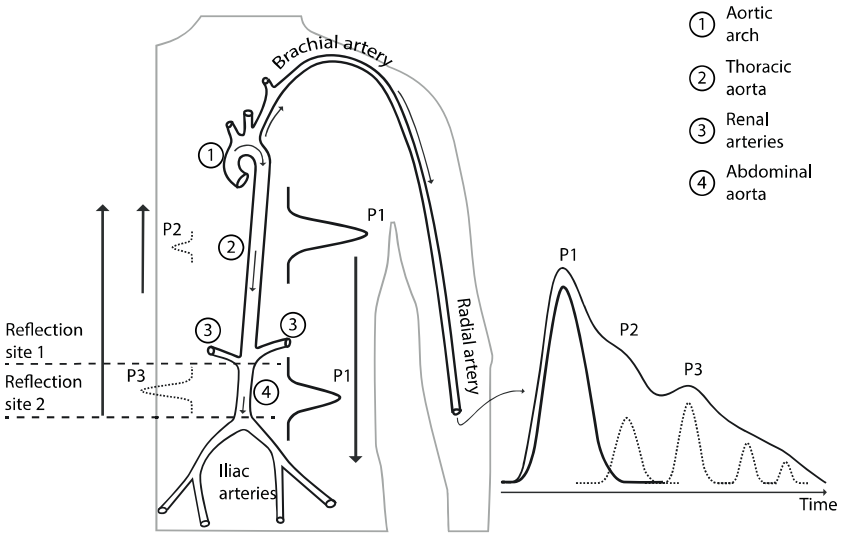

Figure 2. Morphology and origin of the PPG pulse. On the left, a PPG pulse and correspondent forward and reflected waves are presented. On the right, a sketch of the arterial system from the aorta/arm to the iliac arteries (Baruch *et al* 2011).

their morphological characteristics. We determine the characteristic points by analyzing the derivatives of the PPG signal. The physiological basis of this approach was firstly reported (Cook 2001, Wisely and Cook 2001) where L.B. Cook observed the similarity between the arterial flow waveform and the first derivative of the PPG waveform. Therefore, the point in time where the PPG first derivative is the steepest corresponds to the onset of the pulse, which can be determined as a maximum in the PPG third derivative.

To detect these characteristic points, the PPG signal is firstly differentiated using a five-point digital differentiator (Abramowitz and Stegun 2012) (equations (1)–(3)), resulting in first to third order derivatives (d1_ppg, d2_ppg and d3_ppg).

$$d1ppg = f'(t) = \frac{f(t-2h) - 8f(t-h) + 8f(t+h) - f(t+2h)}{12h^2} \quad (1)$$

$$d2\ ppg = f''(t) = \frac{-f(t-2h) + 16f(t-h) - 30f(t) + 16f(t+h) - f(t+2h)}{12h^2} \quad (2)$$

$$d3\ ppg = f'''(t) = \frac{-f(t-2h) + 2f(t-h) - 2f(t+h) + f(t+2h)}{2h^3} \quad (3)$$

where f is the PPG time series, t is the time index and h is the sampling time.

The 1st derivative local maxima (d1_ppg_lmax) with absolute amplitude greater than a threshold ThR are detected, where ThR is selected based on an adaptive thresholding of the d1_ppg data cumulative histogram (using a 10 s window) (Sun *et al* 2005). ThR was defined as the greater value bellow which 90% of the observations are found. Consequently, the d3_ppg local minima (d3_ppg_lmin) corresponding to the d1_ppg local maxima are also identified in order to detect the onset/offset of each PPG beat (see figure 3). These are identified as the peak with greater amplitude (d3_ppg_lmax) prior to the previously identified most relevant valley, the d3_ppg_lmax (Chan *et al* 2007).

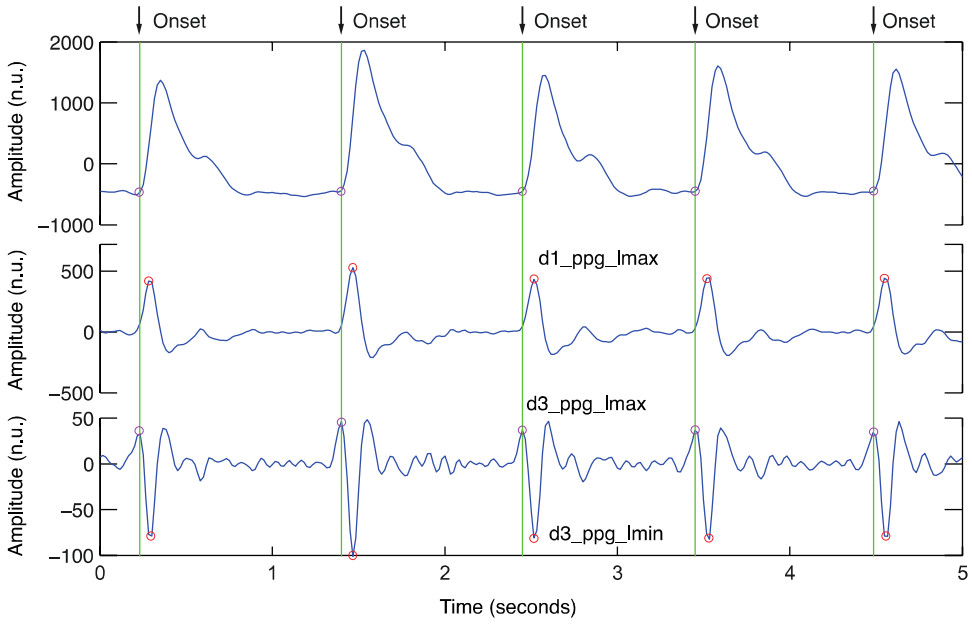

Figure 3. Plot of PPG signal derivatives (order 1–3) and representation of the detected characteristic point for the detection of the onset of each individual PPG pulse.

2.3. Feature extraction

In order to detect PPG motion artifacts it is essential to extract a set of features capable of discriminating clean from corrupted PPG sections. These features were extracted resorting on the analysis of the time and period domain analysis of the PPG. In the time domain analysis, the main goal is to capture the changes in the morphological features of the PPG pulses. In the period domain, the characteristics of principal components of the period spectrum and their relationships are evaluated.

2.3.1. Time domain analysis. In clean PPG signals, the changes on the PPG pulse morphology are mainly caused by cardiovascular changes. Contrarily, PPG signals corrupted by motion artifacts present abnormal, erratic and 'random' characteristics which can be detected from the analysis of each pulse. To assess these changes, the morphology of the PPG pulses and their relationships with the neighboring pulses are analyzed, leading to the definition of the following characteristics: (1) pulse amplitude; (2) pulse length; (3) peak distance; (4) trough depth difference; (5) peak height difference; (6) pulse skewness; and (7) pulse kurtosis. Along with the morphological characteristics proposed by Sukor *et al* (2011) (pulse amplitude, pulse length and trough depth difference), four other characteristics are introduced in the present time domain analysis of PPG signal.

As illustrated in figure 4 the pulse amplitude is defined as the difference between the pulse peak height and its preceding trough depth (pulse onset), the pulse length is the time interval between the onset of two consecutive pulses and the peak distance is the time interval between maxima of two consecutive pulses. The difference between the peak height and peak depth of two consecutive pulses was also considered. As can be observed, these characteristics change drastically in the presence of motion artifacts, showing an erratic pattern. Contrarily, clean PPG

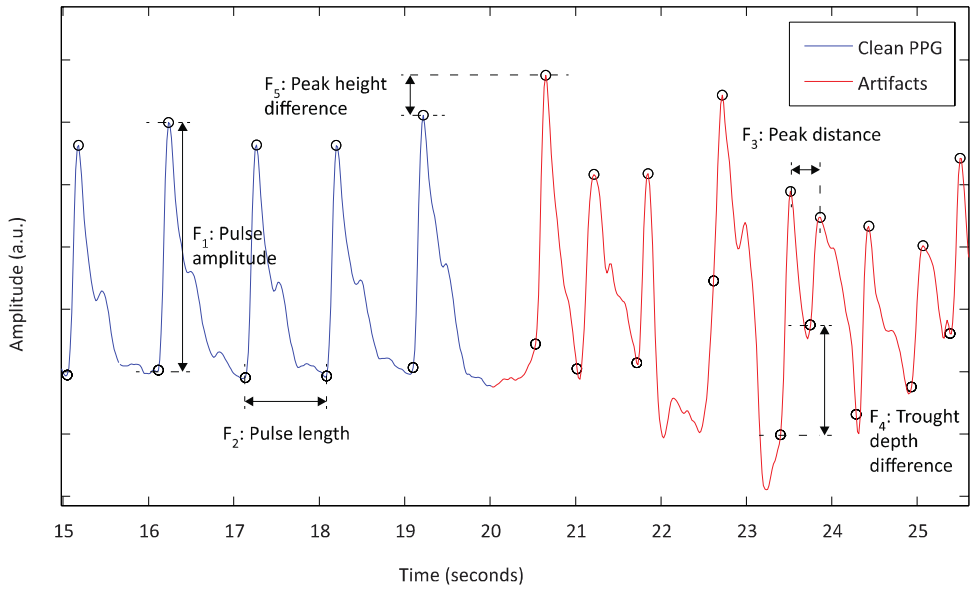

Figure 4. Plot of a PPG signal with clean and motion artifact corrupted sections. Representation of the PPG pulses morphological characteristics extracted during time domain analysis step.

sections exhibit slow variations in the aforementioned characteristics, which are a result of a variety of cardiovascular and respiratory factors (e.g. vasomotion/compliance effects, changes in venous pooling related to heart rate/cardiac output variations, blood pressure changes and respiratory modulations) (Addison *et al* 2012). For example, the PPG pulse amplitude, which is related to changes in the intrathoracic pressure during respiration (Addison *et al* 2012), exhibits slow variations in the clean PPG sections when compared to the corrupted PPG sections, where it exhibits strong and inconsistent changes between pulses.

Since the shape of the PPG pulse is highly affected by motion artifacts it is expected to see random changes in the corrupted PPG pulses symmetry and 'peakedness', which were assessed using skewness (equation (4)) and kurtosis (equation (5)).

$$Ch_6 = \frac{E\left(f_P\left(x\right) - \overline{f_P\left(x\right)}\right)^3}{\sigma^3} \tag{4}$$

$$Ch_7 = \frac{E\left(f_P\left(x\right) - \overline{f_P\left(x\right)}\right)^4}{\sigma^4} \tag{5}$$

where $f_P\left(x\right)$ is the PPG pulse, $\overline{f_P\left(x\right)}$ is the mean of $f_P\left(x\right)$, σ is the standard deviation of $f_P\left(x\right)$, and $E(t)$ represents the expected value of the quantity t.

From the analysis of various types of PPG pulses, one observed that when motion artifacts are present, the aforementioned characteristics vary considerably. Contrarily, in clean PPG signals the PPG pulses are similar and therefore there is almost no variation in its characteristics, since PPG height and regularity are related to blood volume and heart rate, respectively. These physiological properties are not expected to change abruptly between consecutive pulses. Hence, rather then evaluating the values of the proposed characteristics, as suggested

in (Sukor *et al* 2011), we aim to to capture their variations. The changes in the pulse characteristics were evaluated using equation (6), resulting in the features F_1 to F_7.

$$F_i = \Delta\,(Ch_i) = |Ch_i\,(j) - Ch_i\,(j-1)\,| \tag{6}$$

where, Ch_i is the ith characteristic and j is the pulse (section) index.

2.3.2. Period domain analysis. To assess the period characteristics of the PPG signal, the Discrete-time Short Time Fourier Transform (STFT) was applied in the period domain. Let the $[x_n, ..., x_{n+N-1}]$ be the sequence defining the section of the PPG signal under analysis. For a sampling frequency SF, the frequency 'bin' k of the N-point STFT corresponds to the frequency $f_k = k\,.\,SF\,/\,N$ Hz, that is, $s_k = 1\,/\,f_k = N\,/(k\,.\,SF)$ s= $N\,/\,k$ samples. The STFT in the period domain, i.e. PD-STFT, defined as

$$X\,(n,\ s)\ =\ \sum_{m=0}^{L-1} x_{n+m} w_m \mathrm{e}^{-j2\pi n/s} \tag{7}$$

is the expression for the DFT of the windowed sequence $x_{n+m}w_m$ of the kth period bin. $s = 1, 2, \ldots, N-1$ samples is the range of possible periods in the aforementioned sequence.

To choose the size of the sequences (L) and the forward step (Δn), that is related to the section overlapping ($L - \Delta n$) one must take into account: (i) the stationary of the analyzed signal section; (ii) the tradeoff between the PD-STFT period and temporal resolution; (iii) the temporal resolution needed for the subsequent analysis.

Considering the aforementioned issues, the PD-STFT was applied using a rectangular-shaped sliding window with approximately 3 times the fundamental period of the PPG signal (i.e. periods from 0 to approximately one and a half beat). The fundamental period was defined as the maximum of the period domain spectrum calculated from the first 5 s of each PPG signal. The overlap between consecutive windows was set to be approximately 85%. Thus, we assume the stationarity of the signal in the analyzed section and guarantee an appropriate trade-off frequency resolution of the computed PD-STFT. Furthermore, by choosing 85% window overlap size we ensure that the analysis output has the reasonable temporal resolution (i.e. half of a beat) necessary for further analysis and motion artifact detection. Moreover, a good tradeoff between the computational complexity of the algorithm and the acquired temporal resolution is also achieved. The fundamental period was extracted and updated based on the period analysis of small sections (5 s) of the PPG signal.

From the obtained period domain spectra characteristic features are extracted. This procedure resorts on the principle that, similarly to the morphology of the PPG signal, the PD-STFT also exhibits a regular shape representing the main features of the signal. From an analysis of the PD-STFT of various PPG classes (Dawber *et al* 1973) one observed that the PD-STFT of a clean PPG signal consists of three major spikes (P_1, P_2 and P_3) positioned at different locations and with different widths, heights and areas (figure 5). The most relevant spike corresponds to the fundamental period of the PPG signal, i.e., the length of the cardiac cycle (beat). The remaining spikes are thought to be associated with the location and amplitude of the waves reflected from the periphery towards the aorta. Based on these assumptions, the power spectra of several uncorrupted and motion corrupted PPG sections were analyzed.

We observed that the power spectra of PPG sections corrupted with motion artifacts presented several random components that do not represent the fundamental characteristics of the underlying uncorrupted signal, resulting in random and significant changes in the period

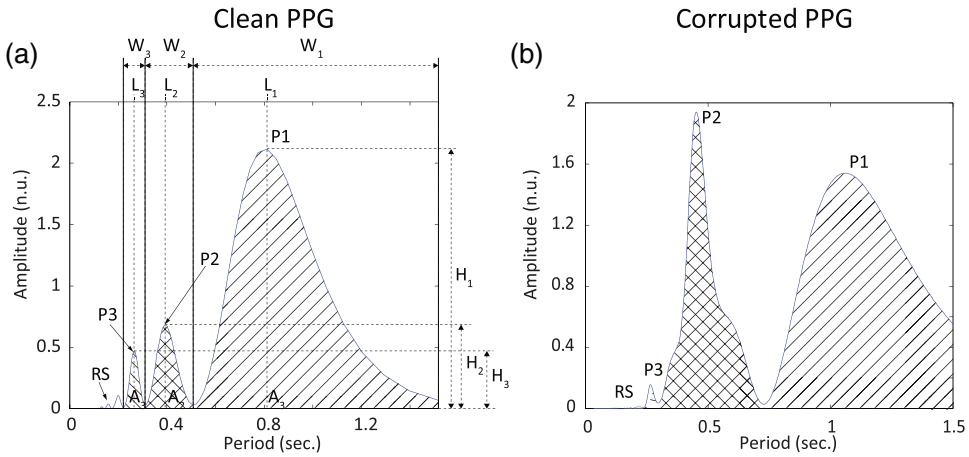

Figure 5. Representation of the PPG signal period domain spectrum, its major components (P_1, P_2 and P_3) and the remaining spectrum (RS) for: (*a*) clean and (*b*) corrupted PPG sections.

domain characteristics. In figure 6 it is possible to observe significant changes in the power, location and length of the main components of the spectra between 20 s and 42 s, where the PPG signal is corrupted by motion artifacts.

To capture these variations, the PD-STFT of each PPG section was analyzed and the following characteristics were defined (see figure 5): (1) height (H); (2) location (L); (3) width (W); and (4) area (A). These characteristics are defined as $pCh_{1,\ldots,4} : \{H, L, W, A\}$, while the three most relevant spikes and the remaining spectrum are defined as P_1, P_2, P_3 and RS. The variations of $P_{1,2,3}$ characteristics were evaluated by equation (8), resulting in the features $F_{8,\ldots,19}$, which are presented in figure 7.

$$F_{8,\ldots,19} = \Delta\left(pCh_i^{P_k}\right) = \left|pCh_i^{P_k}(j) - pCh_i^{P_k}(j-1)\right|, \text{ for } i = 1, \ldots, 4 \text{ and } k = 1, 2, 3 \tag{8}$$

where, pCh_i is the ith period characteristic, k is the spike index and j is the pulse (section) index.

Additionally, the relationship between characteristics of the two most relevant spikes (P_1 and P_2) was also assessed and was defined as follows:

$$F_{20,\ldots,23} = \Delta\left(pCh_i^{P_1} - pCh_i^{P_2}\right), \; i = 1, \ldots, 4 \tag{9}$$

An example of the rate of changes of the relationship between the two most relevant peaks characteristics, i.e. $F_{20,\ldots,23}$ are presented in figure 8.

The area $\left(pCh_4\right)$ of the *RS* and its relationship with the sum of the three most relevant peaks area was also considered:

$$F_{25} = \Delta\left(\frac{pCh_4^{RS}}{pCh_4^{P_1} + pCh_4^{P_2} + pCh_4^{P_3}}\right) \tag{10}$$

An example of the rate of change of the aforementioned characteristics, i.e., $F_{24} = \Delta\left(Ch_4^{RS}\right)$ and F_{25}, is presented in figure 9.

Assuming that the main period characteristics of the PPG signal are represented by the most relevant components in the distribution and that the remaining components are the result

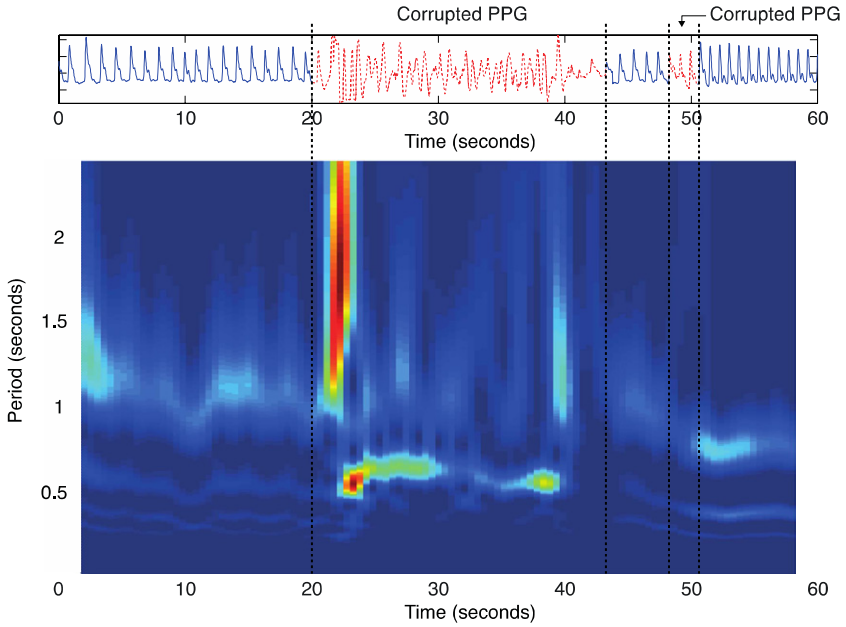

Figure 6. Period domain spectrogram of the PPG signal showing clear changes in the spectra fundamental characteristics in the presence of motion artifacts.

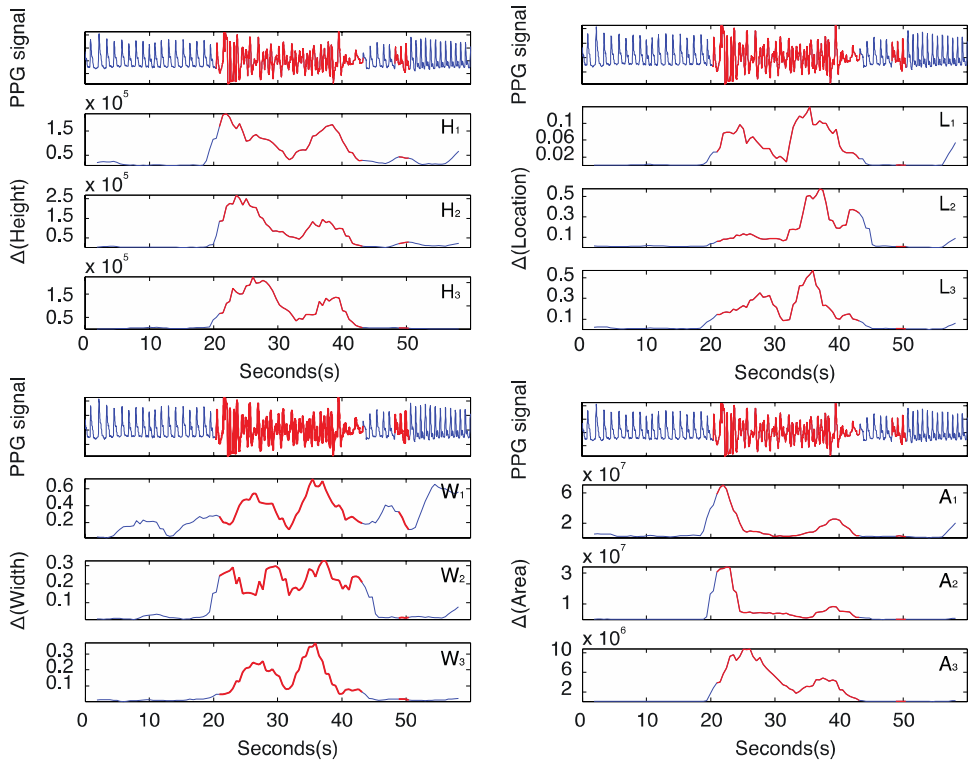

Figure 7. Rate of changes of the three most relevant spikes characteristics (Height, Location, Width and Area).

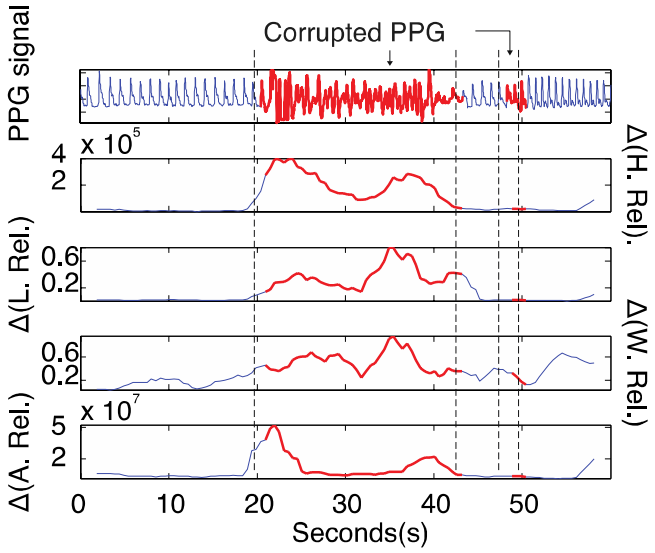

Figure 8. Rate of change of the relationship between the characteristics of the two most relevant peaks (P_1 and P_2).

of noise and motion artifacts, a model of the original distribution was created based on the 3 most relevant spikes, using Gaussian functions. The parameters of each Gaussian are determined based on the height $\left(Ch_1^{Pi}\right)$ and location $\left(Ch_2^{Pi}\right)$ of the detected spikes $(i = 1, \ldots, 3)$. The spectrum model (X^m) was defined as:

$$\mathrm{X}^m(s) = \sum_{i=1}^{3} pCh_1^{Pi} \mathrm{e}^{-\frac{\left(s-pCh_2^{Pi}\right)^2}{2a_{Pi}^2}}, \; a_{Pi} = \frac{FWHM_{Pi}}{2\sqrt{2\ln 2}} \tag{11}$$

where s is the period and $FMHM_{Pi}$ is the full width at half maximum of the spike Pi and ln is the natural logarithm.

The comparison between the computed spectrum model (X^m) and the original spectrum (X^o) was then evaluated using Kullback–Leibler divergence measure (equation (12)).

$$F_{26} = D_{KL}\left(X^m; X^o\right) = \sum_s X^m(s) \ln\left(\frac{X^m(s)}{X^o(s)}\right) \tag{12}$$

where s is the period.

The rationale behind this comparison is that the increase in the spectrum's complexity, as a result of the inclusion of random components, can be detected by an increase in the Kullback–Leibler divergence between the original spectrum and the computed spectrum model (see figure 9—bottom).

2.4. Feature selection

In the feature selection step, the objective is to select a subset that contains the most relevant and least redundant features for the discrimination of motion artifacts. This enables the interpretability of the classification model to be built upstream, and improves the efficiency classification model and its generalization capability.

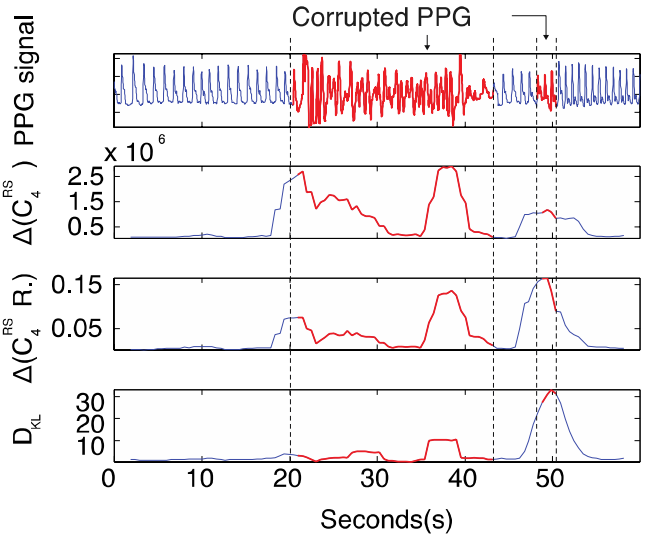

Figure 9. Rate of change of characteristics 24 and 25, and feature 26.

In this paper the feature selection process was performed using the Normalized Mutual Information Feature Selection (NMIFS) method, proposed by Estevez at al. (2009), which is an enhancement to its predecessor methods, the Battiti's MIFS (Battiti 1994), MIFS-U (Kwak and Chong-Ho 2002) and mRMR (Peng *et al* 2005). The main enhancement of the NMIFS method over its predecessors is the introduction of the Normalized Mutual Information (*nMI*) (equation (13)) as a measure of redundancy and the fact that there is no need for user defined parameters. The selection criterion used in the NMIFS method is presented in equation (14).

$$nMI\left(F_i;F_s\right)=\frac{MI\left(F_i;F_{se}\right)}{\min\left\{H\left(F_i\right),H(F_{se})\right\}} \tag{13}$$

F_i and F_j are the features i and j of a set of features F, $MI(F_i,F_j)$ is the Mutual Information (MI) between features i and j and $H\left(F_{\mathrm{se}}\right)=\sum_{f_{\mathrm{se}}\in \mathrm{SE}} P\left(F_{\mathrm{se}}\right)\log P\left(F_{\mathrm{se}}\right)$ is the entropy.

$$G \triangleq \mathrm{MI}\left(\mathrm{CL};F_i\right)-\frac{1}{|\mathrm{SE}|}\sum_{F_{\mathrm{se}}\in \mathrm{SE}} nMI\left(F_i;F_{\mathrm{se}}\right) \tag{14}$$

Where G is the NMIFS score, $\mathrm{SE}=\{F_{\mathrm{se}}\}$, for $\mathrm{se}=1,\ldots,|\mathrm{SE}|$ is the subset of selected features and CL is the classes variable.

2.5. Classification

A Support Vector Machine (SVM) model has been adopted for the discrimination between motion artifacts and clean PPG. The classification process was performed using the algorithm C-Support Vector Classification (C-SVC) algorithm (Chang and Lin 2011), with a radial basis function kernel.

Given the training vector $Tv^i\in R^n, i=1,\ldots,l$, and the correspondent classes label $Cl^i\in\{-1,1\}$, the C-SVC optimization problem requires the solution for:

Table 1. Volunteers characteristics (average ± standard deviation).

	Healthy	CVD
Age	27.4 ± 3.7	62 ± 13.5
Weight	72.5 ± 8	87.9 ± 21.4
BMI	24.4 ± 2.9	31.5 ± 6.9
Male/female	8/0	5/2

$$\min_{w,b,\xi} \frac{1}{2} w^T w + C \sum_{i=1}^{l} \xi_i \tag{15}$$

$$\text{subject to } Cl^i \left(w^T \phi\left(Tv^i\right) + b\right) \geq 1 - \xi_i, \;\; \xi_i \geq 1 \tag{16}$$

Here, the function ϕ maps the training vectors Tv^i into a higher dimensional space, and the cost, $C>0$, is the penalty parameter for the error term. The radial basis function kernel, $K\left(Tv^i, Tv^j\right) = \phi(Tv^i)^T \phi\left(Tv^j\right)$ is defined by:

$$K\left(Tv^i, Tv^j\right) = \exp\left(-\gamma \| Tv^i - Tv^j \|^2\right), \; \gamma > 0 \tag{17}$$

where the parameter gamma (γ) is a RBF kernel specific parameter.

3. Results and discussion

3.1. Experimental protocol

To evaluate the performance of the proposed algorithm, a data collection study was conducted aiming at the collection of photoplethysmograpic (PPG) signals from 15 volunteers: 8 healthy volunteers were enrolled at the Faculty of Sciences and Technology of the Coimbra University and 7 patients with cardiovascular diseases (CVD) were enrolled at the cardiovascular department infirmary of the Hospital Center of Coimbra University. The biometric characteristics of the 15 subjects involved in the present study are summarized in table 1.

The PPG waveform was recorded from the tip of the index finger using an infrared transmission finger probe with a HP-CMS monitor and was digitized at a sampling frequency of 125 Hz.

In order to conduct a wide variety of motion artifact patterns, the subjects were asked to execute two runs of eleven different types of hand and body movements (see figure 10), resulting in 22 records of 60 s for each subject. In order to correctly and timely execute the movements, each volunteer was guided by a slideshow, which showed the expected movement pattern, the next movement and the time to the next movement. Additionally, a trained technician also assisted the volunteers during the whole process.

The volunteers were asked to perform each movement in the 20–40 s. time interval of each run. A technician annotated each record in order to identify the exact time interval where the motion artifacts occurred.

The study was authorized by the ethical committee of the Centro Hospitalar de Coimbra in 2010 under the protocol 'Assessment of cardiac function using heart sounds, ICG and PPG'.

3.2. Feature selection

The NMIFS algorithm was applied to the whole database containing the records of both healthy and CVD volunteers. From the analysis of the computed NMIFS scores, the 8 most

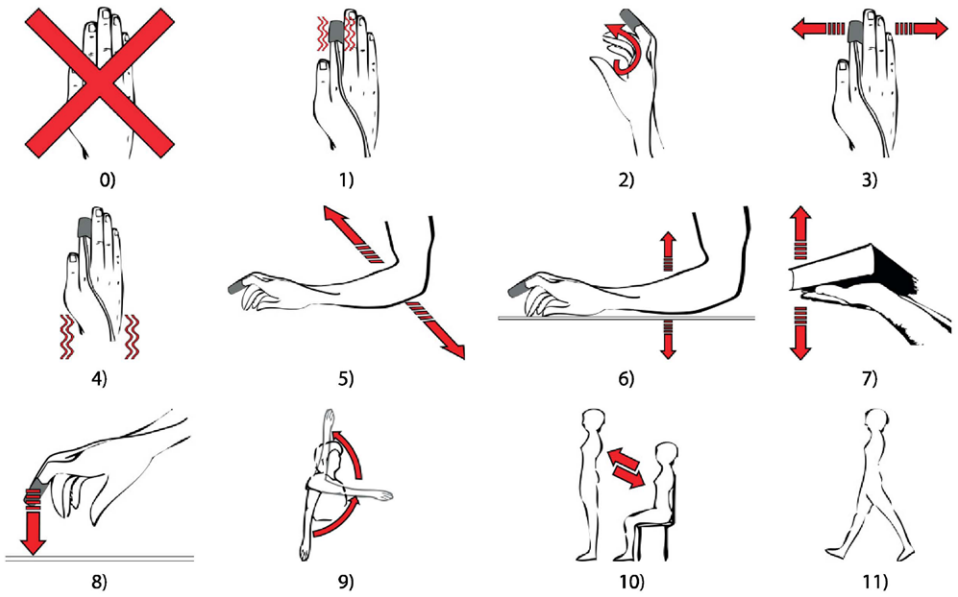

Figure 10. Movements performed by the volunteers. (0) No movement; (1) Disturbance of the PPG probe, causing variations in the contact point between fingertip and probe; (2) Gently bending of the index finger; (3) Repeated movement of the wrist left and right; (4) Shaking the wrist; (5) Repeated movement of the epsilateral arm in the horizontal plane; (6) Repeated movement of the epsilateral arm in the vertical plane; (7) Lifting and lowering a book with both hands; (8) Repeated tapping of the table with the index finger; 9) Repeated raising and lowering of the arm; (10) Repeated sitting down and standing up; (11) Slow walking in a straight line.

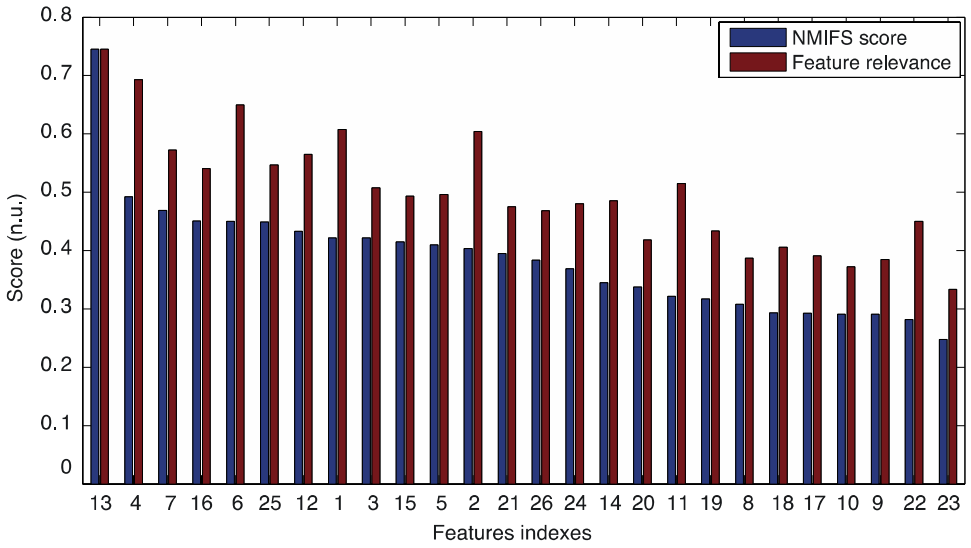

Figure 11. NMIFS and relevance scores for the 26 features extracted from the time $(F_{1,\ldots,7})$ and period $(F_{8,\ldots,26})$ domain analysis.

Table 2. Results achieved by the proposed methodology in Global, healthy and CVD subsets.

	Performance metric (avg ± std)		
Context	SE	SP	ACC
Global	84.3 ± 0.8	91.5 ± 0.5	88.5 ± 0.4
Healthy	78.4 ± 1.2	94.4 ± 0.6	87.5 ± 0.6
CVD	91 ± 0.8	88.4 ± 0.9	89.5 ± 0.6

relevant features were selected, corresponding to 4 features from the time domain and 4 features from the period domain. From the time domain, the selected features are pulse amplitude (F_1), trough depth difference (F_4), pulse skewness (F_6) and pulse kurtosis (F_7). In the period domain, the location of the 2nd and 3rd major spikes (F_{12} and F_{13}), the length of the 3rd major spike (F_{16}) and relationship of the major spikes area with the remaining spectrum (F_{25}) were selected. The most relevant selected feature derive from the period domain analysis, showing its importance in the proposed methodology.

In figure 11 we present the scores achieved by the NMIFS algorithm as well as the relevance scores ($\mathrm{M}I(CL; F_i)$, equation (14)).

3.3. Classification

The 176 recorded signals were analyzed and each section was classified using the proposed methodology and compared to the manually annotated classification. The performance of the algorithm was evaluated for the global, healthy and CVD dataset, as well as to each of the 11 motion sources.

In order to generate a classification model that can accurately predict the testing data and to avoid the over fitting problem, it is essential to find the parameters gamma (γ) and cost (C) that best suit the present classification problem. Therefore, a grid-search method using 10-fold cross-validation was used for this proposal. The global dataset was randomly partitioned into 10 equal size subsets. From the 10 subsets, 9 subsets were used for training and the remaining subset was used for testing. The cross-validation process was repeated 10 times with each of the k subsets used exactly once as the validation data and its accuracy is the average accuracy in each testing step. The cross-validation process was repeated several times with groups of exponentially growing gamma/cost pairs ($C = 2^{-5}, 2^{-3}, \ldots, 2^{15}$ and $\gamma = 2^{-15}, 2^{-13}, \ldots, 2^{9}$). The parameters that best fit the current classification problem were defined as: $C = 2^{5.33}$ and $\gamma = 2^{6.35}$.

The validation of the proposed methodology was performed using a 10-fold cross-validation scheme. In this process, the global dataset was randomly partitioned into 10 equally sized subsets with the same percentage of samples from each patient and each motion artifact source. Nine subsets were used for training the classification model, while the remaining subset was used for validation. The data of the validation subset corresponding to each context was used to validate the classification model regarding each subject group and motion artifacts source. This process was repeated for each of the 10 subsets. The 10-fold cross validation procedure was conducted 20 times. The performance of the proposed methodology was defined by the average ± standard deviation (over the 20 repetitions) of the following metrics: sensitivity (SE) and specificity (SP), and accuracy (ACC).

Table 2 summaries our results. The proposed methodology achieved a good performance in the classification of both corrupted and clean PPG sections, with an overall accuracy of 88.5%, which corresponds to a sensitivity of 84.3% and a specificity of 91.5% during

Table 3. Comparison of the results achieved by the proposed method and the methods proposed in literature (Sukor *et al* 2011, Krishnan *et al* 2008) in healthy volunteers.

	Performance metric (avg ± std)		
Healthy	SE	SP	ACC
Proposed method	78.4 ± 1.2	94.4 ± 0.6	87.5 ± 0.6
Sukor *et al* (2011)	89 ± 10	77 ± 19	83 ± 11
Krishnan *et al* (2008)	91/97	94/80	n.d.

Table 4. Results achieved by the proposed methodology for each of the 11 motion artifacts sources.

	Performance metric (avg ± std)		
Context	SE	SP	ACC
Movement 1	84.7 ± 3	92.6 ± 1.6	89.7 ± 1.5
Movement 2	90 ± 1.9	91.7 ± 1.8	91 ± 1.3
Movement 3	72.7 ± 3	93.5 ± 1.4	85.1 ± 1.3
Movement 4	83.9 ± 2.6	92.7 ± 1.7	89.3 ± 1.5
Movement 5	81.6 ± 2.9	91.9 ± 1.7	87.9 ± 1.6
Movement 6	85.5 ± 2.6	91.5 ± 1.5	89 ± 1.5
Movement 7	88.1 ± 2.4	90.6 ± 1.9	89.4 ± 1.5
Movement 8	77.5 ± 2.7	89.8 ± 1.9	84.6 ± 1.6
Movement 9	89.6 ± 2	92.2 ± 1.7	91 ± 1.2
Movement 10	87.6 ± 2.1	89.3 ± 1.8	88.5 ± 1.4
Movement 11	83.9 ± 2.4	90.9 ± 2.1	88 ± 1.5

validation. Looking into more detail in the specific subject groups, for healthy subjects the accuracy decreased to 87.5%, whereas for the CVD patients an increase can be observed to 89.5%. However, while in the CVD dataset the proposed methodology is able to discriminate corrupted PPG sections from the clean ones with high sensitivity (91.0%) and specificity (88.4%), in the healthy dataset, there is a significant decrease in sensitivity (78.4%). These results show that the proposed methodology is able to detect motion artifacts more accurately in CVD volunteers when compared to healthy volunteers. One possible reason for this difference in the presented results relies on the different characteristics of the PPG signal within healthy and CVD subjects. Due to ageing and the appearance of cardiovascular complications, the compliance of the systemic vascular wall decreases (i.e. arterial stiffening), leading to the disappearance of the dicrotic notch and therefore changing the morphological complexity of the PPG waveform in the CVD volunteers. Additionally, the appearance of abnormal cardiovascular events (e.g. arrhythmias) in CVD volunteers also affects the period characteristics of the PPG waveform, leading to the misclassification of clean PPG sections and reducing the model specificity in the subject group. Since the extracted features mainly reflect the changes in these characteristics, it is expectable to have variations in the extracted features discrimination capability and therefore different optimal feature space for healthy and CVD subsets. The presented results suggest that the discrimination capability of the selected features is dependent on the analyzed context, i.e. the analyzed volunteer subset, affecting the proposed methodology performance within healthy and CVD subjects, as shown in table 2.

It is not possible to perform a fair comparison between the proposed algorithm and state of the art, since different datasets were adopted, resorting on dissimilar populations and protocols. However, a comparison of algorithms performance within the Healthy

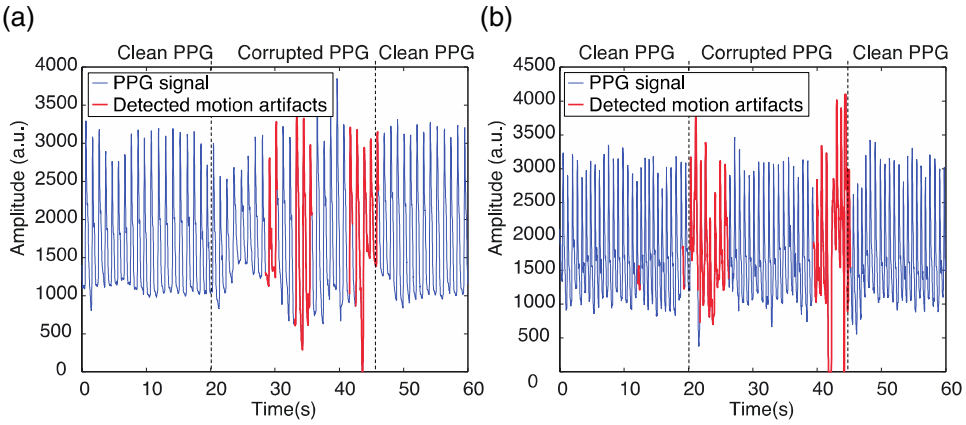

Figure 12. Examples of PPG signals when a performance decrease in the proposed methodology was observed. (*a*) Volunteer 4/Record 5/Movement 3. (*b*) Volunteer 3/ Run 15/Movement 8.

population can still be done. From table 3 we present a comparison of the results achieved by the current algorithm with the methods presented in literature. On the one hand, it is possible to observe that the specificity and accuracy of the current algorithm are greater (SP: +17.4% and ACC: +4.5%) compared to the algorithm presented by Sukor *et al* (2011). Contrarily, the sensitivity of the current algorithm remains lower than the later method (SE: −10.6%). Nonetheless, the algorithm proposed in (Sukor *et al* 2011) exhibits a excessive uncertainty in the results, revealed by the high standard deviation (from 10% to 19%) of the used metrics. On the other hand, one can observe that the current algorithm was not able to outperform the one proposed by Krishnan *et al* (2008), with a much lower sensitivity (SE: −12.6%) and a marginally higher specificity (SP: +0.4). The author did not report the accuracy of the proposed algorithm and therefore we were not able to compare both algorithms using this metric.

From table 4 it can be observed that the majority of the movement artifacts are identified with accuracy over 88%. However, there are two exceptions for the 3rd and 8th movement artifacts where a decrease in the detection accuracy has been observed (85.1% and 84.6%, respectively). This is a result of an evident increase of the algorithm's inability to detect properly the corrupted PPG sections, shown by the decrease in sensitivity to 72.7 and 77.5%, respectively. On the other hand, the algorithm's specificity, that is, the ability to detect non-corrupted PPG sections is still high.

The performance decrease for the 3rd and 8th movement artifacts is possibly associated with how the volunteers perform the requested movements. Two possible reasons are the: i) Low corruption of PPG data resultant from the incorrect execution of the performed movement and; ii) Increase in the periodicity of the performed movements.

During the execution of the 3rd movement, (see figure 10) several volunteers gently lifted the wrist/probe, causing no friction between the PPG probe and wrist with the table, and therefore resulting in low corruption of PPG data. Additionally, during the execution of movement 8, it was observed that several volunteers performed this task in a periodic fashion (contrarily to what is expected in real scenarios), leading to contamination of the PPG data with periodic artifacts. Since the present methodology is based on the analysis of the changes in the period components of the PPG data, artifacts with an intrinsic periodicity typically cannot be

detected. In figure 12, we present two examples where the aforementioned problems occurred and consequently a decrease the proposed algorithm performance has been observed.

4. Conclusion

In the current paper a novel methodology for the detection of motion artifacts in photoplethysmographic signals has been proposed. Our approach is based on the analysis of the time and period domain analysis of the PPG leading to the extraction of a total of 26 features. Contrarily to clean PPG signals, were changes on the PPG pulse morphology are mainly caused by cardiovascular changes, corrupted PPG signals show abnormal, erratic and 'random' pulse characteristics. To assess these, the morphology of the PPG pulses and their relationships with neighboring pulses was analyzed contributing to the extraction of eight time domain 8 features. Features extracted from the period domain resorts on the principle that, the PD-STFT also exhibits a regular shape representing the main features of the signal similar to the morphology of the PPG signal. From the period spectra analysis, it was found that a clean PPG signal consists of three major spikes with different locations, lengths and amplitudes, being the most relevant spike a result of the fundamental period of the PPG signal, and the remaining spikes associated to location and amplitude of the waves reflected from the periphery towards the aorta. Moreover one observed that in corrupted sections of the PPG signal, several random components that do not represent the fundamental characteristics of the underlying uncorrupted signal in the presence of motion artifacts are present, leading to random and significant changes in the period domain characteristics. To capture these changes, 18 features were extracted from the analysis of the main characteristics of the period domain spectra of the PPG signal.

In order increase the classification model generalization capability and interpretability, the extracted features were ranked using the NMIFS algorithm and the 8 most relevant features were selected, corresponding to 4 features from the time domain (pulse amplitude, trough depth difference, pulse skewness and pulse kurtosis) and 4 features from the period domain (2nd and 3rd major spikes, the length of the 3rd major spike and relationship of the major spikes area with the area remaining spectrum).

The discrimination between motion artifacts and clean PPG sections was performed using C-Support Vector Classification algorithm (Chang and Lin 2011), with a radial basis function kernel. The identification of the most suitable gamma (γ) and cost (C) parameters was performed using a 10-fold cross-validation grid-search method.

The proposed methodology for motion artifacts detection was validated on 8 healthy volunteers enrolled a the Faculty of Sciences and Technology of the Coimbra University and 7 CVD patients enrolled at the cardiovascular department infirmary of the Hospital Center of Coimbra University. A 10-fold cross-validation scheme was repeated 20 times with the following performance metrics: sensitivity (SE), specificity (SP), and accuracy (ACC).

The results achieved by the current algorithm in the global dataset (SE: 84.3% and SP: 91.5%) suggest that the characteristics of period components of the PPG signal can be used as discriminative features for motion artifact detection. Additionally, the results achieve for each of the volunteers subsets, show that the proposed methodology is able to detect motion artifacts more accurately in CVD volunteers (SE: 91% and SP: 88.4%) when compared to healthy volunteers (SE: 78.4% SP: 94.4%), suggesting a different discrimination capability of both time and period domain features for each of the volunteers subsets. Finally, the results achieved for each of the motion artifact sources show that the proposed methodology is able to detect motion artifacts with high accuracy regardless the performed movement.

Acknowledgments

The authors would like to express their gratitude for the support of 'Centro Hospitalar de Coimbra' and specially the effort of Dr Leitão Marques in facilitating the arrangements for the data acquisition component of the present study.

This work was supported by CISUC (Center for Informatics and Systems of University of Coimbra) and by EU projects HeartCycle (FP7-216695), iCIS (CENTRO-07-ST24-FEDER-002003).

Declaration of interest

Jens Muehlsteff is employed by Philips Research in the Netherlands.

References

Abramowitz M and Stegun I A 2012 *Handbook of Mathematical Functions: with Formulas, Graphs, and Mathematical Tables* (Dover Publications). New York, USA.

Addison P *et al* 2012 Developing an algorithm for pulse oximetry derived respiratory rate (RRoxi): a healthy volunteer study *J. Clin. Monit. Comput*. **26** 45–51

Allen J 2007 Photoplethysmography and its application in clinical physiological measurement *Physiol. Meas.* **28** R1

Baruch M *et al* 2011 Pulse decomposition analysis of the digital arterial pulse during hemorrhage simulation *Nonlinear Biomed. Phys.* **5** 1

Battiti R 1994 Using mutual information for selecting features in supervised neural net learning *Trans. Neur. Netw.* **5** 537–50

Chan G H *et al* 2007 Automatic detection of left ventricular ejection time from a finger photoplethysmographic pulse oximetry waveform: comparison with Doppler aortic measurement *Physiol. Meas*, **28** 439

Chang C-C and Lin C-J 2011 LIBSVM: a library for support vector machines *ACM Trans. Intell. Syst. Technol.* **2** 27:1–27

Cook L B 2001 Extracting arterial flow waveforms from pulse oximeter waveforms *Anaesthesia* **56** 551–5

Dawber T R, Thomas H E and McNamara P M 1973 Characteristics of the dicrotic notch of the arterial pulse wave in coronary heart disease *Angiology* **24** 244–5

Estevez P A *et al* 2009 Normalized mutual information feature selection *Neural Netw IEEE Trans* **20** 189–201

Foo J Y A 2006 Comparison of wavelet transformation and adaptive filtering in restoring artefact-induced time-related measurement *Biomed. Signal Process. Control.* **1** 93–8

Foo J and Wilson S 2006 A computational system to optimise noise rejection in photoplethysmography signals during motion or poor perfusion states *Med. Biol. Eng. Comput.* **44** 140–5

Gibbs P and Asada H H 2005 Reducing motion artifact in wearable bio-sensors using MEMS accelerometers for active noise cancellation *American Control Conf*. Proc. of the 2005

Graybeal J M and Petterson M T 2004 Adaptive filtering and alternative calculations revolutionizes pulse oximetry sensitivity and specificity during motion and low perfusion Engineering in Medicine and Biology Society *IEMBS '04. 26th Annual Int Conf of the IEEE.* San Francisco, California, USA.

Han H, Kim M J and Kim J 2007 Development of real-time motion artifact reduction algorithm for a wearable photoplethysmography *Conf. Proc. IEEE Eng. Med. Biol. Soc.* **2007** 1538–41

Kim B S and Yoo S K 2006 Motion artifact reduction in photoplethysmography using independent component analysis *Biomed. Eng. IEEE Trans* **53** 566–8

Kim S H, Ryoo D W and Bae C 2007 Adaptive noise cancellation using accelerometers for the PPG signal from forehead *Conf. Proc. IEEE Eng. Med. Biol. Soc*. **2007** 2564–7

Krishnan R, Natarajan B and Warren S 2008 Analysis and detection of motion artifact in photoplethysmographic data using higher order statistics Acoustics, Speech and Signal Processing *IEEE Int. Conf. on ICASSP 2008.* Las Vegas, California, USA.

Kunchon S, Desudchit T and Chinrungrueng C 2009 Comparative evaluation of adaptive filters in motion artifact cancellation for pulse oximetry Signal Processing & Its Applications *5th Int Colloquium on CSPA 2009. Kuala Lumpur, Malaysia, 2009.*

Kwak N and Chong-Ho C 2002 Input feature selection for classification problems *Neural Netw. IEEE Trans.* **13** 143–59

Lee C M and Zhang Y T 2003 Reduction of motion artifacts from photoplethysmographic recordings using a wavelet denoising approach. *IEEE EMBS Asian-Pacific Conf.* on Biomedical Engineering Kyoto-Osaka-Nara, Japan, 2003.

Lee J *et al* 2004 Design of filter to reject motion artifact of pulse oximetry *Comput. Stand. Interfaces* **26** 241–9

Peng H, Fulmi L and Ding C 2005 Feature selection based on mutual information criteria of max-dependency, max-relevance, and min-redundancy *Pattern Anal. Mach. Intell. IEEE Trans.* **27** 1226–38

Raghuram M *et al* 2012 HHT based signal decomposition for reduction of motion artifacts in photoplethysmographic signals IEEE Int. *Instrumentation and Measurement Technology Conference (I2MTC).* 2012 IEEE International (pp. 1730-1734). IEEE.

Reddy K A and Kumar V J 2007 Motion artifact reduction in photoplethysmographic signals using singular value decomposition. *Instrumentation and Measurement Technology Conf. Proc.* IMTC 2007. Warsaw, Poland, 2007.

Reddy K A, George B, Kumar V J 2008 Motion artifact reduction and data compression of photoplethysmographic signals utilizing cycle by cycle fourier series analysis *Instrumentation and Measurement Technology Conf. Proc.*IMTC 2008. IEEE *2008*

Reisner A *et al* 2008 Utility of the photoplethysmogram in circulatory monitoring *Anesthesiology* **108** 950–8

Shang A B *et al* 2007 Development of a standardized method for motion testing in pulse oximeters *Anesth. Analg.* **105** S66–77

Sukor J A, Redmond S J and Lovell N H 2011 Signal quality measures for pulse oximetry through waveform morphology analysis *Physiol. Meas*. **32** 369

Sun Y, Chan K and Krishnan S 2005 Characteristic wave detection in ECG signal using morphological transform *BMC Cardiovasc. Disord* **5** 28

Wisely N A and Cook L B 2001 Arterial flow waveforms from pulse oximetry compared with measured Doppler flow waveforms *Anaesthesia* **56** 556–61

Wood L B and Asada H 2007 Low variance adaptive filter for cancelling motion artifact in wearable photoplethysmogram sensor signals *Conf. Proc. IEEE Eng. Med. Biol. Soc.* **2007** 652–5

Yan Y-S, Poon C and Zhang Y-T 2005 Reduction of motion artifact in pulse oximetry by smoothed pseudo Wigner-Ville distribution *J. NeuroEng. Rehabil.* **2** 3

Yousefi R, xNourani C and Panahi I 2012 Adaptive cancellation of motion artifact in wearable biosensors *Engineering in Medicine and Biology Society (EMBC) Annual Int. Conf. IEEE* (San Diego, CA: IEEE)

Chapter 5.
ASSESSMENT OF CARDIOVASCULAR FUNCTION FROM MULTI-GAUSSIAN FITTING OF FINGER PHOTOPLETHYSMOGRAM

This chapter consists of the following article:

Assessment of Cardiovascular Function from Multi-Gaussian Fitting of Finger Photoplethysmogram

R. Couceiro, P. Carvalho, R. P. Paiva, J. Henriques, I. Quintal, M. Antunes, J. Muehlsteff, C. Eickholt, C. Brinkmeyer, M. Kelm and C. Meyer

Submitted for publication in *Physiological Measurement*, 2015.

Journal impact factor in 2013: 1.617

Assessment of Cardiovascular Function from Multi-Gaussian Fitting of Finger Photoplethysmogram

R Couceiro[1], P Carvalho[1], R P Paiva[1], J Henriques[1], I Quintal[2], M Antunes[3], J Muehlsteff[4], C Eickholt[5,6], C Brinkmeyer[5], M Kelm[5] and C Meyer[6]

[1] Center for Informatics and Systems of the University of Coimbra, Polo II, 3030–2 90 Coimbra
[2] Echocardiography Department of the Centro Hospitalar de Coimbra, Coimbra, Portugal
[3] Centro de Cirurgia Cardio-Torácica of the Centro Hospitalar da Universidade de Coimbra, Coimbra, Portugal
[4] Philips Research Laboratories Europe, Eindhoven, Netherlands
[5] Heinrich-Heine University Hospital Düsseldorf, Division of Cardiology, Pneumology, and Angiology, Düsseldorf, Germany
[6] Department of Electrophysiology, University Heart Center, University Hospital Eppendorf, Hamburg, Germany

E-mail: rcouceir@dei.uc.pt

Abstract

Monitoring of cardiovascular function on a beat-to-beat basis is fundamental to protect patients in different settings including emergency medicine and interventional cardiology but still bears technical challenges and several limitations. In the present study we propose a new method for the extraction of cardiovascular performance surrogates from the analysis of the Photoplethysmographic (PPG) signal alone.

In the current study we propose the use of a Multi-Gaussian (MG) model consisting of five Gaussian functions to decompose the PPG pulses into its main physiological components. From the analysis of these components, we aim to extract estimators of the left ventricular ejection time, blood pressure and vascular tone changes. Using a multi-derivative analysis of the components related with the systolic ejection, we investigate which are the characteristic points that best define the left ventricular ejection time (LVET). Six LVET estimates were compared with the echocardiographic LVET in a database consisting of 68 healthy and cardiovascular diseased volunteers. The best LVET estimate achieved a low absolute error (15.41±13.66 ms), and a high correlation (ρ=0.78) with the echocardiographic reference.

To assess the potential use of the temporal and morphological characteristics of the proposed MG model components as surrogates for blood pressure and vascular tone, six parameters have been investigated. The stiffness index (SI), the T_{1_d} and T_{1_2} were defined as the time span between the MG model forward and reflected waves, while the reflection index (RI), the R_{1_d} and the R_{1_2} were defined as their amplitude ratio. Their association to reference values of blood pressure and total peripheral resistance was investigated in 43 volunteers exhibiting hemodynamic instability. A good correlation was found between the majority of the extracted and reference parameters, with an exception to R_{1_2} (amplitude ratio between the main forward wave and the first reflection wave), which correlated low with all the reference parameters. The highest correlation (ρ_p = 0.45) was found between T_{1_2} and the total peripheral resistance index (TPRI), while in the patients that experienced syncope, the highest agreement (ρ_p = 0.57) was found between SI and systolic blood pressure (SBP) and mean blood pressure (MBP).

In conclusion, the presented method for the extraction of surrogates of cardiovascular performance might improve patient monitoring and warrants further investigation.

Keywords: Photoplethysmography, digital volume pulse, Multi-Gaussian model, left ventricular ejection time, blood pressure, vascular tone.

1. Introduction

Photoplethysmography (PPG) is an optical measurement technique used to monitor non-invasively and continuously changes in blood volume of microvascular bed of tissues [1]. The waveform, i.e., the photoplethysmogram, has a widespread range of clinical applications and is commonly acquired in clinical settings to infer arterial oxygen saturation [2]. Since the signal morphology is similar to the arterial blood pressure waveform, the study of the PPG became popular within the scientific community as a potential non-invasive tool, especially in the assessment of the cardiovascular and autonomic function [1]. Anesthesia care, critical care and emergency medicine are the main clinical areas where the PPG is already widely applied [1]. Furthermore, it is already being used in interventional cardiology and in ambulatory and recreational settings, e.g. for pulse measurement in sport watches.

The analysis of the PPG waveform dates back to early 1930s, when manual measurement and feature extraction techniques were often used [1]. More recently, several approaches have been proposed to extracted relevant information about the cardiovascular function. One of the most recognized approaches is Double Differentiation Analysis (DDA), which is based on the analysis of PPG second derivative. Since the signal processing is simple and can be easily implemented in real-time applications it became very popular in contemporary research. Relationships between these identified waves within a pulse have been associated with several demographic and physiological parameters such as aging, large artery stiffness and blood pressure [3]. However, DDA lacks robustness in the presence of seriously damped and noisy signals, which can complicate the correct identification and characterization of the PPG pulse components. Thus, an alternative approach consisting in the decomposition of PPG pulse into individual waves was proposed, which is called Pulse Decomposition Analysis (PDA).

The ejection of blood from the left ventricle creates a pressure wave called arterial pulse pressure wave. As the main pressure wave (P1 - illustrated in Fig. 1) travels down the systemic vascular network it reaches several sites causing reflection due to significant changes in arterial resistance and compliance. The first one is the juncture between thoracic and abdominal aorta, which causes the first wave reflection (P2 - illustrated in Fig. 1) and commonly known as second or late systolic wave. At the second reflection site, the juncture between the abdominal aorta and common iliac arteries, the main wave is reflected once again, and appears as a second wave reflection (P3 - illustrated in Fig. 1) [4]. A small dip, called dicrotic notch, is commonly observed between the first and second wave reflections (P2 and P3, respectively). There are additionally minor reflections and re-reflections in the systemic vascular structure with lower amplitudes of the reflection waves. These pulse reflections are also observed in a similar, but smoother fashion, in the photoplethysmogram morphology [5, 6].

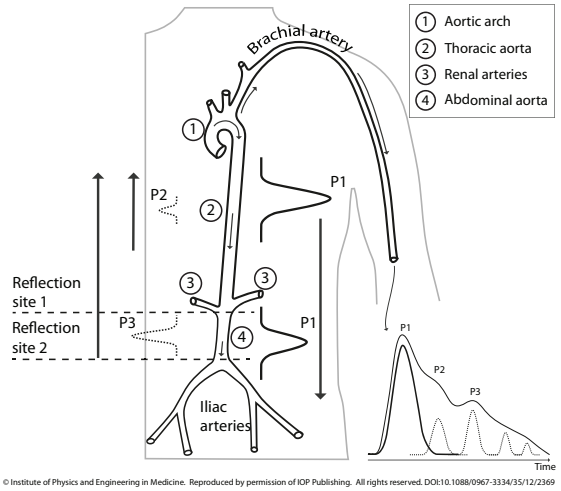

Fig. 1 – Morphology and origin of the PPG pulse. On the left, a sketch of the arterial system from the aorta/arm to the iliac arteries. On the right, a PPG pulse decomposed in the correspondent forward pulse (P1) and pulses reflected at the first (P2) and second (P3) reflection sites.

Several variations of the PDA methodology have been proposed in literature e.g. inference of a different number of components (2 to 5) and use of different kernels (Gaussian, Rayleight and Logarithmic normal function) in order to model the PPG pulse. In [6] a two-pulse synthesis model is proposed to decompose the PPG pulse as a sum of two Rayleight functions, while in [7] a sum of five logarithmic normal functions have been used. Moreover, a sum of up to three [4], four [8, 9] and five [10] Gaussian functions have also been used to model the PPG pulse. While in [9] it was suggested that the PPG pulse can be accurately modeled using only three Gaussian functions, in [10] the author highlights the need of using five Gaussian functions to reach an acceptable fitting error. Obviously, there is a controversy on the ideal number of the model components.

Pulse reflections carry important information about the cardiovascular system. One example is the augmentation index (AI) usually associated with aging and arterial stiffening [1, 4, 11]. The stiffness index (SI) and reflection index (RI) were associated with large artery stiffness [12], the velocity of a pulse wave in large arteries [13], pulse pressure [4], small artery stiffness [13] and vascular tone [14, 15].

In the assessment of cardiac function, the current non-invasive gold standard is cardiovascular magnetic resonance (CMR) [16]. However, its expensiveness, the requirement of trained personal and the lack of portability make it unsuitable for primary, home care and ambulatory scenarios. Thus, Echocardiography (ECHO) is becoming increasingly popular ambulatory professional care, driven by the development of inexpensive and portable handheld devices. As the former gold standard in the evaluation of cardiac function, it is widely available and provides a straightforward determination of indexes such as the velocity of pressure rise, the velocity of ejection, the extension of ejection and the ejection fraction [17]. Nevertheless, it also requires trained personal and does not support the recording of long-term measurements, which are still major disadvantages for its application in p-health scenarios.

The healthy of the myocardial cells is intrinsically related with the timings of the myocardial relaxation and contraction events, which are coordinated by the recycling of the intracellular calcium ions. From these events, the timings of the left ventricle systole and diastole are of major importance, since it is the left ventricle role to supply blood into the systemic circulation. The two main functions of the left ventricle are the systolic ejection (preceded by the pre-ejection period – PEP) and the diastolic filling. The PEP is the time span from the start of ventricular depolarization and the opening of the aortic valve and is composed electro-mechanical delay and by the isovolumetric contraction time (IVCT). The left ventricular ejection time (LVET) is defined by the time span between the opening and closure of the aortic valve. The diastolic filling is preceded by the isovolumetric relaxation time (IVRT). The assessment of systolic time intervals (STIs) has been widely investigated as a measure of myocardial performance since the 1960s. A widely recognized index of left ventricular function is the ratio between the PEP and LVET, which was proposed by Weissler et al. [18].

LVET is commonly associated with stroke volume and has been indicated as a valuable prognostic parameter related to hypovolemia [19], an important predictor of mortality in patients with cardiac amyloidosis [20] and a robust and independent predictor of light chain amyloidosis mortality [21]. Moreover, a shortened LVET was associated with poor prognosis in patients with precapillary pulmonary hypertension hospitalized in the ICU because of heart failure [22]. It can been assessed using several modalities, such as impedance cardiography (ICG) [23], phonocardiography (PCG) [24-26], and PPG [27, 28]. Using the PPG waveform, LVET inference was firstly introduced in a study on the analysis of the ear densitogram [29], were it was suggested that the onset and offset of the systolic ejection could be recognized in the morphology of the first derivative. Based on this study, Chan et al. [27] proposed an algorithm for the assessment of LVET based on a rule-based combination of three LVET measures extracted from a multi-derivative analysis of the finger photoplethysmogram. However, similar problems to those encountered on the DDA can be found on this high-order derivatives based analysis, where noise can be a critical factor [27].

In this paper, we propose a method for the assessment of cardiovascular surrogates based on the decomposition of the PPG pulse into its forward and reflection waves, using a Multi-Gaussian (MG) model formulation. The proposed methodology resorts on the segmentation of the PPG pulse into systolic and diastolic phases and consequent modeling of the segmented phases into a sum of three and two Gaussian functions motivated by the underlying physiology of the PPG pulse. We identified three main parameters related with cardiovascular function derived from the pulse decomposition. The LVET was assessed from the systolic phase of the fitted model a multi-derivative analysis approach. In order to investigate which are the characteristic points that best define the LVET, six LVET estimates were calculated and compared with the

reference echocardiographic LVET. Aiming the evaluation the performance of the LVET detection algorithm in a wide range of PPG pulse morphologies hemodynamic characteristics, the algorithm was tested in healthy and cardiovascular diseased populations. Additionally, from the analysis of the location and amplitudes of the PPG pulse components (forward wave, late systolic wave and reflection waves), 6 parameters were extracted. The stiffness index (SI), the T_{1_d} and the T_{1_2} were defined as the time span between the main forward and reflected waves, while the reflection index (RI), the R_{1_d} and the R_{1_2} were defined as the ratio of their amplitudes. The association of these indexes with blood pressure and vascular tone changes was assessed by their correlation with reference values of systolic (SBP), diastolic (DBP) and mean (MBP) blood pressure, pulse pressure (PP) and total peripheral resistance index (TPRI), in both healthy and hemodynamic unstable patients.

The remainder of the paper is organized as follows. The proposed methodology for PPG modeling and assessment of cardiovascular surrogates is presented in section 2. In 3 the experimental protocol used in the present study is described. The main results are presented and discussed in section 4 and finally, we present our main conclusions in section 5.

2. Methods

The proposed methodology consists of the followings steps: 1) Pre-processing and baseline removal; 2) Segmentation; 3) Multi-Gaussian modeling of the PPG pulses; 4a) Estimation of LVET and 4b) Estimation of blood pressure and vascular tone surrogates.

2.1. Pre-processing

The susceptibility of the PPG signal to ambient light at the photo-detector, poor blood perfusion of the peripheral tissues and motion artifacts [30] is well known. In order to minimize the influence of these factors in the subsequent phases of the PPG analysis, a pre-processing stage is required. At this stage, high frequency components in the acquired signal, such as the interference of the power sources, are removed using a low-pass Butterworth filter with a 18Hz cut-off frequency [27], ensuring the preservation of the physiological relevant information (usually bellow 15 Hz [31]). Additionally, low frequency components, commonly associated with changes in capillary density and venous blood volume [2], temperature variations, acquisition instruments or subject movements [32], were suppressed by subtracting a 2 second window moving average filtered version to the original PPG signal [27].

2.2. Segmentation

The main objective in this step is to segment a PPG signal stream into individual PPG pulses per heart beat. From each detected PPG pulse, the morphological characteristics are inferred afterwards.

To detect the PPG pulses, an approach similar to [33] was applied. Firstly, the PPG signal is differentiated using a five-point digital differentiator [34] (from (1) to (4)), resulting in first to fourth order derivatives ($d1_{ppg}$, $d2_{ppg}$, $d3_{ppg}$ and $d4_{ppg}$).

$$d1_{ppg} = f'(t) = \frac{f(t-2h) - 8f(t-h) + 8f(t+h) - f(t+2h)}{12h^2} \quad (1)$$

$$d2_{ppg} = f''(t) = \frac{-f(t-2h) + 16f(t-h) - 30f(t) + 16f(t+h) - f(t+2h)}{12h^2} \quad (2)$$

$$d3_{ppg} = f'''(t) = \frac{-f(t-2h) + 2f(t-h) - 2f(t+h) + f(t+2h)}{2h^3} \quad (3)$$

$$d4_{ppg} = f''''(t) = \frac{f(t-2h) - 4f(t-h) + 6f(t) - 4f(t+h) + f(t+2h)}{2h^3} \quad (4)$$

where f is the PPG time series, t is the time index and h is the sampling time.

From the analysis of the $d1_{ppg}$, the local maxima (d1_ppg_lmax) with absolute amplitude greater than a threshold ThR are detected. Here, the ThR is selected based on an adaptive thresholding of the $d1_{ppg}$ data

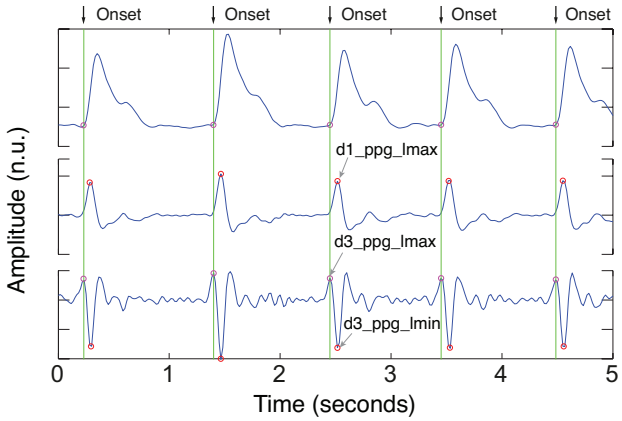

Fig. 2 – Plot of PPG signal derivatives (order 1 and 3) and representation of the detected characteristic points for the detection of the onset of each individual PPG pulse.

cumulative histogram (calculated within 10 seconds time windows), and was defined as the greater value bellow which 90% of the observations are found.

Following the work proposed by Chan et al. [27], the PPG pulse onset was considered to be the point $d1_{ppg}$ presenting a rapid inflection (just before d1_ppg_lmax), which corresponds to a maximum in the $d3_{ppg}$ (d3_ppg_lmax). The motivation behind this approach was firstly reported by L.B. Cook [35, 36], who observed a significant resemblance between the PPG signal's first derivative and the arterial flow waveform.

The detection of the d3_ppg_lmax characteristic point was accomplished in two phases: 1) detection of the $d3_{ppg}$ local minima (d3_ppg_lmin) corresponding to the $d1_{ppg}$ local maxima (see Fig. 2) and 2) identification of the peak with greater amplitude (d3_ppg_lmax) prior to the previously identified most relevant valley.

2.3. Multi-Gaussian modeling of PPG pulse

The first step of the modeling process is an additional preprocessing of the PPG pulses, which may still exhibit minor baseline and amplitude fluctuations and can negatively affect the subsequent modeling phases. Therefore, the linear trend is removed and the amplitude of each PPG pulse is normalized to the unit.

In the second step, the PPG pulse is separated into systolic and diastolic phases. The systolic phase, primarily associated with the ventricular ejection, was defined as the portion between the onset of the PPG pulse and the dicrotic notch. The diastolic phase, resulting from the reflections and re-reflections of the main PPG pulse in the systemic vascular network, was defined as the portion of the PPG pulse between the dicrotic notch and the pulse offset. The two phases of the PPG pulse are illustrated in Fig. 3.

The detection of the reference point correspondent to the dicrotic notch was defined as local maxima of the $d2_{ppg}$ (d2_ppg_lmax) within a [0.2-0.4]s interval and its boundaries as the negative-to-positive/positive-to-negative zero crossings of the $d2_{ppg}$ [8]. Although this strategy can be effective in PPG pulse morphologies where the dicrotic notch is highly prominent, in cases where the pulse is severely damped this task can be deeply compromised due to the existence of multiple d2_ppg_lmax and the absence of zero crossings in an acceptable temporal window (i.e., very far from d2_ppg_lmax – an example in shown in Fig. 4). In such cases, the identification of the dicrotic notch boundaries relies on the identification of the points in $d2_{ppg}$ with the steepest slope, i.e., the negative-to-positive/positive-to-negative in the $d4_{ppg}$ closer to the reference point. The selection of the dicrotic notch among multiple candidates is performed based on a joint analysis of the candidate characteristics, i.e., their amplitude, area and length.

In our previous work [28], we modeled the PPG pulse as a mixture of four Gaussian functions, related with the main pulse and corresponding reflections in the arterial path. However, depending on the morphology of the PPG pulse, this model may lead to inaccurate approximations, especially in rapid inflections close to the PPG pulse onset during the systolic rise. Based on these observations and aiming the reduction of the error between the proposed PPG model and the data, the main forward pulse is modeled as a mixture of two Gaussian functions instead of just one. Thus, by increasing the number of degrees of freedom of the proposed model, we expect to decrease the error between the model and the data and to determine the PPG pulse components more accurately. The formulation of the proposed 5-Gaussian model is presented as follows:

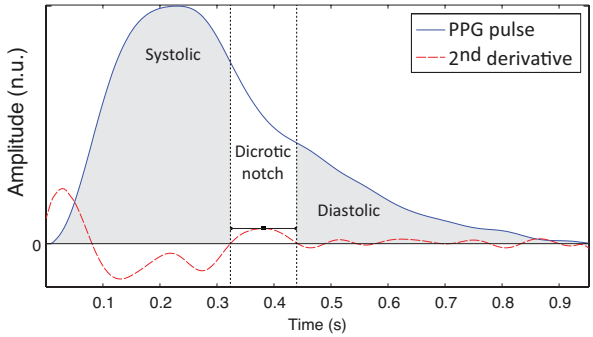

Fig. 3 – Representation of the systolic and diastolic phases of the PPG pulse based on the detection of the notch (inflection) onset and offset.

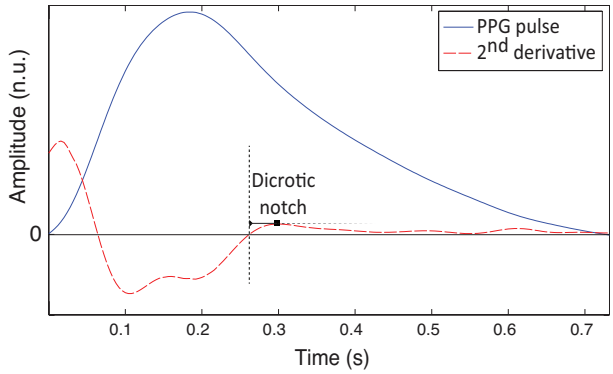

Fig. 4 – Example of a damped PPG pulse with no positive-to-negative zero crossings after the local maxima of the $d2_{ppg}$ (d2_ppg_lmax).

$$f_m(t,\beta_j) = \sum_{j=1}^{5} g_j(t,\beta_j), \qquad for\ \beta_j = \{a,b,c\}_j$$
$$g_j(t,\beta_j) = a_j\, e^{\frac{-(t-b_j)^2}{2c_j^2}} \tag{5}$$

where the parameters a_j, b_j and c_j correspond to the amplitude, location and width of the Gaussian function j. Here, the first two Gaussian functions ($g_{1\_2} = g_1 + g_2$) correspond to the ventricular ejection and the third Gaussian function (g_3) is related to the first pulse reflection at the junction between the thoracic and abdominal aorta, presented in Fig. 5. The fourth (g_4) and fifth (g_5) Gaussian functions derive from the reflection at the juncture between abdominal aorta and common iliac arteries [4] and minor reflections and re-reflections in the systemic structure, respectively (see Fig. 5).

According to [10], the positions of the *a*, *b*, *c*, *d* and *e* waves (here called W_a, W_b, W_c, W_d and W_e waves and illustrated in Fig. 6) defined by DDA [37] can provide an insight about the locations of the individual components of the PPG pulse. Additionally, from the inspection of the PPG pulse morphology and the corresponding 2nd derivative, we observed that the negative peak after W_e (i.e., W_f) can provide information about the location of the 2nd reflection wave and, therefore, it was included in the present work. Based on the waves identified Fig. 6, the initial parameters and corresponding boundaries of the Multi-Gaussian model were determined using a Heuristic approach similar to the one proposed in [10]. The initial parameters and boundaries of the proposed model are presented in TABLE 1.

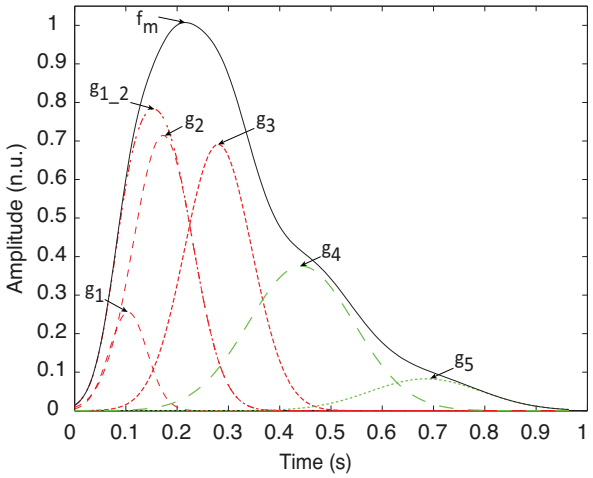

Fig. 5 – Representation of the Multi-Gaussian model of a PPG pulse and individual Gaussian functions correspondent to the main forward wave and consequent reflections at the arterial pathway. $\boldsymbol{g_{1\_2}}$ represents the main forward wave, consisting on the sum of $\boldsymbol{g_1}$ and $\boldsymbol{g_2}$.

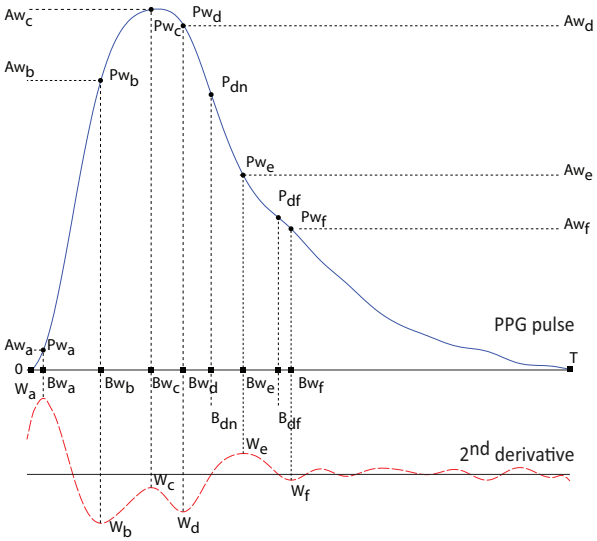

Fig. 6 – Characteristic waves proposed by Takazawa et al. [37] using DDA and an additional W_f wave used in the definition of the initial parameters and boundaries.

TABLE 1 - INITIAL PARAMETERS AND CORRESPONDING LOWER AND UPPER BOUNDARIES (LB AND UB, RESPECTIVELY) OF THE PROPOSED MULTI-GAUSSIAN MODEL.

Parameter	a_i		b_i		c_i	
	Initial value	Boundaries [lb,ub]	Initial value	Boundaries [lb,ub]	Initial value	Boundaries [lb,ub]
i=1	$0.7*Aw_a$	$[0.5*Aw_a, Aw_b]$	Bw_a	$[Bw_a, Bw_b]$	$Bw_a/3$	$[0, Bw_b/3]$
i=2	$0.9*A_{sys}^{\dagger}$	$[0.5*A_{sys}^{\dagger}, A_{sys}^{\dagger}]$	Bw_b	$[Bw_a, Bw_c]$	$Bw_b/3$	$[Bw_a/3, Bw_d/3]$
i=3	$0.5*A_{sys}^{\dagger}$	$[0.2*A_{sys}^{\dagger}, 0.8*A_{sys}^{\dagger}]$	Bw_d	$[Bw_b, B_{dn}]$	$Bw_d/3$	$[Bw_b/3, B_{dn}/3]$
i=4	$0.8*A_{dias}^{\ddagger}$	$[0, A_{dias}^{\ddagger}]$	Bw_f	$[B_{df}, T]$	$\min(Bw_f, (T-Bw_f))/3$	$[0, B_{df}]$
i=5	$0.3*A_{dias}^{\ddagger}$	$[0, A_{dias}^{\ddagger}]$	B_{dias}	$[Bw_f, T]$	$T-avg(T-Bw_f)$	$[0, B_{df}]$

$^{\dagger}A_{sys} = \max([A_2, A_3, A_4])$

$^{\ddagger}A_{dias} = \max(PPG(B_{dn}, \dots, T))$

To adjust the model parameters a least squares method combined with the interior point algorithm [38] has been adopted. Let $f(n), n \in [1, N]$ be the normalized PPG pulse, where N is the total number of samples

composing $f(n)$. Using the least squares method, the goal is to find the solution, that minimize the sum of the squared residuals as presented bellow:

$$f_{MSE}(\beta) = \frac{1}{N}\sum_{n=1}^{N}[f(n) - f_m(n,\beta)]^2 \tag{6}$$

where $f_m(n,\beta)$ is the MG model with the set of parameters $\beta_j = \{a,b,c\}_j, j = 1,\dots,5$. Using the interior point algorithm [38], we aim to solve following nonlinear constrained optimization problem

$$\begin{aligned} min \quad & f_{MSE}(\beta) \\ subject\ to \quad & g(\beta) \leq 0 \\ & lb \leq \beta \leq ub \end{aligned} \tag{7}$$

where $g(\beta) \leq 0$ and $lb \leq \beta \leq ub$ are the inequality constrains and the boundaries to which the parameters are subject. By constraining the parameters to pre-specified boundaries and relationships between them, we aim to assure the physiological foundations on the model, as well as to increase its robustness. Based on the study proposed by Baruch et al. [4], the inequality constraints are summarized bellow:

- $a_1 - a_2 \leq 0 \ \wedge \ a_1 - a_3 \leq 0$: the main objective of g_1 is to increase the fitness of the proposed model in the first portion of the systolic rise. Since it belongs to the main forward wave, we confine the amplitude of g_1 must be smaller than the following two (g_2 and g_3).
- $a_3 - a_2 \leq 0 \ \wedge \ a_4 - a_2 \leq 0$: the forward pulse has the highest amplitude [4] and therefore the amplitude of g_2 must be greater than g_3, g_4 and g_5.
- $a_5 - a_4 \leq 0$: since g_5 is a result of reflections and re-reflections in the arterial pathway, this wave is expected to have very low amplitude, i.e. the smallest within the diastolic phase. Therefore we restrict the amplitude of the last reflected wave (g_5) smaller than the second reflected pulse (g_4).
- $b_1 \leq b_2 < b_3 \leq b_4 \leq b_5$: in order to guarantee that the aforementioned relationships prevail, the location of the Gaussian functions must be increasingly larger.

2.4. Assessment of left ventricular ejection time

As the main pressure wave, created by the ejection of blood from the left ventricle, travels in the arterial pathway, it suffers from dampening, which affects both the rise and decay of the pulse. Additionally, the reflection of the main pulse in the two major reflection sites also causes drastic changes on the diastolic phase of the measured PPG pulse [27]. In order to avoid these potential sources of error, one implemented a data driven approach that resorts on the analysis of the components corresponding to the systolic phase of the PPG pulse, herein called as the systolic model (g_{sys}). g_{sys} was defined as the sum of the Gaussian functions corresponding to the main forward wave (g_1 and g_2) and late systolic peak (g_3). Since the morphological characteristics of the pulse wave (at the beginning of the aorta) change as the pulse travels the pathway, it is expectable that the time span between the onset and offset of the g_{sys} model do not exactly match the time span between the onset and offset of the left ventricular ejection. Therefore, we aim to investigate which are the characteristic points at the beginning and end of the g_{sys} model that better represent the LVET. For that purpose, a data driven approach based on a multi-derivative analysis of the g_{sys} model has been implemented. g_{sys} was differentiated using (1) to (3), resulting in the derivatives up to the 3rd order and six LVET estimates ($LVETc_i$) from the analysis of the systolic model derivatives:

- LVETc1 – Time span between systolic (D3sp) and diastolic (D3dp) peaks of the systolic model 3rd derivative.
- LVETc2 – Time span between systolic peak of the systolic model 3rd derivative (D3sp) and the notch in the systolic model 1st derivative (D1nt).

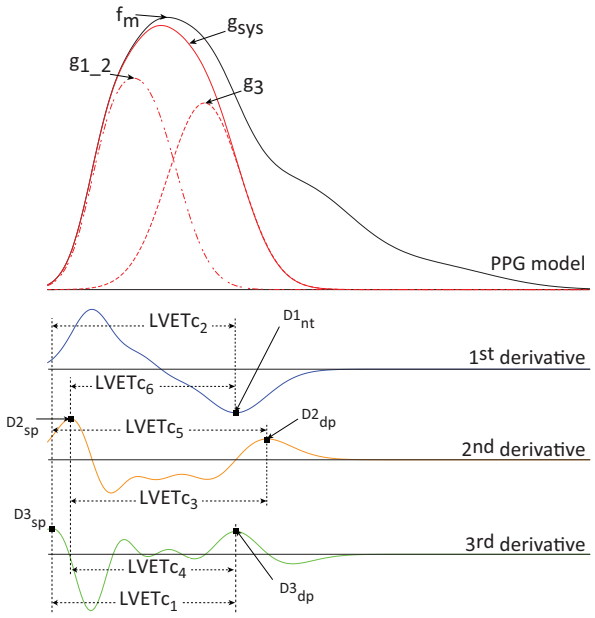

Fig. 7 – Representation of the systolic model derivatives and respective characteristic points and LVET estimates.

- LVETc3 – Time span between systolic (D2sp) and diastolic (D2dp) peaks of the systolic model 2nd derivative.
- LVETc4 – Time span between systolic peak of the systolic model 2nd derivative (D2sp) and diastolic peak of the systolic model 3rd derivative (D3dp).
- LVETc5 – Time span between systolic peak of the systolic model 3nd derivative (D3sp) and diastolic peak of the systolic model 2nd derivative (D2dp).
- LVETc$_6$ – Time span between systolic peak of the systolic model 2nd derivative (D2$_{sp}$) and the notch in the systolic model 1st derivative (D1$_{nt}$).

The characteristic points and respective LVET estimates are illustrated in Fig. 7.

2.5. Assessment of blood pressure and vascular tone surrogates

Several parameters have been suggested in the literature as potential surrogates of blood pressure and vascular tone changes [1, 4, 11, 12, 39-41]. In the current paper, we investigate two major parameters called stiffness index (SI) and reflection index (RI). The SI is associated with the velocity of a pulse wave in large arteries [13] and large artery stiffness [12]. It also correlates with pulse pressure [4] and is defined by the time span between the forward (P_s) and reflected waves (P_d), as illustrated in Fig. 8, that is:

$$SI = B_d - B_s \tag{8}$$

Additionally, the RI, associated with small artery stiffness [13] and changes in vascular tone [14, 15], is defined by the ratio between the amplitudes of both waves the forward (P_s) and reflected waves (P_d), described as follows:

$$RI = \frac{A_d}{A_s} \tag{9}$$

Additionally, we also aim to investigate the temporal and amplitude relationship between the main forward wave (P_1) with the late systolic wave (P_2) and the reflected waves (P_d) described by the 4 additional indexes (T_{1_2}, T_{1_d}, R_{1_2}, R_{1_d}), presented from (10) to (13).

$$T_{1\_2} = B_2 - B_1 \tag{10}$$

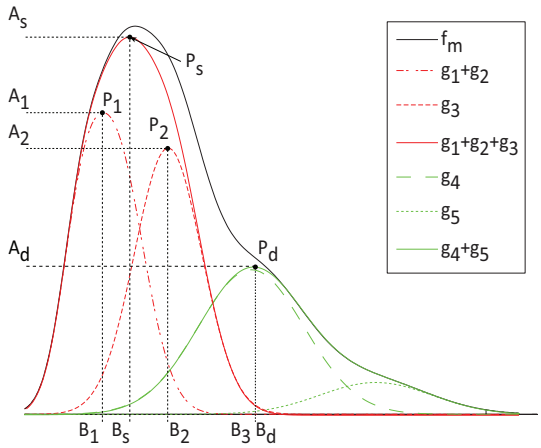

Fig. 8 - Representation of the PPG beat morphology and the defined characteristic points used to extract stiffness and reflection indexes (SI and RI, respectively).

$$T_{1\_d} = B_d - B_1 \tag{11}$$

$$R_{1\_2} = \frac{A_2}{A_1} \tag{12}$$

$$R_{1\_d} = \frac{A_d}{A_1} \tag{13}$$

While the indexes T_{1_d}, and R_{1_d}, are closely related with the SI and RI, the indexes R_{1_2} have been associated to changes the impedance mismatch of the aortic artery and is closely related with augmentation index, which has been associated aging and arterial stiffening [1, 4, 11].

3. Data collection

3.1. Experimental setup

Two databases were used in the current work. The evaluation of the LVET detection algorithm was performed on a database collected at the "Centro Hospitalar de Coimbra" (CHC), while for the investigation of the SI, T_{1_d}, T_{1_2}, RI, R_{1_d} and R_{1_2}, a database provided by the Heinrich-Heine University Hospital Düsseldorf was used. The protocols used for the collection of these databases are outlined bellow.

3.1.1. Protocol for the assessment of cardiac function surrogates

The data considered in the present paper for the assessment of cardiac function was collected in a study conducted in "Centro Hospitalar de Coimbra" (CHC) aiming at the simultaneous acquisition of PPG and Echocardiography.

In this study, patients of two distinct groups were enrolled: 1) 33 healthy subjects and 2) 35 subjects suffering from various cardiovascular diseases (CVDs) including coronary artery disease, heart failure, and comorbidities such as hypertension. All volunteers gave written informed consent to participate in this study, which was authorized by the CHC's ethical committee in 2010 under the protocol "Assessment of cardiac function using heart sounds, ICG and PPG". The characteristics of the population considered in the present study are summarized in TABLE 2.

The ECG and PPG signals were recorded with a HP-CMS monitor and stored on a laptop at a sampling frequency of 500 Hz and 125 Hz, respectively. Echocardiography (in Doppler mode, with ECG) was conducted using a Vivid 7 system from General Electric, which produces images with a temporal resolution of 500 Hz (Fig. 9). The ECG signals acquired simultaneously by the two systems described above were used to synchronize the signals streams.

The measurement protocol was supervised and conducted by an authorized medical specialist. It consisted of several acquisitions of ECHO in doppler mode and PPG collected at the right hand index finger using an infrared transmission finger probe.

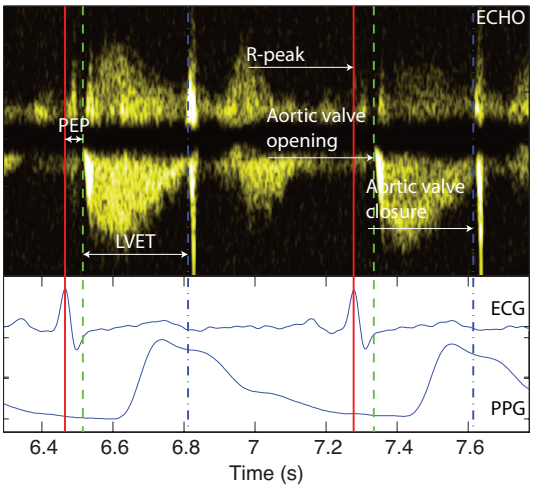

Fig. 9 - Annotation of aortic valve timings using Doppler mode ECHO.

TABLE 2 – CHARACTERISTICS OF THE VOLUNTEERS ENROLLED IN THE STUDY FOR THE ASSESSMENT OF CARDIAC FUNCTION.

	Healthy (#33)	CVD (#35)
Age	29± 8	58± 17
Weight	74.3 ± 11.1	70.6 ± 12.6
BMI	24± 2	25± 3
Male/female	32/1	20/15

A clinical expert annotated the ECHO-doppler images. The time instant corresponding to the opening of the aortic valve was defined as onset of the left ventricular outflow lobe, while the closure of the aortic valve was defined immediately before the closing click onset, produced by the residual reflux after the closure of the aortic valve cusps. An example is shown in Fig. 9.

In this study a total of 2081 heartbeats have been annotated, of which 1109 beats correspond to healthy volunteers and 972 beats correspond to CVD subjects.

3.1.2. Protocol for the assessment of blood pressure and vascular tone surrogates

The data screened in this paper for the assessment of blood pressure and vascular tone surrogates was acquired in a study at the Heinrich-Heine University Hospital Düsseldorf, Division of Cardiology, Pneumology and Angiology aiming at the collection of bio-signals for the development of algorithms capable of detecting and predicting hemodynamic instability in patients suspected to be at risk for a sudden loss of consciousness.

In this study, 55 patients with unexplained syncope were scheduled for diagnostic head-up tilt table tests (HUTT), following the recommendations of the European Society of Cardiology (ESC). The study was approved by the local ethics committee and complied with international standards (ClinicalTrials.gov identifier: NCT01262508). All volunteers gave written informed consent to participate.

The HUTT protocol consisted of four phases: 1) the patient was at rest in supine position for at least 15 min; 2) the patient did a passive standing exercise (70º) for 20 min; 3) in the absence of syncope, the phase (2) was extended by 15 min with sublingual administration of min 400 µg of glycerol trinitrate (GTN); 4) the patient was tilted back to supine position. At any time, if a syncope episode occurred, the patient was brought back to supine position immediately for recovery and the HUTT protocol was stopped. The nurse accompanying the study documented any prodromal symptoms (e.g. dizziness, sweat, tremor, etc.) during the procedure.

Data of 12 patients had to be removed due to the presence of heart rhythm other than sinus rhythm or poor data quality in BP and PPG signals. The characteristics of the resulting study population consisting of 43 patients are summarized in TABLE 3.

The ECG and PPG signals were acquired with a Philips MP50 patient monitor and stored on a laptop. Blood pressure was continuously measured (beat-to-beat) using a "Taskforce Monitor" [12]. Data coming from both systems were aligned in time via the synchronously detected ECG signals. Details of the acquisition system can be found in [42].

TABLE 3 – CHARACTERISTICS OF THE VOLUNTEERS ENROLLED IN THE STUDY FOR THE ASSESSMENT OF BLOOD PRESSURE AND VASCULAR TONE SURROGATES.

	Tilt positive (#21)	Tilt negative (#22)
Age [y]	57±18	63±17
Weight [kg]	86±15	74±13
BMI [kg/m2]	27.1±4.6	26±5
Male/female	13/8	10/12
GTN‡ (yes/no)	15/6	15/7

‡ Glycerol trinitrate

3.2. Data synchronization

The synchronization of the data obtained during the before mentioned studies was performed using an algorithm based on the minimization of the error between the RR intervals time series assessed from the ECG's of both systems, using the minimum least squares error criterion. Let $RR_1(k)$, k=1,…,K, and RR $RR_2(m)$, m=1,…,M (K<M) be the RR intervals time series of the ECGs to be synchronized. The time instant *t* at which both time series are synchronized is:

$$t = \underset{w=0,\ldots,M-K}{\operatorname{argmin}} f_{sync}(w) \tag{14}$$

$$f_{sync}(w) = \frac{1}{K}\sum_{k=1}^{K} \left(RR1\ (k+w) - RR2\ (k)\right)^2 \tag{15}$$

where f_{sync} is the synchronization time series.

4. Results and discussion

4.1. Estimation of Left Ventricular Ejection Time

The algorithms' performance for LVET inference was analyzed for the whole dataset described in section 3.1.1, referred to as global dataset in the following, and in the two subsets that compose it. These are the subset of healthy volunteers, called the healthy subset and the subset of volunteers with cardiovascular diseases, called the CVD subset.

To evaluate the performance achieved by the proposed algorithm, four performance metrics have been adopted. Let $LVET_{MEAS}$:{$LVETc_1$,…, $LVETc_6$, $LVET_{CHAN}$} be the measured beat-to-beat LVET values, corresponding to estimate 1 to 6 and the LVET obtained using the algorithm proposed by Chan et al. [27], respectively, and $LVET_{ECHO}$ be the reference beat-to-beat LVET values assessed using ECHO-doppler. The abbreviation "Error" stands for the error between measured and reference values ($LVET_{MEAS} - LVET_{ECHO}$), while "Abs. Error" concerns to the absolute estimation error ($|LVET_{MEAS} - LVET_{ECHO}|$). The "Abs. Error Perc." stands for the percentage of absolute estimation error ($|LVET_{MEAS} - LVET_{ECHO}|/\overline{LVET_{ECHO}}$). The agreement between measured LVET and $LVET_{ECHO}$ was analyzed by assessing the correlation coefficients between the two variables in each dataset (Global, healthy and CVD). Additionally, the correlation coefficients were also calculated for each volunteer and the average and standard deviation over each dataset was calculated. The Pearson correlation coefficient was calculated if the variables were normally distributed, while the Spearman's correlation coefficients were used otherwise. The p-values corresponding to the coefficients shown in TABLE 4 were low (p<0.05), enabling the rejection of the hypothesis of no correlation.

The agreement between $LVET_{MEAS}$ and $LVET_{ECHO}$ was also analyzed using the Regression plots (Fig. 10) and the Bland-Altman plot (Fig. 11). Error distributions were tested for gaussianity using the Kolmogorov–Smirnov test. Accordingly, statistical analysis was performed using the paired Student test and the two-sided Wilcoxon signed rank test and the values shown in TABLE 4 have been found to be statistically relevant (p<0.001).

In TABLE 4 we present the results achieved by our algorithm approach for all extracted LVET estimates. One observes that the best estimation performance was achieved by the $LVETc_6$ estimate (measured between $D2_{sp}$ and $D1_{nt}$), with an absolute estimation error of 15.41±13.66 ms, corresponding to a percentage of error of

TABLE 4 - SUMMARY OF THE RESULTS ACHIEVED BY THE PROPOSED LVET ESTIMATION ALGORITHM AND THE ALGORITHM PROPOSED BY CHAN ET AL. [27]. ALL THE PRESENTED VALUES ARE STATISTICALLY SIGNIFICANT.

Context	Measured LVET	Error (msec.) Avg ± std	Abs. Error (msec.) Avg ± std	Abs. Error (%) Avg ± std	ρ	ρ Avg ± std	Range
Global	$LVET_{CHAN}$	18.75±19.78	23.01±14.60	8.19±5.20	0.75*	0,58±0,19	[186.2;388.9]
	$LVETc_1$	22.35±23.91	28.43±16.21	10.19±5.81	0.70*	0,56±0,16	
	$LVETc_2$	22.66±19.68	26.13±14.76	9.37±5.29	0.77*	0,56±0,17	
	$LVETc_3$	47.02±23.93	47.74±22.46	17.12±8.05	0.75	0,55±0,16	
	$LVETc_4$	-6.57±24.09	18.72±16.51	6.71±5.92	0.70*	0,59±0,18	
	$LVETc_5$	75.9±23.99	75.96±23.78	27.24±8.53	0.68*	0,54±0,15	
	$LVETc_6$	-6.22±19.63	15.41±13.66	5.53±4.9	0.78*	0,58±0,17	
Healthy	$LVET_{CHAN}$	31.19±12.26	31.03±12.66	11.7±4.61	0.71*	0,48±0,11	[186.2;318.6]
	$LVETc_1$	36.15±14.84	36.7±13.43	13.85±5.07	0.84	0,45±0,1	
	$LVETc_2$	31.69±13.92	31.99±13.21	12.07±4.99	0.86	0,5±0,14	
	$LVETc_3$	57.09±18.51	57.12±18.43	21.56±6.96	0.76	0,52±0,14	
	$LVETc_4$	7.63±14.38	12.91±9.91	4.87±3.74	0.73*	0,49±0,14	
	$LVETc_5$	85.76±18.91	85.76±18.91	32.37±7.14	0.74	0,48±0,11	
	$LVETc_6$	3.03±13.66	10.88±8.79	4.11±3.32	0.72*	0,52±0,15	
CVD	$LVET_{CHAN}$	6.49±15.93	13.48±10.68	4.52±3.58	0.88*	0,66±0,2	[213.5;388.9]
	$LVETc_1$	7.19±20.16	17.75±11.95	5.99±4.04	0.84*	0,67±0,14	
	$LVETc_2$	11.59±19.39	18.72±12.63	6.32±4.27	0.84*	0,61±0,19	
	$LVETc_3$	34.69±23.38	36.07±21.2	12.18±7.16	0.81*	0,59±0,18	
	$LVETc_4$	-21.94±20.16	23.99±17.67	8.1±5.97	0.84*	0,69±0,15	
	$LVETc_5$	63.82±23.37	63.9±23.16	21.58±7.82	0.80*	0,61±0,17	
	$LVETc_6$	-17.65±19.04	20.63±15.75	6.97±5.32	0.85*	0,63±0,18	

*Estimated values using Spearman's correlation.

5.53±4.9%. The performance of the remaining estimates in the global dataset, are much less good ranging from 26.13±14.76 to 75.96±23.78 ms. An exception is observed for the $LVETc_4$ estimate (measure between $D2_{sp}$ and $D3_{dp}$) that obtained an absolute estimation error of 18.72±16.51 ms, representing an increase in the estimation error percentage of about 1% (3 ms). The correlation between the measured LVET estimates and the echocardiographic LVET reference was high and ranged from 0.68 ($LVETc_5$) to 0.78 ($LVETc_6$).

The results regarding the evaluation of the proposed LVET estimates in both Healthy and CVD subsets are also presented in TABLE 4. In the Healthy subset, we observed a decrease in the absolute estimation error of about 5ms for both $LVETc_4$ and $LVETc_6$, representing a reduction of about 1-2%. Contrarily, a decrease in the performance of the remaining estimates was observed for this subset, with an increase in the estimation error ranging from 3 to 5%. The agreement between both measure and reference LVET's increased for all the LVET estimates, with an exception to $LVETc_6$, where a decrease of about 6% was observed. Contrarily to the results observed in the Healthy subset, in the CVD subset we observed a decrease in the performance achieved by $LVETc_4$ (23.99±17.67 ms) and $LVETc_6$ (20.63±15.75 ms) and a decrease in the absolute estimation error of the remaining LVET estimates. Moreover, an increase in the agreement between measured and reference LVET values was also observed in this study group, being $LVETc_6$ the estimate with highest correlation coefficient (ρ=0.85).

The correlation coefficients calculated in a patient-by-patient basis presented results similar (but lower, ≈ 0.15 less) to those calculated in each dataset, showing a lower agreement between the measured LVET values and the $LVET_{ECHO}$, which is mainly explained by the absence of marked trend within each volunteer measured values.

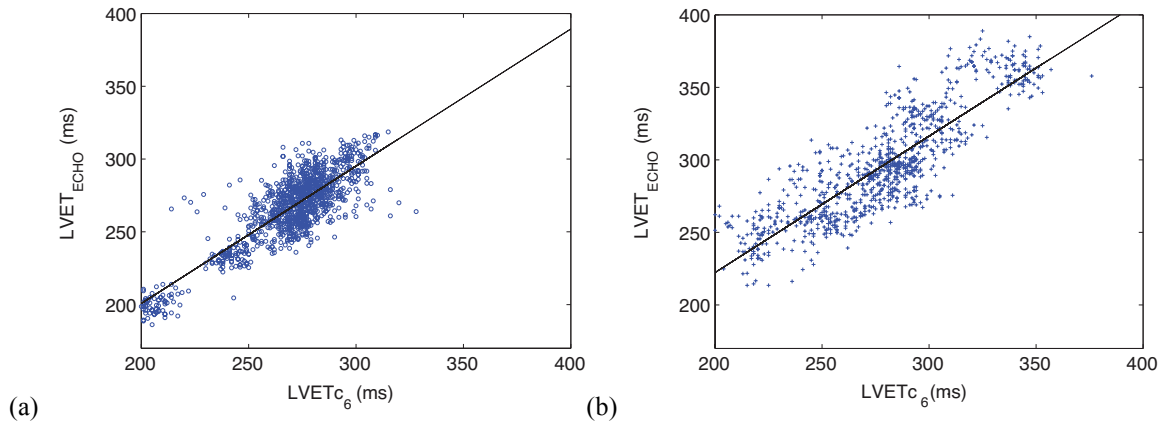

Fig. 10 – Regression plots of $LVETc_6$. (a) Healthy subset ($\rho = 0.72$): best linear fit $y = 12.05 + 0.94x$. (b) CVD subset ($\rho = 0.85$): best linear fit $y = 34.27 + 0.94x$.

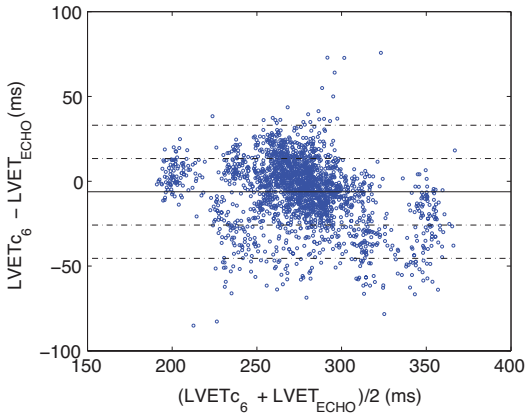

Fig. 11 - The Bland-Altman plot of the measured ($LVETc_6$) and reference LVET using the proposed algorithm in the Global dataset.

Comparing the best LVET estimate ($LVETc_6$) with the LVET obtained using the algorithm proposed by Chan et al. [27], one observes that the best estimation performance was achieved by our method, which obtained better estimation performance (15.41±13.66 msec. vs 23.01 ± 14.60 msec.) and higher correlation (0.78 vs 0.75). In the healthy context, a significant improvement as been achieved by $LVETc_6$ (Abs. Error: 10.88±8.79 msec. and ρ=0.72) compared to the algorithm by Chan et al. [27] (Abs. Error: 31.03 ± 12.66 msec. and ρ=0.71). In contrast, Chan's method performs better for CVD patients compared to our implementation (13.48 ± 10.68 msec. vs 20.63±15.75 msec). Finally, Chan's algorithm achieved a better correlation coefficient for CVD patients (ρ=0.88 vs ρ=0.85).

In Fig. 10 we present the regression plots corresponding to the best LVET estimate ($LVETc_6$) in both Healthy and CVD subsets. For the healthy subset (Fig. 10 (a)), the best linear fit corresponds to a 0.94 slope, which is very close to unity. This agrees with the low estimation error achieved by $LVETc_6$ and the high correlation value presented in TABLE 4. For the CVD subset Fig. 10 (b)), a similar slope of 0.94 was achieved, but with a greater dispersion of the reference/measure LVET pairs.

The agreement between the $LVETc_6$ and $LVET_{ECHO}$ was also assessed via Bland-Altman plot, presented in Fig. 11 for the Global dataset. The horizontal solid line represents the mean error while the dashed lines denote the level of agreement between $LVETc_6$ and $LVET_{ECHO}$, i.e. mean ± standard deviation and mean ± 2 standard deviation. One can observe that the average error is close to zero and the estimation error is not evenly distributed around the whole range of LVET values, particularly in the higher range where a greater dispersion is shown.

The presented results show that the characteristic points that better define the onset and end of the ventricular ejection on the PPG pulse are the systolic peak defined in the second derivative and the notch defined the 1st derivative. Not surprisingly, these two points do not match exactly the onset and offset of the PPG main forward wave resultant from the ventricular ejection. This can be explained by the temporal and

morphological changes experienced by the main pulse as it travels from the left ventricle to the peripheral sites. The reduction of arterial compliance [5] and the increase peripheral resistance [1], due to the changes in the arterial wall composition and the tapering of the arteries, dampens the main pulse, and therefore a temporal shift is observed in the onset and offset of the PPG pulse. Instead, the characteristic points corresponding to the boundaries of the ejection in the PPG systolic model are determined by the characteristic points corresponding to the maximum acceleration at the systolic rise of the systolic model and by the minimum velocity during its decay. Contrarily, the remaining LVET estimates calculated form the characteristic points closer to the onset/offset of the systolic model present a higher error, resulting from an overestimation.

Our results also indicate a discrepancy in the estimation of LVET within Healthy and CVD patients. In the Healthy dataset, the absolute estimation error achieved by $LVETc_6$ was very low (ap. 10.9 ms), while in the CVD the absolute error almost doubled (ap. 20.6ms) accentuated by the underestimation of the LVET (error: -17.65±19.04ms). One possible reason for the underestimation of LVET in the CVD population is the dependence of the pulse transmission on the PWV. One common characteristic observed in aging and in populations with cardiovascular diseases, is the increase of the pulse wave velocity, mainly due to the increase of the vascular resistance and stiffness, which leads to a faster transmission of reflected waves along the arterial pathway and early appearance in the PPG pulse [1, 11]. With the aging of the arteries (and the presence of atherosclerosis), there is a progressively return of the reflected waves, which can arrive so early during systole that it becomes difficult to distinguish the two phases [12]. This phenomenon is believed to negatively affect the proposed algorithm in two aspects. The first is the increase in the uncertainty in the identification of the systolic and diastolic phase boundaries, which consequently affects the remaining modeling process. The second is the overestimation of the Gaussian parameters related with the reflected waves in the diastolic phase, due to the attempt of the model to fit the increased (in amplitude and length) falling edge of the diastolic phase. As a consequence of this overestimation, the amplitude and length systolic model is diminished leading to an underestimation of the $LVETc_6$. Another characteristic that is believed to accentuate the problematic is the elongation of the systolic rising edge, commonly associated with aging. As a result of this elongation, the characteristic points corresponding to the maximum acceleration of the systolic model appear at a later instant and therefore a decrease in the LVET estimate is observed.

4.2. Assessment of blood pressure and vascular tone surrogates

In this section we analyze the relationship between the extracted blood pressure and vascular tone surrogates with the reference blood pressure and total peripheral resistance values. The relationship was evaluated in the dataset composed by all volunteers (Global dataset) and in the subset composed by volunteers where greater blood pressure changes are observed, i.e., the tilt positive group (Tilt positive dataset). The relationship between variables was evaluated for the upright position phase of the HUTT protocol. The extracted reference values used in the present analysis are: systolic (SBP), diastolic (DBP) and mean blood pressure (MBP), pulse pressure (PP) and total peripheral resistance index (TPRI). These parameters were compared with the extracted surrogates, i.e., SI, T_{1_d}, T_{1_2}, RI, R_{1_d} and R_{1_2}, in order to identify the parameters that better characterize blood pressure and vascular tone changes, and their level of agreement with those parameters.

Let m=1,…,M with M=43 be the volunteers, x_{meas}={SI, T_{1_2}, T_{1_d}, RI, R_{1_2}, R_{1_d}} the measured parameters and x_{ref}={SBP,DBP,MBP,PP,TPRI} the reference parameters, assessed in a beat-to-beat basis. The agreement (ρ_p) between the measured and reference parameters for each volunteer using the Pearson correlation coefficient was defined as:

$$\rho_p(x_{meas}, x_{ref}) = \frac{1}{M}\sum_{m=1}^{M} \left|\rho(x_{meas}, x_{ref})\right| \tag{16}$$

In TABLE 5 and TABLE 6 we present the Pearson correlation coefficients ρ_p achieved by each extracted features and the reference parameters, for the global and tilt positive datasets. The p-values corresponding to the coefficients shown in TABLE 5 and TABLE 6 were low ($p<0.05$), enabling the rejection of the hypothesis of no correlation.

From TABLE 5 and TABLE 6, one can observe that the parameter achieving the best correlation coefficient in the global dataset is the T_{1_2}, which presented a correlation with TPRI, SBP of 0.45 and 0.43, respectively.

TABLE 5 – CORRELATION BETWEEN THE EXTRACTED (SI, T_{1_D} AND T_{1_2}) AND REFERENCE PARAMETERS (SBP, DBP, MBP, PP, TPRI).

Parameters	Absolute Correlation coefficient (ρ_p)			Range
	SI (Global/Tilt positive)	T_{1_d} (Global/Tilt positive)	T_{1_2} (Global/Tilt positive)	
SBP	0.41 / 0.57	0.39 / 0.53	0.43 / 0.49	[22.3;247.1] mmHg
DBP	0.42 / 0.54	0.41 / 0.51	0.40 / 0.41	[1.7;141.5] mmHg
MBP	0.41 / 0.57	0.38 / 0.53	0.40 / 0.43	[8.3;168.5] mmHg
PP	0.33 / 0.41	0.34 / 0.39	0.41 / 0.47	[0; 147.7] mmHg
TPRI	0.41 / 0.51	0.37 / 0.46	0.45/ 0.46	[215.7;7427.2] dyne*s*m^2/cm^5

TABLE 6 – CORRELATION BETWEEN THE EXTRACTED (RI, R_{1_D} AND T_{1_2}) AND REFERENCE PARAMETERS (SBP, DBP, MBP, PP, TPRI)

Parameters	Absolute Correlation coefficient (ρ_p)			Range
	RI (Global/Tilt positive)	R_{1_d} (Global/Tilt positive)	R_{1_2} (Global/Tilt positive)	
SBP	0.40 / 0.52	0.36 / 0.49	0.21 / 0.23	[22.3;247.1] mmHg
DBP	0.38 / 0.46	0.37 / 0.43	0.23 / 0.25	[1.7;141.5] mmHg
MBP	0.40 / 0.52	0.37 / 0.44	0.22 / 0.24	[8.3;168.5] mmHg
PP	0.37 / 0.44	0.33 / 0.40	0.25 / 0.26	[0; 147.7] mmHg
TPRI	0.43 / 0.5	0.42 / 0.45	0.26 / 0.27	[215.7;7427.2] dyne*s*m^2/cm^5

Additionally, the parameter SI and T_{1_d} were also moderately correlated with the reference blood pressure measurements and with the TPRI, with values ranging from 0.37 (between T_{1_d} and TPRI) to 0.42 (between SI and DBP). Similarly, the parameters RI and R_{1_d} also showed a good agreement with the reference parameters (excluding PP) being the highest correlation with TPRI ($\rho_p = 0.43$ and $\rho_p = 0.42$, respectively). The parameter R_{1_2} showed to be weakly associated with each of the reference parameters, with ρ_p ranging from 0.21 to 0.26.

Regarding the results in the tilt positive group, one can observe a marked increase in the agreement between the majority of the measured and reference parameters. In this group of patients, the highest agreement was found between the SI and MBP ($\rho_p = 0.57$), SBP ($\rho_p = 0.57$) and DBP ($\rho_p = 0.54$). Not surprisingly, the parameter T_{1_d} also presented a high agreement with MBP and SBP ($\rho_p = 0.53$). The parameter most closely associated with TPRI in the tilt positive volunteers was the SI ($\rho_p = 0.51$). The parameter T_{1_2} showed to be more closely associated with the SBP, PP and TPRI, with a level of agreement of 0.49, 0.47 and 0.46, respectively. From TABLE 6, one can observe a similar (but lower) agreement between the parameters RI, R_{1_d} and R_{1_2} and the reference parameters, with the highest level of agreement being found between RI and SBP ($\rho_p = 0.52$) and between RI and TPRI ($\rho_p = 0.50$). The parameter R_{1_2} presented low correlation ($\rho_p \epsilon [0.23; 0.27]$) with all the reference parameters.

The level of agreement between the surrogate that presented the best results (i.e., SI) and the SBP are illustrated by the regression plots present in Fig. 12 a) and b), for two volunteers. A linear model SBP = A*SI+B was applied on the data extracted from volunteer 7 (Fig. 12 a)) and volunteer 36 (Fig. 12 b)). For volunteer 7, the best linear fit corresponds to a negative slope A=-1.8, which is very far from the unit. For volunteer 36, the best linear fit corresponds to similar slope A=-2.28. From Fig. 12 it is possible to observe a strong linear and negative correlation between SI and SBP, especially for lower values of SBP (high values of SI). The higher dispersion SI/SBP points for high SBPs, particularly above 130 mmHg, suggest a higher uncertainty in the SI measurement, resulting from the increasingly overlapping of the forward and reflected waves.

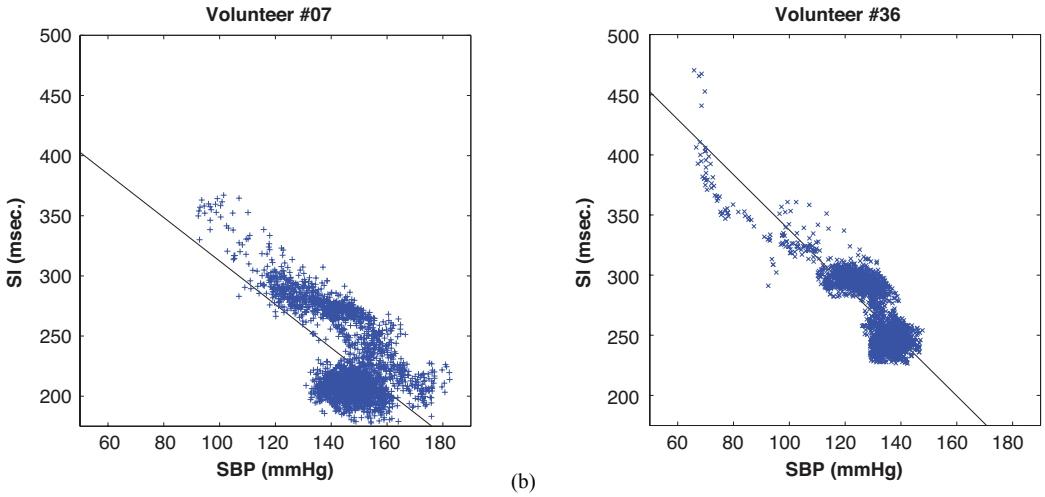

(a) (b)

Fig. 12 – Regression plots of SI-SBP. (a) Volunteer #07 (ρ = 0.-0.64): best linear fit $SBP_e = -1.8*SI + 491$. (b) Volunteer #36 (ρ = -0.84): best linear fit $SBP_e = -2.28*SI + 565.6$.

The results presented in this section suggest that the extracted parameters can be associated with changes in blood pressure and vascular resistance. The presented results regarding the SI and T_{1_d} parameters for SBP, DBP and MBP are consistent with those found by Millasseau et al. [43] (ρ_p =0.48/0.68/0.51 for SBP/DBP/MDP), by Padilla et al. [44] (ρ_p =0.41/0.40/0.44 for SBP/DBP/MDP) and by Brillante et al. [45] (ρ_p =0.42/0.52/0.51 for SBP/DBP/MDP). Contrarily, the low agreement between RI and blood pressure measurements reported by in [43-45] (ρ_p<0.18 for SBP, ρ_p< 0.28 for DBP and ρ_p<0.24 for MBP) was not found in our analysis, where the correlation found with SBP, DBP and MBP was above 0.38 for the global dataset and above 0.46 for the tilt positive dataset. The low correlation found between the R_{1_2} and SBP was not consistent with the association between reported by Baruch et al. [4]. This discrepancy is mainly explained by the normalization of the PPG pulse performed in the present study, and by the modalities used in the study reported in [4]. While Baruch et. al [4] used the absolutes amplitudes of the main forward and first reflection waves (assessed from the arterial blood pressure waveform) to estimate R_{1_2}, in the present study the R_{1_2} parameter was assessed from the normalized pulse (assessed from the photoplethysmogram). The lower correlation between SI, T_{1_d} and PP ($\rho_p \approx 0.33$) found in the present study is in agreement with that found by Padilla et al. [44] ($\rho_p = 0.24$), but not with the association outlined in [4].

The increase in the agreement between the SI, RI and the reference parameters, from the global dataset to the tilt positive dataset, show the importance of these parameters in the assessment of blood pressure and vascular tone changes, specially in cases where acute vasodilatation is present, which is the case of the patients suffering from syncope (tilt positive group).

5. Conclusions and Outlook

The PPG is a promising tool to deploy solutions for ambulatory and personal health applications. Its successful utilization still lacks convincing signal processing methods that are reliable and accurate enough for the extraction and sophisticated interpretation of PPG waveform characteristics, beyond simple heart rate determination.

In the present study an algorithm for the extraction of cardiovascular performance surrogates from the photoplethysmographic (PPG) waveform is introduced. The proposed methodology is based on the segmentation of the PPG signal, and consequently modeling each PPG pulse as a sum of 5 Gaussian functions. Using the reference echocardiographic LVET values extracted using Echocardiography from 68 Healthy and Cardiovascular diseased volunteers, we were able to evaluate the performance of six LVET estimates. The best LVET estimate ($LVETc_6$) achieved a low estimation error (ap. 15 ms) and a high correlation (ρ=0.78) on a dataset composed by 2081 annotated heartbeats. Although $LVETc_6$ did not present the best estimation error for the population with cardiovascular diseases, a high correlation (ρ=0.85) with the reference LVET was still achieved, supporting the use of the PPG for the assessment of LVET changes.

The relationship between the amplitude and location of the Multi-Gaussian model waves was also investigated in the current paper, leading to the definition of 6 parameters related to stiffness and reflection indexes. Their relationship with reference values of blood pressure and total peripheral resistance extracted from a Taskforce Monitor was evaluated in the tilt positive group. We were able to conclude that the extracted surrogates are associated with both changes in blood pressure and total peripheral resistance. T_{1_2} index was found to have the highest correlation within the overall dataset, presenting a moderate agreement with the total peripheral resistance ($\rho_p = 0.45$) and with SBP ($\rho_p = 0.43$). Moreover, a similar agreement was found between SI and the reference parameters (excepting PP), with the coefficients ranging from 0.41 to 0.42. In the tilt positive group, the stiffness index presented the highest agreement with mean blood pressure and systolic blood pressure ($\rho_p = 0.57$). Although this surrogate exhibits a good level of agreement with the majority of the remaining reference parameters ($\rho_p = 0.51$ to $\rho_p = 0.57$), a lower correlation was found with the pulse pressure ($\rho_p = 0.41$). Moreover, an exception was also observed for the parameter R_{1_2}, corresponding to the amplitude ratio between the main forward pulse and the first reflection at the renal reflection site, which exhibit a low correlation with all the reference parameters ($\rho_p = 0.22$). The results obtained during the current analysis suggest that the stiffness and the reflection indexes can be robustly estimated from the analysis of the systolic and diastolic components of the proposed model. Moreover, the good correlation with the reference parameters suggest that these indexes can provide valuable information about blood pressure and vascular tone changes and especially in patients presenting hemodynamic instability.

Acknowledgments

The authors would like to express their gratitude for the support of “Centro Hospitalar de Coimbra” and specially the effort of Dr. Leitão Marques in facilitating the arrangements for the data acquisition component of the present study. We also thank Sandy Gläser for excellent technical support.

This work was supported by CISUC (Center for Informatics and Systems of University of Coimbra) and by EU projects HeartCycle (FP7-216695), HeartSafe (PTDC-EEI-PRO-2857-2012) and iCIS (CENTRO-07-ST24-FEDER-002003).

Jens Muehlsteff is employed by Philips Research in the Netherlands.

C.M. and C.E. are funded by the Research Committee of the medical faculty of the University of Düsseldorf. C.M. also holds a research grant from Biotronik and the Hans-und-Gertie-Fischer-Stiftung.

References

[1] J. Allen, "Photoplethysmography and its application in clinical physiological measurement," *Physiological Measurement,* vol. 28, p. R1, 2007.

[2] A. Reisner, P. A. Shaltis, D. McCombie, and H. H. Asada, "Utility of the Photoplethysmogram in Circulatory Monitoring," *Anesthesiology,* vol. 108, pp. 950-958 10.1097/ALN.0b013e31816c89e1, 2008.

[3] S. C. Millasseau, J. M. Ritter, K. Takazawa, and P. J. Chowienczyk, "Contour analysis of the photoplethysmographic pulse measured at the finger," *J Hypertens,* vol. 24, pp. 1449-56, Aug 2006.

[4] M. Baruch, D. Warburton, S. Bredin, A. Cote, D. Gerdt, and C. Adkins, "Pulse Decomposition Analysis of the digital arterial pulse during hemorrhage simulation," *Nonlinear Biomedical Physics,* vol. 5, p. 1, 2011.

[5] M. O'Rourke, "Mechanical Principles in Arterial Disease," *Hypertension,* vol. 26, pp. 2-9, July 1, 1995 1995.

[6] D. Goswami, K. Chaudhuri, and J. Mukherjee, "A New Two-Pulse Synthesis Model for Digital Volume Pulse Signal Analysis," *Cardiovascular Engineering,* vol. 10, pp. 109-117, 2010/09/01 2010.

[7] M. Huotari, A. Vehkaoja, K. Määttä, and J. Kostamovaara, "Pulse waveforms are an indicator of the condition of vascular system," in *World Congress on Medical Physics and Biomedical Engineering May 26-31, 2012, Beijing, China*. vol. 39, M. Long, Ed., ed: Springer Berlin Heidelberg, 2013, pp. 526-529.

[8] U. Rubins, "Finger and ear photoplethysmogram waveform analysis by fitting with Gaussians," *Medical and Biological Engineering and Computing,* vol. 46, pp. 1271-1276, 2008.

[9] C. Liu, D. Zheng, A. Murray, and C. Liu, "Modeling carotid and radial artery pulse pressure waveforms by curve fitting with Gaussian functions," *Biomedical Signal Processing and Control,* vol. 8, pp. 449-454, 9// 2013.

[10] L. Wang, L. Xu, S. Feng, M. Q. H. Meng, and K. Wang, "Multi-Gaussian fitting for pulse waveform using Weighted Least Squares and multi-criteria decision making method," *Computers in Biology and Medicine,* vol. 43, pp. 1661-1672, 11// 2013.
[11] M. F. O'Rourke, A. Pauca, and X. J. Jiang, "Pulse wave analysis," *British Journal of Clinical Pharmacology,* vol. 51, pp. 507-522, 2001.
[12] S. C. Millasseau, R. P. Kelly, J. M. Ritter, and P. J. Chowienczyk, "Determination of age-related increases in large artery stiffness by digital pulse contour analysis," *Clin Sci (Lond),* vol. 103, pp. 371-7, Oct 2002.
[13] S. S. DeLoach and R. R. Townsend, "Vascular Stiffness: Its Measurement and Significance for Epidemiologic and Outcome Studies," *Clinical Journal of the American Society of Nephrology,* vol. 3, pp. 184-192, 2008.
[14] P. J. Chowienczyk, R. P. Kelly, H. MacCallum, S. C. Millasseau, T. L. G. Andersson, R. G. Gosling, *et al.*, "Photoplethysmographic assessment of pulse wave reflection: Blunted response to endothelium-dependent beta2-adrenergic vasodilation in type II diabetes mellitus," *J Am Coll Cardiol,* vol. 34, pp. 2007-2014, December 1 1999.
[15] A. Laucevicius, L. Ryliskyte, Z. Petruioniene, MildaKovaite, and N. Misonis, "First Experience With Salbutamol - Induced Changes In The Photoplethysmographic Digital Volume Pulse," presented at the Seminars in Cardiology, 2002.
[16] F. Andre, C. Celik, H. Abdel-Aty, M. Santos, E. Giannitsis, H. Katus, *et al.*, "Comparison of parameters for left ventricular volumes and function between echocardiography and cardiovascular magnetic resonance in a large group of cardiac patients," *Journal of Cardiovascular Magnetic Resonance,* vol. 15, p. E74, 2013.
[17] T. C. Gillebert, N. V. de Veire, M. L. De Buyzere, and J. D. Sutter, "Time intervals and global cardiac function. Use and limitations," *European Heart Journal,* vol. 25, pp. 2185-2186, December 1 2004.
[18] A. M. Weissler, W. S. Harris, and C. D. Schoenfield, "Systolic Time Intervals in Heart Failure in Man," *Circulation,* vol. 37, pp. 149-159, February 1 1968.
[19] T. Geeraerts, P. Albaladejo, A. D. Declère, J. Duranteau, J.-P. Sales, and D. Benhamou, "Decrease in Left Ventricular Ejection Time on Digital Arterial Waveform during Simulated Hypovolemia in Normal Humans," *The Journal of Trauma and Acute Care Surgery,* vol. 56, pp. 845-849, 2004.
[20] D. Bellavia, P. A. Pellikka, T. P. Abraham, G. Al-Zahrani, A. Dispenzieri, J. Oh, *et al.*, ""Hypersynchronization" by Tissue Velocity Imaging in Patients with Cardiac Amyloidosis," *Heart,* May 12, 2008 2008.
[21] R. Q. Migrino, R. K. Mareedu, D. Eastwood, M. Bowers, L. Harmann, and P. Hari, "Left Ventricular Ejection Time on Echocardiography Predicts Long-Term Mortality in Light Chain Amyloidosis," *Journal of the American Society of Echocardiography,* vol. 22, pp. 1396-1402, 2009.
[22] B. Sztrymf, S. Günther, E. Artaud-Macari, L. Savale, X. Jaïs, O. Sitbon, *et al.*, "Left ventricular ejection time in acute heart failure complicating precapillary pulmonary hypertension," *Chest,* vol. 144, pp. 1512-1520, 2013.
[23] T. Ono, M. Miyamura, Y. Yasuda, T. Ito, T. Saito, T. Ishiguro, *et al.*, "Beat-to-Beat Evaluation of Systolic Time Intervals during Bicycle Exercise Using Impedance Cardiography," *The Tohoku Journal of Experimental Medicine,* vol. 203, pp. 17-29, 2004.
[24] P. Carvalho, R. P. Paiva, R. Couceiro, J. Henriques, I. Quintal, J. Muehlsteff, *et al.*, "Assessing systolic time-intervals from heart sound: a feasibility study," in *31st Annual International Conference of the IEEE Engineering in Medicine and Biology Society, 2009. EMBS 2009*, 2009, pp. 3124-8.
[25] R. P. Paiva, P. Carvalho, X. Aubert, J. Muehlsteff, J. Henriques, and M. Antunes, "Assessing PEP and LVET from heart sounds: algorithms and evaluation," in *31st Annual International Conference of the IEEE Engineering in Medicine and Biology Society, 2009. EMBS 2009*, 2009, pp. 3129-33.
[26] R. P. Paiva, P. Carvalho, R. Couceiro, J. Henriques, M. Antunes, I. Quintal, *et al.*, "Beat-to-beat systolic time-interval measurement from heart sounds and ECG," *Physiological Measurement,* vol. 33, p. 177, 2012.
[27] G. H. Chan, P. M. Middleton, B. G. Celler, L. Wang, and N. H. Lovell, "Automatic detection of left ventricular ejection time from a finger photoplethysmographic pulse oximetry waveform: comparison with Doppler aortic measurement," *Physiological Measurement,* vol. 28, p. 439, 2007.
[28] R. Couceiro, P. Carvalho, R. P. Paiva, J. Henriques, M. Antunes, I. Quintal, *et al.*, "Multi-Gaussian fitting for the assessment of left ventricular ejection time from the Photoplethysmogram," in *EMBC2012*, San Diego, 2012.
[29] V. Quarry-Pigott, R. Chirife, and D. H. Spodick, "Ejection time by ear densitogram and its derivative. Clinical and physiologic applications," *Circulation,* vol. 48, pp. 239-46, Aug 1973.
[30] J. A. Sukor, S. J. Redmond, and N. H. Lovell, "Signal quality measures for pulse oximetry through waveform morphology analysis," *Physiological Measurement,* vol. 32, p. 369, 2011.

[31] A. A. R. Kamal, J. B. Harness, G. Irving, and A. J. Mearns, "Skin photoplethysmography — a review," *Computer Methods and Programs in Biomedicine,* vol. 28, pp. 257-269.
[32] K. Pilt, K. Meigas, M. Rosmann, J. Lass, and J. Kaik, "An Experimental Study of PPG Probe Efficiency Coefficient Determination on Human Body," in *14th Nordic-Baltic Conference on Biomedical Engineering and Medical Physics*. vol. 20, A. Katashev, Y. Dekhtyar, and J. Spigulis, Eds., ed: Springer Berlin Heidelberg, 2008, pp. 311-314.
[33] Y. Sun, K. Chan, and S. Krishnan, "Characteristic wave detection in ECG signal using morphological transform," *BMC Cardiovascular Disorders,* vol. 5, p. 28, 2005.
[34] M. Abramowitz and I. A. Stegun, *Handbook of Mathematical Functions: with Formulas, Graphs, and Mathematical Tables*: Dover Publications, 2012.
[35] L. B. Cook, "Extracting arterial flow waveforms from pulse oximeter waveforms," *Anaesthesia,* vol. 56, pp. 551-555, 2001.
[36] N. A. Wisely and L. B. Cook, "Arterial flow waveforms from pulse oximetry compared with measured Doppler flow waveforms," *Anaesthesia,* vol. 56, pp. 556-561, 2001.
[37] K. Takazawa, N. Tanaka, M. Fujita, O. Matsuoka, T. Saiki, M. Aikawa*, et al*., "Assessment of Vasoactive Agents and Vascular Aging by the Second Derivative of Photoplethysmogram Waveform," *Hypertension,* vol. 32, pp. 365-370, August 1, 1998 1998.
[38] R. A. Waltz, J. L. Morales, J. Nocedal, and D. Orban, "An interior algorithm for nonlinear optimization that combines line search and trust region steps," *Mathematical Programming,* vol. 107, pp. 391-408, 2006/07/01 2006.
[39] J. Muehlsteff, A. Ritz, T. Drexel, C. Eickholt, P. Carvalho, R. Couceiro*, et al*., "Pulse Arrival Time as surrogate for systolic blood pressure changes during impending neurally mediated syncope," in *34th Annual Int. Conf. of the IEEE Eng. in Medicine and Biology Society, EMBC 2012*, 2012, pp. 4283-4286.
[40] C. Meyer, G. Morren, J. Muehlsteff, C. Heiss, T. Lauer, P. Schauerte*, et al*., "Predicting neurally mediated syncope based on pulse arrival time: algorithm development and preliminary results," *J Cardiovasc Electrophysiol,* vol. 22, pp. 1042-8, Sep 2011.
[41] J. Muehlsteff, T. Correia, R. Couceiro, P. Carvalho, A. Ritz, C. Eickholt*, et al*., "Detection of hemodynamic adaptations during impending syncope: Implementation of a robust algorithm based on pulse arrival time measurements only," *35th Annual Int. Conf. of the IEEE Eng. in Medicine and Biology Society, EMBC 2013,* vol. 2013, pp. 2291-4, 2013.
[42] R. Couceiro, P. Carvalho, R. P. Paiva, J. Muehlsteff, J. Henriques, V. Schulze*, et al*., "Characterization of surrogate parameters for blood pressure regulation in neurally-mediated syncope," in *35th Annual Int. Conf. of the IEEE Eng. in Medicine and Biology Society, EMBC 2013*, 2013, pp. 5381-5385.
[43] S. C. Millasseau, R. P. Kelly, J. M. Ritter, and P. J. Chowienczyk, "The vascular impact of aging and vasoactive drugs: comparison of two digital volume pulse measurements*," *American Journal of Hypertension,* vol. 16, pp. 467-472, June 1, 2003 2003.
[44] J. Padilla, E. Berjano, J. Sáiz, R. Rodriguez, and L. Fácila, "Pulse Wave Velocity and Digital Volume Pulse as Indirect Estimators of Blood Pressure: Pilot Study on Healthy Volunteers," *Cardiovascular Engineering,* vol. 9, pp. 104-112, 2009/09/01 2009.
[45] D. G. Brillante, A. J. O'sullivan, and L. G. Howes, "Arterial stiffness indices in healthy volunteers using non-invasive digital photoplethysmography," *Blood Pressure,* vol. 17, pp. 116-123, 2008.

Chapter 6.
REAL TIME PREDICTION OF NEURALLY MEDIATED SYNCOPE

This chapter consists of the following article:

Real Time Prediction of Neurally Mediated Syncope

R. Couceiro, P. Carvalho, R. P. Paiva, J. Muehlsteff, J. Henriques, C. Eickholt, C. Brinkmeyer, M. Kelm, C. Meyer

IEEE Journal of Biomedical and Health Informatics (J-BHI), accepted for publication, 2015.

DOI:10.1109/JBHI.2015.2408994

Journal impact factor in 2012: 1.978

Real Time Prediction of Neurally Mediated Syncope

R. Couceiro, P. Carvalho, R. P. Paiva, J. Muehlsteff, J. Henriques, C. Eickholt, C. Brinkmeyer, M. Kelm, C. Meyer

***Abstract*— Neurally mediated syncope (NMS) patients suffer from sudden loss of consciousness, which is associated with a high rate of falls and hospitalization. NMS negatively impacts a subject's quality of life and is a growing cost issue in our aging society, as its incidence increases with age.**

In the present paper we present a solution for prediction of NMS, which is based on the analysis of the electrocardiogram (ECG) and photoplethysmogram (PPG) alone. Several parameters extracted from ECG and PPG, associated with reflectory mechanisms underlying NMS in previous publications, were combined in a single algorithm to detect impending syncope. The proposed algorithm was evaluated in a population of 43 subjects. The feature selection, distance metric selection and optimal threshold were performed in a subset of 30 patients, while the remaining data from 13 patients was used to test the final solution. Additionally, a leave-one-out cross validation scheme was also used to evaluate the performance of the proposed algorithm yielding the following results: sensitivity (SE) – 95.2%; specificity (SP) – 95.4%; positive predictive value (PPV) – 90.9%; false positive rate per hour (FPRh) - 0.14 h^{-1} and prediction time (aPTime) - 116.4s.

***Index Terms*— Neurally Mediated Syncope; Electrocardiogram; Photoplethysmogram; Blood pressure regulation and variability; Autonomic nervous system.**

I. Introduction

SYNCOPE is a transient and self-limiting loss of consciousness, resulting from a transient global cerebral hypoperfusion and is characterized by a rapid onset, short duration and spontaneous complete recovery [1]. Also referred to as vasovagal and neurocardiogenic syncope, NMS belongs to a broader group of syncope known as reflex syncope, which is responsible for 21% of syncope episodes [1].

In the latest Framingham Study [2] involving 7814 participants between 20 and 96 years old it was reported an incidence rate of 6.2 per 1000 person-years. Moreover, the incidence of syncope was shown to increase with age, ranging from 2.6 to 5.4 per 1000 person-years between 20 and 69 years old. The same study shows a sharp rise to 11.1 and 19.5 per 1000 person-years within the 70-79 and above 80 years old populations [2, 3].

The main causes of syncope are generally benign. However, it is associated with frequent hospitalizations and accounts for 1-3% of all emergency department (ED) visits, as well as 1-6% of all hospital admissions in general [2, 4]. Moreover, in the U.S. approximately 4% of syncope patients discharged from the ED experience severe adverse events (e.g. readmission or death) within 72 hours [4].

The recurrence of syncope episodes gains special emphasis in elderly populations, where morbidity is particularly high. Fear of falling often leads to reduced physical and social activity, which is associated with increased mental decline and incidence of medical conditions. Subsequent institutionalization is a common consequence of syncope in this age group [1].

The main advances in syncope treatment and prevention focus on lifestyle modifications, which include the education of patients regarding the awareness and avoidance of triggers, the early recognition of prodromal symptoms, and performance of counter measures to abort the syncope episode [1]. Thus, the development of a non-invasive and non-intrusive, as well as cost-efficient personal p-health system to alert patients in case of an impending syncope might: 1) provide an opportunity for the patient to perform early counter-maneuvers (e.g. physical counterpressure maneuvers - PCMs) and avoid or delay syncope, as well as 2) help in diagnostics of underlying pathophysiological mechanisms with better personalized treatment options.

A. Background and state of the art

Orthostatic intolerance is thought to be one of the most common triggers of reflex syncope [5]. Investigators believe that the abrupt and excessive amount of venous blood pooling during standing posture is responsible for a decrease in the venous blood return to the heart resulting in more vigorously ventricle contractions and excessive stimulation of the ventricular mechanoreceptors. As a result, a "paradoxical"

This work was supported by CISUC (Center for Informatics and Systems of University of Coimbra) and by EU projects HeartCycle (FP7-216695), iCIS (CENTRO-07-ST24-FEDER-002003), Welcome (FP7-ICT-2013-10) and HeartSafe (PTDC-EEI-PRO-2857-2012).

R. Couceiro, P. Carvalho, R. P. Paiva and J. Henriques are with University of Coimbra, Department of Informatics Engineering, Science and Technology Faculty of the University of Coimbra, Coimbra, Portugal (e-mail: {rcouceir, carvalho, ruipedro, jh}@dei.uc.pt)

J. Muehlsteff is with Philips Research Laboratories Europe, Eindhoven, Netherlands (e-mail: Jens.Muehlsteff@philips.com)

C. Eickholt, C. Brinkmeyer M. Kelm and C. Meyer are with Heinrich-Heine University Hospital Düsseldorf, Division of Cardiology, Pneumology, and Angiology (e-mail: {Christian.Eickholt, Christoph.Brinkmeyer, Malte.Kelm, Christian.Meyer}@med.uni-duesseldorf.de) and with Department of Electrophysiology, University Heart Center, University Hospital Eppendorf, Hamburg, Germany. C.E. and C.M.(email: Chr.Meyer@uke.de)

withdrawal in sympathetic tone can occur i.e. cardioinhibition and vasodepression. This process is associated with a decrease in blood pressure and finally syncope [6]. Although the increase in parasympathetic activity (cardioinhibition) is commonly observed during NMS, hypotension due to vasodepression is considered as the primary mechanism leading to the loss of consciousness [7].

Several studies have been proposed in the literature for NMS prediction, differing on the objectives, methods and used modalities. The most common approach is the early prediction of the head-up tilt table test (HUTT) outcome based on an analysis of HR and BP parameters before and after tilt, i.e., during the supine position and early passive standing position. These methods are mainly focused on the analysis of the HR and/or SBP variability using either time or frequency domain techniques, or both. The time domain methods focus on the evaluation of temporal changes of HR during the supine and upright positions, using statistical features, such as mean, standard deviation [8-11], variance and kurtosis [12], or even doing simple comparisons between the HR in both phases [13, 14]. The frequency domain methods are mainly based on the evaluation of the characteristics of the low (LFr: 0.04-0.15Hz) and high (HFr: 0.15-0.40Hz) frequency components (e.g., power and area) and on the relationship between the characteristics of those components (the LFr/HFr ratio) as measures of sympathovagal balance [10, 11, 15-17]. Additionally, methods using indices of myocardial contractility assessed from peak endocardial acceleration [18], from transthoracic impedance cardiography [19, 20] and from the arterial blood pressure waveform [21] have also been proposed in the literature.

In contrast with the early prediction approach, the real time prediction problem has only been addressed in the later years, where hemodynamic changes are continuously monitored during the whole HUTT protocol. Rather than focusing on the hemodynamic responses resulting from the change of posture, the real-time approaches continuously assess the risk of an impending syncope episode from the monitored hemodynamic parameters. Since the mechanisms underlying the occurrence of syncope are characterized by fast dynamics and are not limited to changes of posture, these approaches are believed to have a wider scope concerning the real-life scenarios. Here, the changes in heart rate (HR) and continuously measured systolic blood pressure (SBP) have also been considered [22, 23]. Virag et al [22] proposed a method for real time prediction of impending syncope based on the time and frequency analysis of the HR and SBP signals, while Mereu et al. [23] evaluated the prediction ability of HR and BP (SBP, MBP, DBP and PP) trends and the ratio between the dRR (1^{st} derivative of RR) with those trends. However, current non-invasive blood pressure monitoring systems have several disadvantages. Most obviously their application is cumbersome due to bulky and expensive hardware, as well as complicated handling with the need for frequent calibrations [24]. These limitations become critical in unsupervised environments such as at home or in ambulatory scenarios, where low cost and easy-to-use devices are essential. More recently, several authors focused on the evaluation of changes of the pulse arrival time (PAT) alone [25], as a surrogate for SBP changes, or combined with HR changes [26, 27] and, finally, prediction of syncope. In our previous works [25, 28] we established and validated a method for syncope prediction using PAT and evaluated the possible mechanisms underlying the development of NMS.

B. Main contributions and paper organization

In the present paper, we propose a complete framework with tailored algorithms for prediction of NMS by analyzing changes of several cardiovascular parameters that characterize the chronotropic (HR), inotropic (left ventricular ejection time - LVET), vascular tone and blood pressure (PAT, stiffness index – SI – and reflection index - RI, respectively). These parameters were extracted from the joint analysis of the electrocardiogram (ECG) and photoplethysmogram (PPG), which can be acquired easily and non-obtrusively with state-of-the-art equipment. The parameters were normalized and led to the definition of ten features. The best seven features were selected and the distance to the orthostatic reference was calculated using the Minkowski distance metric. A threshold-based approach was adopted to detect impending syncope.

The remainder of the paper is organized as follows. The proposed solution for syncope prediction is presented in section II. The experimental protocol used in the present study is described in section III. The main results and respective discussion are presented in IV. Finally, we present our main conclusions in section V.

II. METHODS

The main steps of the proposed solution are illustrated in Fig. 1, which are: 1) Detection of motion artifacts; 2) Parameter extraction and post-processing; 3) Feature evaluation and; 4) Syncope prediction.

A. Detection of motion artifacts

It is well known that the PPG signal is prone to several sources of error (e.g. motion artifacts), which can be a serious obstacle in the reliable extraction of the derived parameters, especially in uncontrolled environments such as home care

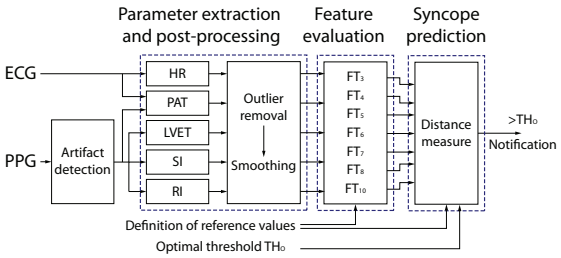

Fig. 1 - Schematic representation of the proposed algorithm structure. Heart rate (HR), pulse arrival time (PAT), left ventricular ejection (LVET), stiffness index (SI) and reflection index (RI) are extracted from the analysis electrocardiogram (ECG) and photoplethysmogram (PPG), which are post-processed and evaluated in order to extract seven features. Syncope prediction is performed using a threshold-based approach applied to the distance of the extracted features to an orthostatic stable reference. A notification is generated if the distance measure surpasses a predefined optimal threshold (TH_o).

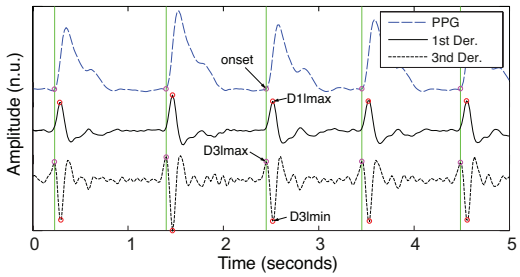

Fig. 2 - Segmentation of the photoplethysmogram (PPG) using a multiple-order derivative analysis approach.

and ambulatory scenarios. Therefore, it is important to detect the sections of the PPG signal that are corrupted and consequently shall not be included in the subsequent steps of the analysis. In the proposed framework we adopted a motion artifact detection algorithm using features from the time and period domain of the PPG signal [29]. The classification of the corrupted/clean PPG sections is performed using a C-Support Vector Classification (C-SVC) algorithm [30], with a radial basis function kernel. The classification model was fed with 8 inputs calculated from the rate of change of the time and period domain characteristics of the PPG signal. The time domain features were extracted from the morphological characteristics of the PPG signal:

1) Pulse amplitude - difference between the pulse peak height and its preceding trough depth (pulse onset);

2) Trough depth difference – Difference between the foot height of consecutive pulses;

3) Pulse skewness – Evaluation of the pulse symmetry;

4) Pulse kurtosis – Evaluation of the pulse "peakedness".

To extract the period domain features, the Discrete-time Short Time Fourier Transform (STFT) was applied, and the most relevant characteristics of the spectra were evaluated: 1) Location of the spectrum 2nd major spike; 2) Location of the spectrum 3rd major spike; 3) Length of the spectrum 3rd major spike and; 4) Ratio between the area of the three major spikes and the area of the remaining spectrum.

B. Parameter extraction

Chronotropic and inotropic changes were assessed via HR and LVET.

The HR was derived from the analysis of the ECG signal and was defined as the time span between consecutive R-peaks, detected by a Pan-Tompkins algorithm [31].

The LVET was assessed from the PPG analysis using an extension of the algorithm proposed in [32]. First, the PPG signal is band-pass filtered in a 0.23-18 Hz frequency band to remove high frequency noise and the baseline fluctuations. Second, the onset of each PPG pulse is detected using a multiple-order derivative analysis approach. Derivatives from order 1 to 3 (f'_{ppg} to f'''_{ppg}, respectively) are calculated using a five-point digital differentiator [22] and the onset of each PPG pulse is defined as the local maxima (D3lmax) on the f'''_{ppg} preceding the local minima (D3lmin) that corresponds to the f'_{ppg} local maxima (D1lmax), as presented in Fig. 2. To detect the Dlmax, a cumulative histogram of the f'_{ppg} data is calculated and the threshold ThR_{PPG} is defined as the greater value bellow which 90% of the observations are found. The f'_{ppg} local maxima with absolute amplitudes greater than ThR_{PPG} are defined as D1lmax [33].

Each extracted PPG pulse was normalized to the unit, the linear trend was removed and the systolic and diastolic phases were identified. The systolic phase associated with the ventricular ejection was defined between the onset of the PPG pulse and the onset of the dicrotic notch (or inflection). The diastolic phase, resulting from pulse reflections in the arterial path, was defined as the portion of the PPG pulse between the offset of the dicrotic notch and the offset of the PPG pulse, as presented in Fig. 3 (top). The onset/offset of the dicrotic notch were defined as the negative-to-positive/positive-to-negative zero crossings between 0.2 and 0.4 seconds [34].

The systolic and diastolic phases were modeled by a sum of three and two Gaussian function, respectively, and PPG pulse model was defined as:

$$f_m(t,\beta_j) = \sum_{j=1}^{5} a_j\, e^{\frac{-(t-c_j)^2}{2b_j^2}}, \qquad \beta_j = \{a,b,c\}_j \tag{1}$$

where the parameters a_j, b_j and c_j correspond to the amplitude, location and length of the Gaussian function j. The sum of the first and second Gaussians ($g_1 + g_2$) correspond to the wave driven by the systolic ejection. The third Gaussian (g_3) is related to the first pulse reflection at the junction between the thoracic and abdominal aorta, presented in Fig. 3 (middle). The fourth and fifth Gaussians (g_4 and g_5) derive from forward pulse reflection at the juncture between abdominal aorta and common iliac arteries [35] and minor reflections and re-reflections in the systemic structure, respectively. The adjustment of the model parameters was achieved minimizing the sum of the squared residuals, using the least squares minimization method, as presented bellow:

$$f_{MSE}(\beta) = \frac{1}{N}\sum_{n=1}^{N}[f(n) - f_m(n,\beta)]^2 \tag{2}$$

where $f_m(n,\beta)$ is the MG model with the set of parameters $\beta_j = \{a,b,c\}_j, j = 1,\dots,5$. Using the interior point algorithm [36], the goal is to solve nonlinear constrained optimization problem presented in (3).

$$\begin{aligned} min \quad & f_{MSE}(\beta) \\ subject\ to \quad & g(\beta) \le 0 \\ & lb \le \beta \le ub \end{aligned} \tag{3}$$

where $g(\beta) \le 0$ and $lb \le \beta \le ub$ are the physiologically driven inequality constrains and the boundaries to which the parameters are subject.

The LVET was defined by the time span between systolic peak of the systolic model 2nd derivative ($D2_{sp}$) and the notch in the systolic model 1st derivative ($D1_{nt}$), as presented in Fig. 3 (bottom).

To assess vascular and blood pressure changes, three highly pressure dependent parameters were also extracted [25, 35, 37,

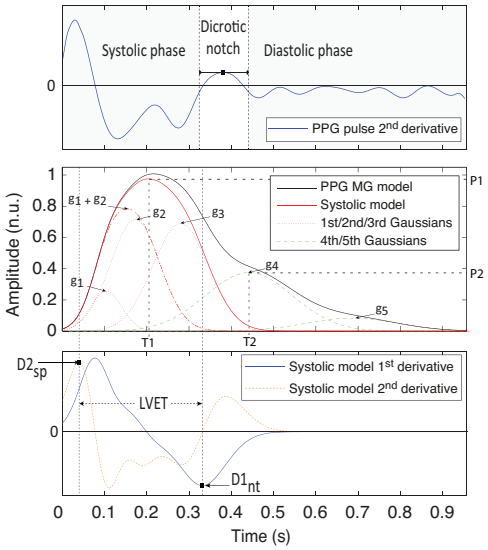

Fig. 3 - Schematic representation of the approach used to determine LVET, SI and RI. Top: 2nd derivative of the PPG pulse for determination of the systolic and diastolic phases. Middle: Gaussian model of the PPG pulse and the characteristic points used to assess stiffness and reflection indexes (SI and RI, respectively). Bottom: 1st and 2nd derivatives of the systolic model used to determine LVET.

38]. The Stiffness Index (SI) is associated with the velocity of a pulse wave in large arteries [39] and correlates with pulse pressure [35] was defined as the time span between the forward wave (g_1+g_2+g_3) and the reflected wave (g_4) and is described by:

$$SI = T2 - T1 \quad (4)$$

where the T1 is the time index corresponding to the maximum of the forward wave (g_1+g_2+g_3) and the T2 is the time index corresponding to the peak of the reflected wave (g_4), as indicated in Fig. 3 (middle).

The Reflection index (RI), associated with small artery stiffness [39], was defined as the ratio between the amplitudes of the forward wave (g_1+g_2+g_3) and the reflected wave (g_4) and is described by:

$$RI = P2/P1 \quad (5)$$

where P is the is the amplitude of the forward wave (g_1+g_2+g_3) and P2 is the amplitude of the reflected wave (g_4), as indicated in Fig. 3 (middle).

Finally, $PAT_{80\%}$ was defined as the time span between the ECG R-peak and the moment in time corresponding to 80% of the PPG pulse amplitude after its onset, which is known to correlate well with a decreasing BP in NMS [11].

C. *Parameter post-processing*

The presence of motion artifacts in the ECG signal and the inappropriate behavior of the parameter extraction algorithms can lead to the appearance of spurious values that do not reflect the undergoing physiological processes and consequently in inaccurate interpretation of data. This issue can be particularly observed in unsupervised monitoring with ill-defined measurement conditions. Therefore, a post-processing step is needed to detect and remove these spurious

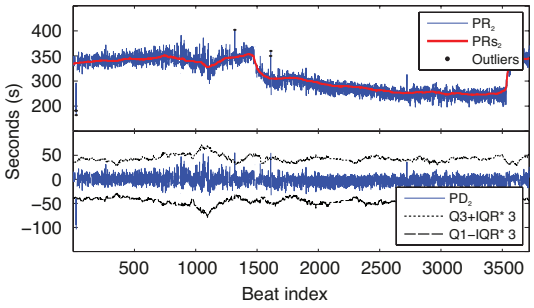

Fig. 4 - Example of the adopted outlier detection approach based on a 121 beat sliding window box plot analysis. Top: Extracted LVET parameter (PR_2) smoothed LVET (PRs_2) and detected outliers. Bottom: LVET parameter difference (PD_2), and outlier detection criterion limits ($Q1 - 3 * IQR$ and $Q3 + 3 * IQR$).

values. In the current framework a sliding window boxplot analysis [40] was adopted to remove outliers from the extracted parameters. First, a smoothed version (PRs_i) of each parameter PR_i was calculated using a moving median average filter (121 beats length – presented in Fig. 4 for the LVET parameter as a red thick line). The extracted PRs_i was subtracted to the parameter time series PR_i according to:

$$PD_i(t) = PRs_i(t) - PR_i(t) \quad (6)$$

where $PD_i(t)$ is the resulting time series without the main trend (presented in Fig. 4 for the LVET parameter – bottom), herein called as parameter difference.

Let $PD_i^w(t) = \{PD_i(t - w, \dots, t + w\}$ be a temporal sliding window over the derived time series PD_i with length $w * 2 + 1$ and centered in the instant t, for the i^{th} parameter. For each window, the lower quartile (Q1: 25th percentile), the upper quartile (Q3: 75th percentile) and the interquartile range ($IQR = Q3 - Q1$) are identified. The PR_i sample at the instant t is considered an outlier if the corresponding PD_i sample (see Fig. 4 - bottom) satisfies the following criterion:

$$PD_i(t) < Q1 - 3 * IQR \vee PD_i(t) > Q3 + 3 * IQR \quad (7)$$

Finally, all the identified outliers are excluded from the extracted parameters time series PR_i.

The rationale behind this approach is that the sporadic parameter values resulting from artifacts and noise can be detected as outliers, which greatly differ from the parameter main trend.

Finally, the parameter time series were linearly interpolated at a 2Hz frequency, which according to [25] is well above the required minimal sample frequency and a Butterworth low-pass filter with a 0.05Hz cutoff frequency was used to reduce high frequency noise.

D. *Feature evaluation and selection*

To develop a robust prediction algorithm, independent from the patient's specific characteristics, the extracted parameters were normalized according to (8) and (9), resulting in a set of ten features in total (summarized in Table I). The first five features were defined as:

$$FT_i(t) = \widetilde{PR}_i(t) = \frac{PR_i(t)}{PRref_i}, i = 1, \dots, 5 \quad (8)$$

where FT_i is the i[th] feature, PR_i is the i[th] parameter, $PRref_i$ is

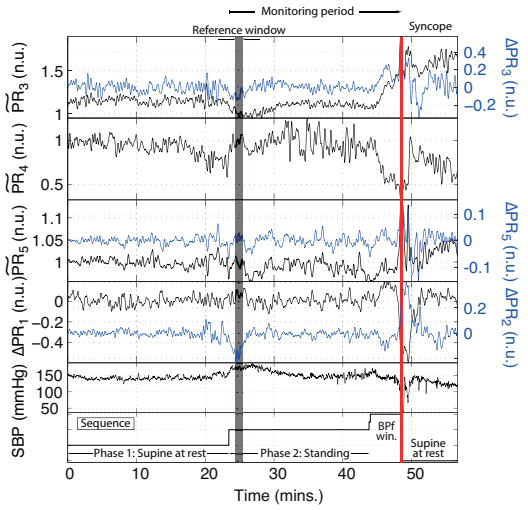

Fig. 5 - HUTT of a 50-year-old patient with syncope onset during GTN provocation. Representation of the seven most discriminant features assessed from the extracted parameters, SBP and HUTT sequence.

the average of each parameter during the second minute (reference window) after the patient was tilted to the upright position and t is the time instant. The selection of the second minute as the reference window ensures that the patient achieves orthostatic stabilization, which typically occurs within less than 1 minute [6].

Additionally, the normalized changes of the extracted parameters during the last 1.5 minutes (the minimum response time according to [25]) were also taken into account as:

$$FT_{i+5}(t) = \Delta PR_i(t) = \frac{PR_i(t) - PR_i(t - 1.5min)}{PRref_i}, \quad i = 1, \dots, 5 \tag{9}$$

The selection of the most appropriate features for syncope prediction was performed using the approach proposed in [41], where the features are selected based on a score metric (FSS) combining their relevance and redundancy, presented in (10). The relevance of each feature was assessed by the area under the curve (AUC) of the receiver operating characteristic (ROC) curve, while its redundancy was assessed by the spearman's rank correlation coefficient (RCC).

$$FSS_i = AUC(FT_i) - \frac{\left|\sum_{FT_j \in S} RCC(FT_i, FT_j)\right|}{|S|} \tag{10}$$

where $AUC(FT_i)$ is the AUC obtained by the i[th] feature, $RCC(FT_i, FT_j)$ is the spearman's rank correlation coefficient between the i[th] and j[th] feature, S is the subset of selected features at each iteration and $|S|$ its cardinality. In sum, seven features were selected corresponding to the highest features selection scores. The feature scores and their ability to predict the onset of syncope are summarized in Table III.

1) Syncope onset detection algorithm

From the analysis of the extracted features immediately before the onset of syncope, we observed significant changes in the majority of the tilt positive patients (Fig. 5). The chronotropic and inotropic variations were reflected in a substantial decrease of ΔPR_1 and increase in ΔPR_2. Moreover,

TABLE I. CORRESPONDENCE BETWEEN PARAMETERS/FEATURES INDEXES AND NAMES

Parameter name	Parameter index	Feature name (1st set)	Feature name (2nd set)
HR	PR_1	$\widetilde{PR}_1$	ΔPR_1
LVET	PR_2	$\widetilde{PR}_2$	ΔPR_2
SI	PR_3	$\widetilde{PR}_3$	ΔPR_3
RI	PR_4	$\widetilde{PR}_4$	ΔPR_4
PAT	PR_5	$\widetilde{PR}_5$	ΔPR_5

a significant drop in blood pressure was reflected in a substantial increase of $\widetilde{PR}_3$, $\widetilde{PR}_5$, ΔPR_3, ΔPR_5 and decrease of $\widetilde{PR}_4$.

To illustrate how the features vary during a head-up tilt testing (HUTT), principal component analysis (PCA) was applied to the selected features in two patients (with/without NMS), and a representation of the first three principal components is shown in Fig. 6. In general, for HUTT positive (po) patient, the trajectory evolves away from the orthostatic stable reference point, just before the onset of syncope. An example of this behavior is presented in Fig. 6 (top) for a 69-year-old patient with manifested syncope and GTN provocation. Contrarily, on HUTT negative (ne) patients the trajectory remains closer to the orthostatic stable state as shown in Fig. 6 (bottom) for a 78-year-old patient with no syncope after GTN administration.

These findings suggest that distance metrics might be used to differentiate the stable state from the risk of an impending event, i.e., to capture changes relative to a stable orthostatic reference at the beginning of the standing period (FTref). In order to choose the distance metric that better suits syncope prediction, several metrics were evaluated using ROC analysis combined with a 5-fold cross validation scheme. The highest

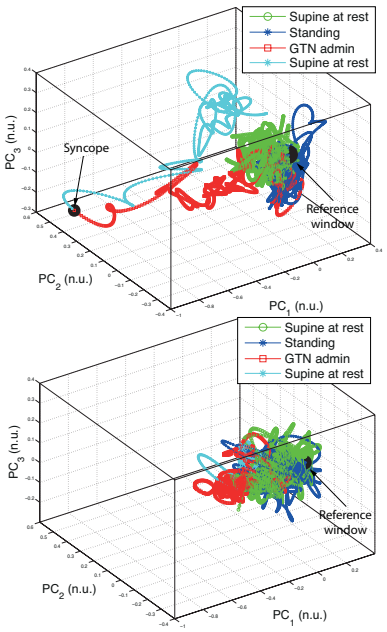

Fig. 6 - Illustration of the trajectory of the three principal components extracted from the most discriminative features, during HUTT procedure. Top: 69-year-old patient with manifested syncope and GTN provocation. Bottom: 78-year-old patient with no syncope and GTN provocation.

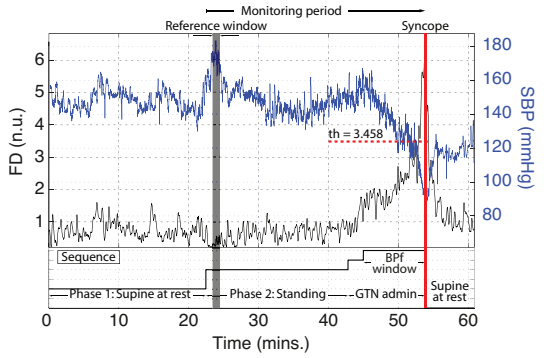

Fig. 7 - HUTT of a 69-year-old patient with manifested syncope and GTN provocation. Top diagram: SBP (blue) and FD (black) time series during HUTT. Bottom diagram: Phases of HUTT. Reference window represent as a black bar, corresponding to the second minute of phase 2. BPf window corresponds time between the start of BP fall and the syncope episode.

F-measure was adopted as the selection criterion leading to the selection of the Minkowski distance metric ($p = 2^{-0.5}$), which was calculated according to (11). Since the proposed measure does not account for the direction of the evolving trajectory, it is necessary to eliminate feature variations that are not associated with the physiological mechanisms underlying NMS, and might negatively affect FD measure. Therefore, the ΔPR_3 and ΔPR_5 values above unit and $\widetilde{PR}_4$ values below unit were set to one. Additionally, ΔPR_1 values below zero, and ΔPR_2, ΔPR_3 and ΔPR_5 values above zero were set to zero.

$$FD(t) = \left(\sum_{i=1}^{7} |FT_i(t) - FTref_i|^p \right)^{1/p}, p = 2^{-0.5} \qquad (11)$$

where $FD(t)$ is the Minkowski distance at the time instant *t*.

Impending NMS was detected when FD crosses a predefined optimal threshold. The SBP, FD and HUTT sequence are presented in Fig. 7 for an example case of 69-year-old patient.

III. Data Collection

A. Study design and HUTT protocol

Data were acquired during scheduled diagnostic head-up tilt table tests (HUTT) from 55 patients with unexplained syncope. All patients gave written informed consent to participate in this study (ClinicalTrials.gov identifier: NCT01262508).

The HUTT protocol followed the recommendation of the European Society of Cardiology (ESC) and consisted of four phases: 1) the patient was lying at rest of at least 15 min; 2) the patient did a passive standing exercise of 20 min at a position of 70º; 3) phase (2) was extended by 15 min, if no syncope occurred, with sublingual administration of 400 µg of glycerol trinitrate (GTN); 4) the patient was tilted back to supine position. The HUTT stopped at any moment in time, if syncope occurred and at the patient was brought back to supine position immediately for recovery. The nurse accompanying the study documented any prodromal symptoms such as dizziness, sweat, tremor, etc. during the procedure.

TABLE II. Patient Characteristics (AVG± STD)

	Tilt positive (n=21)	Tilt negative (n=22)
Age [y]	57±18	63±17
Weight [kg]	86±15	74±13
BMI [kg/m2]	27.1±4.6	26±5
Male/female	13/8	10/12
GTN yes/no	15/6	15/7

According to the guideline of European Society of Cardiology (ESC) the test outcome was classified as positive (po) or negative (ne) [2]. A positive result is characterized by occurrence of syncope or pre-syncope with the presence of bradycardia, hypotension, or both.

Data of 12 patients had to be removed due to BP regulation failures not caused by syncope, presence of arrhythmias or poor data quality in BP and PPG signals. The characteristics of the reaming study population consisting of 43 patients are summarized in Table II.

B. Experimental setup

The patients were monitored using two independent acquisition systems during the whole HUTT protocol.

The ECG-II lead and PPG signal (with sampling frequencies of 500 Hz and 126 Hz, respectively) were acquired using a Philips MP50 patient monitor [42] extended with a data logger functionality. To collect the PPG signal a standard SpO2 sensor was attached to the index finger.

Continuous non-invasive blood pressure (@50Hz) was collected using a "Taskforce Monitor" [43]. Additionally, two ECG leads (@1000 Hz) and an Impedance Cardiography (ICG) signal (@50 Hz) were also acquired. Based on these signals several hemodynamic parameters are provided, such as continuous (beat-to-beat) systolic blood pressure (SBP), total peripheral resistance index (TPRI) and stroke volume (SV).

The synchronization of the data coming from both systems was performed by temporally aligning the RR intervals time series extracted from ECG signals of both acquisition systems.

IV. Results and Discussion

To evaluate the performance of the proposed algorithm two validation schemes have been adopted: 1) Three-way data split validation (shown in Fig. 8); 2) Leave-one-out cross-validation LOO CV).

In the three-way data split validation scheme, the dataset was randomly partitioned into a train/validation and test subsets. The train/validation subset was constructed in order to have approximately 70% of the study population, corresponding to 15 po patients and 15 ne patients. The remaining 13 patients (ap. 30%), i.e., 6 po patients and 7 ne patients, were included in the test subset.

The train/validation subset was used to select the best features, evaluate the performance of the proposed algorithm and select the optimal threshold for syncope prediction. The algorithm performance and optimal threshold were evaluated using a 5-fold cross validation (5f-CV) approach (repeated 20 times). In this process, the training set (4 subsets) is used to find the optimal threshold based on ROC analysis, while remaining subset is used for validation. This process was

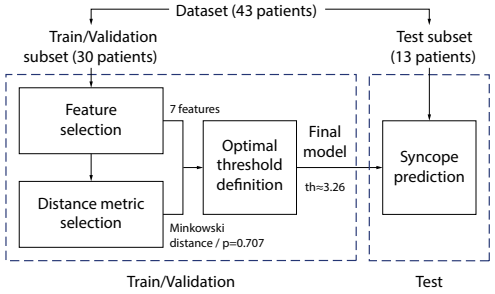

Fig. 8 - Diagram of the adopted three-way data split validation scheme. Train/Validation: Feature selection, distance metric selection and optimal threshold definition. Test: Evaluation of the proposed algorithm prediction capability.

repeated for each of the 5 subsets (folds). The test subset was used to validate the final solution, and test the real algorithms' performance.

In the leave-one-out cross validation scheme, the dataset was partitioned into 43 subsets, corresponding to each patient. From the 43 subsets, 42 subsets were used for training and the remaining subset was used for testing. The cross-validation process was repeated 43 times with each of the 43 subsets being used exactly once as the validation data.

The proposed methodology was evaluated using the following metrics: F-measure (F-m), sensitivity (SE) and specificity (SP), positive predictive value (PPV), false positive rate per hour (FPRh), prediction time average (aPTime) and standard deviation (sPTime).

The detection result was considered a true positive (TP) if an alarm is generated within the time window corresponding to the time between the start of BP fall and the syncope episode (BPf window). Otherwise, the detection result was considered a false positive (FP). A true negative (TN) was assigned if no alarm is generated outside the BPf window, whereas a false negative (FN) is considered if alarms are generated in this period. The FPRh was defined as the number of false positives divided by the sum of all non-BPf windows (in hours) of all patients, while the PTime was defined as the time span between the first alarm and the syncope episode.

In the 5-fold CV the performance of the algorithm was assessed in each iteration and the average was computed. After repeating this process 20 times, the average and standard deviation (avg ± std) of the aforementioned metrics was evaluated. In the LOO CV, the performance of the algorithm was computed based on the countings of each iteration detection result, at the end of the CV process.

A. Motion artifacts detection and parameter post-processing

The percentage of the detected motion artifacts and outliers was assessed for each patient and the results were evaluated using a box plot analysis, which is presented in Fig. 9. It is possible to observe that the percentage of detected motion artifacts is far greater (Median: 21.64%; Mean: 26.68%) than the percentage of detected outliers (Median: 3.94%; Mean: 4.56%). Moreover, the percentage of motion artifacts detected in 3 of the 43 patients was greater than 70%. These results suggest that even in a controlled environment such as the

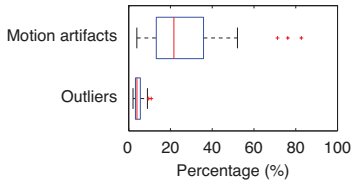

Fig. 9 – Box plot of the percentage of pulses classified as motion artifacts (top) and parameter samples detected as outliers (bottom).

HUTT, the PPG signal is prone to be corrupted with motion artifacts. The results also show a discrepancy between the percentage of detected motion artifacts and outliers, which can be explained by the percentage of false detections of the motion artifacts detection algorithm (approximately 10%). Another possible reason relies on the outlier detection algorithm itself. Since it is based on a boxplot analysis, it is expectable that sections corrupted with motion artifacts result in a high variance in the extracted parameters, which prevents the correct identification of outliers. These results emphasize the importance of combining both motion artifacts and outliers detection algorithms in order to increase the robustness of the syncope prediction method.

Regarding the segmentation of the PPG signal, the adopted algorithm was able to identify the PPG pulses with a sensitivity of 96.27% and a positive predictive value of 97.23% in the current dataset.

B. Feature selection

The feature selection results are presented in Table III. One observes that the feature presenting the highest FSS refers to PAT parameter ($\widetilde{PR}_5$), followed by $\widetilde{PR}_3$, related to SI. The remaining selected features correspond to the normalized changes of HR (ΔPR_1) over a 1.5 minutes window and to the change of RI relatively to the reference window ($\widetilde{PR}_4$). It is also evident that between the 7th and 8th features (separated by a thick red line in Table III) there is a huge gap in the FSS score (≈11.4%). The low performance of the last three features, as indicated by the FSS decrease, resulted in the exclusion these features. In summary, seven features were selected from a total of ten extracted features. Although the best feature ($\widetilde{PR}_5$) extracted from the analysis of the PAT parameter present the highest FSS, it is worth noting that it presents lower SP (90%) and PPV (83.3%), when compared to $\widetilde{PR}_3$ (SP: 96.7% and PPV: 92.3%). Additionally, this feature presents a high FPRh (1.7 h^{-1}) when compared to the selected features, and particularly $\widetilde{PR}_3$ (0.8h^{-1}).

TABLE III. PERFORMANCE OF THE EXTRACTED FEATURES ($FT_{1,\ldots,10}$)

Feature acronym	Score (%)	SE (%)	SP (%)	PPV (%)	FPRh (h^{-1})	aPTime (s)	sPTime (s)
$\widetilde{PR}_5$	94.6*	100.0	90.0	83.3	1.7	101.0	85.4
$\widetilde{PR}_3$	89.6*	80.0	96.7	92.3	0.8	125.2	121.3
ΔPR_1	75.8*	80.0	86.7	75.0	2.4	60.8	72.3
$\widetilde{PR}_4$	71.0*	86.7	83.3	72.2	2.0	113.2	94.2
ΔPR_5	70.7*	80.0	93.3	85.7	0.8	76.4	143.0
ΔPR_3	68.3*	80.0	93.3	85.7	0.3	84.5	84.3
ΔPR_2	67.4*	80.0	73.3	60.0	4.1	90.2	80.6
$\widetilde{PR}_2$	56.0*	93.3	60.0	53.8	5.2	201.6	130.2
$\widetilde{PR}_1$	49.0*	73.3	90.0	78.6	1.2	77.0	142.7
ΔPR_4	35.9*	100.0	10.0	35.7	11.3	206.7	141.8

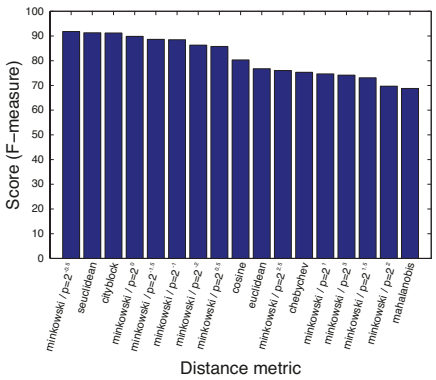

Fig. 10 - Bar plot representing the scores of the evaluated distance metrics.

The selected features with the highest prediction time (aPTime) also derive from the analysis of SI ($\widetilde{PR}_3$: 125.2s), followed by $\widetilde{PR}_4$ (113.2s) and $\widetilde{PR}_5$ (101.0). The aPTime of the remaining features range from 60.8s (ΔPR_1) to 90.2s (ΔPR_2).

C. Distance metric selection

The selection of the most appropriate distance metric was achieved using a 5-fold cross validation scheme (repeated 20 times) and the distance metric obtaining the best F-measure score was chosen. The scores obtained by each distance metric and corresponding parameters are presented in Fig. 10. As shown in Fig. 10, the distance metric presenting the best score is the Minkowski distance with parameter $p = 2^{-0.5}$ and therefore it used in the assessment of the distance between the evolving trajectory and the stable orthostatic reference.

D. Syncope detection

The performance of the proposed algorithm was evaluated in two separate phases. First, the algorithm performance (presented in Table IV – *3W-DS validation*) and the optimal threshold were evaluated using a 5f-CV scheme (repeated 20 times) in train/validation phase. Second, the real prediction capability of the proposed solution (presented in Table IV - *3W-DS test*) was tested on the test subset using the optimal threshold (TH_0).

The optimal threshold (TH_0) was evaluated based on the following criterion:

$$TH_0 = {}^1\!/_N \sum_{n=1}^{N} \left({}^1\!/_K \sum_{k=1}^{K} TH(n,k) \right) \qquad (12)$$

where TH is the threshold calculated at the iteration k on the 5-f CV n^{th} repetition, *N=20* is the number of repetitions of the 5-f CV, *K=5* is the number of 5-f CV iterations/folds. Using (12), the optimal threshold was defined as $TH_0 = 3.458$.

Additionally, the proposed algorithm performance was also evaluated using a leave-one-out cross-validation approach using the whole dataset composed of 43 patients, herein called LOO validation phase (presented in Table IV - LOO validation).

1) Influence of motion artifacts and outliers

In order to evaluate the influence of the artifacts detection and outlier removal steps on the overall performance of the proposed algorithm, each of the before mentioned train/validation and test phases were performed using 4 sets of features, which are:

- Raw data – Features extracted without removing the motion artifacts and outliers
- Data w/o outliers – Features extracted after removing the outliers
- Data w/o artifacts - Features extracted after removing the motion artifacts
- Data w/o artifacts and outliers - Features extracted after removing the motion artifacts and outliers

From Table IV it is possible to observe that in each phase, the performance of the proposed method strongly benefits from the removal of artifacts, outliers and both. It is shown a F-measure increase, during the 3W-DS validation, of 13% with the removal of outliers, approximately 8% with the removal of artifacts and approximately 15% with the removal of both. In the 3W-DS test phase and LOO validation, similar results have been achieved with the exception to the increase in performance from the data w/o outliers to the data w/o artifacts and outliers, where no performance increase has been observed (F-measure: 3W-DS Test - 92.3%; *LOO validation – 93%*).

The removal of outliers and artifacts has also a significant impact on the reduction of false alarms, which can be confirmed by the decrease of the FPRh in each of the validation phases. The number of false alarms was reduced to nearly one quarter by removing the outliers (3W-DS Validation: 0.68 to 0.18 h^{-1}) and to nearly one fifth by removing both artifacts and outliers (3W-DS Validation: 0.68 to 0.15 h^{-1}). These results are even more expressive in LOO validation, where a decrease in the FPRh from 0.75 to 0.14 has been observed.

The removal of outliers and artifacts also affected the prediction time of the proposed algorithm. However, while in the 3W-DS validation (aPTime: 67.9 to 61.0 s) and in the LOO validation (aPTime: 138.8 to 116.4 s) is observed a decrease in the prediction time, in the 3W-DS test phase, the result was the opposite (aPTime: 207.1 to 243.3 s).

These results show the importance to remove artifacts before parameters are extraced. Additionally, they emphasize the importance of combining the artifacts removal with an outlier removal step, focused on the detection of spurious values provided by the parameter extraction algorithm. Since the post-processing step targets the extracted parameters rather than the characteristics of the analyzed signal, it is capable of detecting unreasonable behaviors caused by the parameter extraction algorithms. Therefore, the combination of both algorithms in the present framework results in a great enhancement of the proposed methods' performance.

2) Prediction capability

In the 3W-DS validation phase, the proposed algorithm achieved a SE of 93.3%, associated with high specificity (SP: 96.7%) and positive predictive value (PPV: 94.8%). Moreover, the number of false positives per hour is low (FPRh: 0.15h^{-1}) and a good prediction time was achieved (aPTime: 61s). The variance of the achieved prediction times

TABLE IV. PERFORMANCE OF THE PROPOSED ALGORITHM DURING THE VALIDATION AND TESTING PHASES

Phase	Dataset	Score avg±std (%)	SE avg±std (%)	SP avg±std (%)	PPV avg±std (%)	FPRh avg±std (h^{-1})	aPTime avg±std (s)	sPTime avg±std (s)
3W-DS Validation	*Raw data*	78.8 ± 3.0†	84.0 ± 3.4	86.7 ± 1.6E-14	77.9 ± 2.2	0.68 ± 0.018	67.9 ± 2.4	34.5 ± 7.3
	Data w/o outliers	91.8 ± 2†	89.0 ± 3.3	96.7 ± 0	94.4 ± 0.82	0.18 ± 0.05	65.4 ± 2.6	40.6 ± 5.1
	Data w/o artifacts	86.5 ± 1.9†	85.3 ± 4.2	93.0 ± 2.5	88.7 ± 4.1	0.16 ± 0.236	70.0 ± 9.4	48.7 ± 10.8
	Data w/o artifacts and outliers	93.2 ± 0.06†	93.3 ± 9.1E-15	96.7 ± 1.0E-14	94.8 ± 0.5	0.15 ± 0.007	61.0 ± 1.0	38.6 ± 5.9
3W-DS Test	*Raw data*	75.0†	100	69.2	60.0	0.88	207.1	217.8
	Data w/o outliers	92.3†	100	92.3	85.7	0.15	217.6	197.5
	Data w/o artifacts	83.3†	83.3	92.3	83.3	0.15	197.1	243.2
	Data w/o artifacts and outliers	92.3†	100	92.3	85.7	0.15	243.3	242.5
LOO validation	*Raw data*	69.6†	76.2	79.1	64.0	0.75	138.8	147.0
	Data w/o outliers	93.0†	95.2	95.4	90.9	0.18	107.9	141.6
	Data w/o artifacts	87.8†	85.7	95.4	90.0	0.16	100.9	140.8
	Data w/o artifacts and outliers	93.0†	95.2	95.4	90.9	0.14	116.4	155.5

† F-measure (F-m)

(sPTime) was 38.6s.

In the LOO validation, the proposed algorithm also achieved high performance (SE: 95.2%; SP: 95.4%; PPV: 90.9%), followed by a low FPRh ($0.14h^{-1}$) and a good prediction time (116.4 ± 155.5 s).

In the 3W-DS testing phase, the proposed syncope prediction solution achieved a high SE of 100%, without compromising both specificity (SP: 92.3%) and positive predictive value (PPV: 85.7%). Moreover, the number of false positives per hour is low (FPRh: 0.15 h^{-1}) and a good prediction time was achieved (aPTime: 243.3s). The onset of impending syncope was detected in a range of 62 to 629.5s (presented in Table V) and presented a high variance (sPTime: 242.5s).

Our results obtained in each validation phase show a minor decrease in the proposed algorithm score, from the 3W-DS validation to the LOO validation phase (93.2% against 93%), and from the 3W-DS validation to 3W-DS test phase (93.2% against 92.3%), as presented in Table IV. However, there was a substantial increase in SE (93.3% to 100%) and decrease in PPV (94.8% to 85.7%), from the 3W-DS validation to the 3W-DS test phases. Similarly, there was an increase in SE (93.3% to 95.2%) and decrease in PPV (94.8% to 90.9%), from the 3W-DS validation to the LOO validation. The FPRh was similar in both phases (≈ 0.15 h^{-1}). Contrarily, there was a substantial increase in the prediction time average and standard deviation (65.37±40.6s to 217±197.45s), from the 3W-DS validation to the test phase. This discrepancy between the validation and testing performances reflect the differences in the syncope development timings between patients, suggested by the distinct prodomi times presented in Table V.

In order to evaluate the stability of the proposed method, we evaluated its performance in terms of sensitivity and specificity as a function of the adopted threshold. From Fig. 11 it is possible to observe that the optimal threshold identified during the 3W-DS validation phase is within a large range of possible values (from 3.391 to 4.461) yielding the best performance (SE: 100% and SP: 92.3%), presented in Table IV. Moreover, a reduction in Th_0 of at least 0.28 is needed to decrease the specificity below 84% and a rise of at least 1 to set the sensitivity below 70%. These results indicate that the extracted features provide robust discrimination within a large range of optimal thresholds.

The individual results achieved for each of the 43 patients included in the LOO validation (presented in Table V) show that the proposed solution predicted majority of the syncope events with an acceptable prediction time (over 60 seconds). This time span is enough to inform the patient for the need to start physical counterpressure maneuvers (PCMs) or simply to sit/lay down to avoid falling. Moreover, there was a misdetection in patient #10 (FP=1), which led to the decrease in the SP, PPV and increase in FPRh metrics. It is noteworthy to mention that although it was considered as a FP (as a result of an alarm triggered outside the BPf window), this patient suffered a syncope episode subsequently and therefore should not be considered a false positive. Fig. 12 shows that the optimal threshold is surpassed due to a substantial drop in SBP (>40mmHg) around 57 minutes, which continues to decrease until the moment of syncope. From Table V one observes that onset of prodromal symptoms in the majority of the patients preceded syncope detection (range: 3 to 213 sec.; 90.2 ± 67.2 sec.). Yet, prodromal symptoms in the context of the standardized, clinical HUTT procedure tend to be more pronounced than during "real-life" onset of syncope. Moreover, in the current study even the slight symptoms were

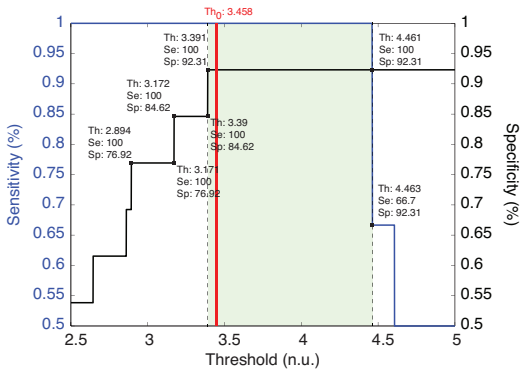

Fig. 11 – Representation of the evolution of the sensitivity and specificity performance metrics as a function of the adopted threshold for the 3W-DS test set (data w/o artifacts and outliers)

TABLE V. PERFORMANCE OF THE PROPOSED ALGORITHM USING THE LOO VALIDATION SCHEME FOR THE 43 PATIENTS

Syncope	Patient	TP	FP	TN	FN	Prediction time (s)	Prodomi (s)
No	#05	0	0	1	0	-	-
Yes	#07	1	0	1	0	82	218.1
Yes	#08	1	0	1	0	8	150.1
Yes	#09	1	0	1	0	62.5	98.2
Yes	#10	1	1	0	0	627.5	759.9
No	#11	0	0	1	0	-	-
Yes	#12	1	0	1	0	36	92.7
Yes	#13	1	0	1	0	86	211.4
No	#14	0	0	1	0	-	-
Yes	#15	1	0	1	0	65	92
No	#16	0	1	0	0	-	-
No	#17	0	0	1	0	-	-
Yes	#18	1	0	1	0	24	167
No	#20	0	0	1	0	-	-
No	#21	0	0	1	0	-	-
Yes	#24	1	0	1	0	71	48
No	#25	0	0	1	0	-	-
Yes	#26	1	0	1	0	145	192
No	#27	0	0	1	0	-	-
No	#28	0	0	1	0	-	-
No	#29	0	0	1	0	-	-
No	#30	0	0	1	0	-	-
No	#31	0	0	1	0	-	-
No	#32	0	0	1	0	-	-
Yes	#33	0	0	1	1	-	368
Yes	#34	1	0	1	0	29.5	26
Yes	#36	1	0	1	0	61.5	50
Yes	#37	1	0	1	0	59,5	43
No	#38	0	0	1	0	-	-
Yes	#39	1	0	1	0	66	43
Yes	#40	1	0	1	0	33	195
No	#41	0	0	1	0	-	-
Yes	#42	1	0	1	0	50	53
No	#43	0	0	1	0	-	-
No	#45	0	0	1	0	-	-
Yes	#46	1	0	1	0	155	368
No	#48	0	0	1	0	-	-
No	#49	1	0	1	0	24	30
Yes	#50	1	0	1	0	181	178
Yes	#53	0	0	1	0	-	-
No	#54	0	0	1	0	-	-
No	#55	0	0	1	0	-	-
Yes	#56	1	0	1	0	461.5	495

recorded as prodromal sensations (e.g. mild dizziness or nausea), which in an ambulatory setting might be ignored by the patients.

An important characteristic of our method is the compromise between a high performance, supported by the high values of SE, SP and PPV (above 85%), and the low false positive rate per hour, in both validation and testing phases. This is essential in the ambulatory p-health setting, since it helps to avoid mistrust and compromised patient compliance due to false positive syncope detections. Moreover, the

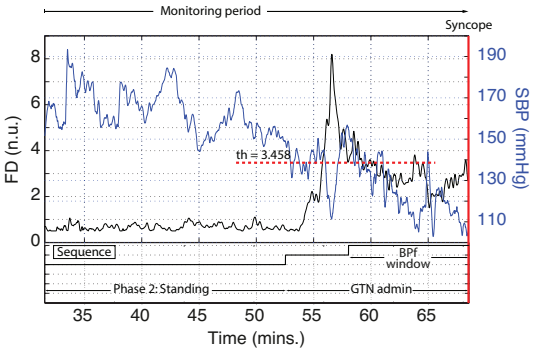

Fig. 12 - HUTT of a 17-year-old patient with syncope after GTN administration.

observed prediction times can give patients the ability to act appropriately, e.g. by performing PCMs or simply to sit/lay down avoiding a fall. PCMs act via the increase of sympathetic activity and vascular resistance to raise BP in order to avoid or to delay NMS. According to [44], the effects of PCMs such as the hand grip maneuver were evident after the first 10s and showed significant BP increases after 2 min. Our results of prediction times ranging from 1 to 9 minutes might be helpful in an early execution of PCMs and therefore could facilitate the timely administration of effective interventions to prevent or delay NMS.

3) Comparison with the state of the art

Performing a fair comparison between our method and the other state of the art methods is a challenging task, considering the heterogeneity of the experimental and test protocols, as well as differences in the populations' demographics. However, keeping these topics in our consideration, the comparison and discussion of the methods prediction performance can still be accomplished.

In Table VI we compare results achieved by our method and methods discussed in literature for real time prediction of NMS. Visibly, our method outperform the others in terms of SE, SP and PPV metrics, excluding the method proposed by Meyer et al. [27] (SE/SP/PPV: 100%), however this study was intended to show basic feasibility under ideal conditions using PAT with a small enrolled number of 14 patients only.

Next to our method is the approach proposed by Virag et al. [22], which focused on the analysis of the HR and SBP trends. The results in this study present a similar performance (SE: 95% and SP: 93%). Although no values were provided regarding the PPV and FPRh, the validation of the proposed method on a much larger population (1155 patients), suggests that the presented results are founded on strong statistics,

TABLE VI. PERFORMANCE OF THE ALGORITHMS PROPOSED IN LITERATURE FOR REAL TIME SYNCOPE PREDICTION

Dataset	SE AVG±STD (%)	SP avg±std (%)	PPV avg±std (%)	FPRh avg±std (h^{-1})	PTime avg±std (s)	Modalities	Number of volunteers
Virag et al. [22]	95	93	-	-	128 ± 216	ECG/ABPW	1155
Mereu et al. [23]	86.2	89.1	-	-	44.1 ± 6.6	ECG/ABPW	145
Eickolt et al. [26]	81	85	-	-	203 ± 227s	ECG/PPG	44
Meyer et al. [27]	100	100	100	-	99 ± 108	ECG/PPG	14
Muhlsteff et al. [25]	90.48	83.33	82.61	-	77.71 ± 71.78	ECG/PPG	43
Proposed method*	95.2	95.4	90.9	0.14	116.4 ± 155.5	ECG/PPG	43

* *LOO validation; Data w/o artifacts and outliers*

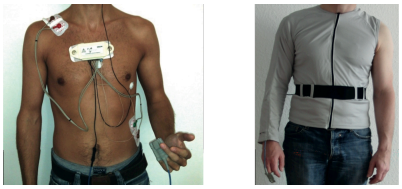

Fig. 13 - Left: SENSATRON system attached to a subject by standard adhesive electrodes. Right: functional textile as user-interface developed within HeartCycle for the SENSATRON device.

which represents a great advantage compared to the other methods discussed before. Nonetheless, the dependence on the analysis of the arterial blood pressure waveform to assess the SBP trends is still a major disadvantage, since the current available sensors still present limitations regarding their long-term applicability. The remaining algorithms proposed by Mereu et al. [23], Eickolt et al. [26] and Muehlsteff et al. [25] presented similar performances regarding the SE and SP metrics (above 80%).

Considering the prediction time, Eickolt et al. [26] reported the best with 203±227s, followed by Virag et al. [22] (128±216s) and than by our approach (116.4±155.5s). The lowest prediction time was achieved by Mereu et al. [23] with 44.1 ± 6.6 s in advance of a syncope.

E. Wearable sensors and real-life scenarios

Our NMS prediction algorithm requires the ECG and PPG signals only, which can be easily acquired in real life. For that purpose, within the EU-funded "HeartCycle" project, a wearable monitoring system called "SENSATRON" has been developed. The "SENSATRON" is a multi-sensor device with a modular design, which can be easily adapted to home and clinical monitoring scenarios. The system can be easily integrated functional textiles [45], as shown in Fig. 13. Data are stored on an on-board memory card and/or can be wirelessly transmitted via Bluetooth to an external hub.

This device features extended functionalities and acquires an ECG, an impedance cardiogram (ICG), near-infrared PPG, infrared PPG, thoracic inductive plethysmogram, skin temperature as well as sound signals from two thorax locations [46]. Additionally, up-to three 3-axis acceleration sensors at the thorax, arms or legs provide information on posture and movements. In fact, context information provided by the acceleration sensors will play a fundamental role in the translation of the proposed algorithm in real life setting, e.g. the detection of motion near the ECG electrodes and PPG sensor. This information can be used in the assistance of the proposed method to improve handling of PPG and ECG motion artifacts and increase the algorithm performance. Additionally, the detection of posture changes provide the temporal windows where orthostatic stabilization is achieved and which time windows shall be used for the normalization of the extracted features. Based on this context information, our algorithm is able to self-calibrate periodically without any human interventions.

V. Conclusions and Future Work

In this work a real time algorithm for syncope prediction based on the evaluation of chronotropic (HR), inotropic (LVET) and vascular tone (SI, RI and PAT) parameters are presented. Features are derived by analysis of ECG and PPG signals only and were combined into a single distance measure. NMS was detected by an appropriately and robust threshold-based approach.

The algorithm was trained and tested on a population of 43 patients using a three-way data split validation scheme. A train/validation subset (30 patients) was used to select the most relevant and least redundant features, the most suitable distance metric and to define the optimal threshold for syncope prediction. The threshold was found using a 5-fold cross validation approach, repeated 20 times. The prediction capability of was evaluated in the test subset of 13 patients (SE: 100%; SP: 92.3%; PPV: 85.7%; FPRh: 0.15 h^{-1}; aPTime: 243.3s) and in all 43 patients using a leave one out cross validation scheme (SE: 95.2%; SP: 95.4%; PPV: 90.9%; FPRh: 0.14 h^{-1}; aPTime: 116.4s).

Our results highlight the potential importance of a combined analysis of the extracted parameters in the prediction of impending NMS. Additionally, we demonstrate the robustness of the algorithm approach against artifacts, which will be key feature to transfer our method into to ambulatory and p-health settings.

Future work will focus on the adaptation and deployment of the proposed framework into a continuous monitoring (24/7) wearable system. Moreover, the validation of the algorithm in real life scenarios such as home care and ambulatory will be also under our concern. Finally, the improvement of the usability of the system and respective sensors will also be one of our primary interests.

Acknowledgment

We thank the medical and nursing staff of the Neurocardiology Unit, Division of Cardiology, Pneumology and Angiology, University Düsseldorf, for supporting this study. We thank especially Sandy Gläser for excellent technical support.

References

[1] A. Moya, R. Sutton, F. Ammirati, J. J. Blanc, M. Brignole, J. B. Dahm, *et al.*, "Guidelines for the diagnosis and management of syncope (version 2009)," *Eur Heart J,* vol. 30, pp. 2631-71, Nov 2009.

[2] N. Colman, K. Nahm, K. S. Ganzeboom, W. K. Shen, J. Reitsma, M. Linzer, *et al.*, "Epidemiology of reflex syncope," *Clin Auton Res,* vol. 14 Suppl 1, pp. 9-17, Oct 2004.

[3] E. S. Soteriades, J. C. Evans, M. G. Larson, M. H. Chen, L. Chen, E. J. Benjamin, *et al.*, "Incidence and Prognosis of Syncope," *New England Journal of Medicine,* vol. 347, pp. 878-885, 2002.

[4] D. M. Lemonick, "Evaluation of Syncope in the Emergency Department," *American Journal of Clinical Medicine,* vol. 7, 2010.

[5] S. Rosanio, E. R. Schwarz, D. L. Ware, and A. Vitarelli, "Syncope in adults: Systematic review and proposal of a diagnostic and therapeutic algorithm," *International journal of cardiology,* vol. 162, pp. 149-157, 2013.

[6] B. P. Grubb, "Pathophysiology and differential diagnosis of neurocardiogenic syncope," *The American Journal of Cardiology,* vol. 84, pp. 3-9, 1999.

[7] H. Ouyang and J. Quinn, "Diagnosis and Evaluation of Syncope in the Emergency Department," *Emergency Medicine Clinics of North America,* vol. 28, pp. 471-485, 8// 2010.

[8] N. Lippman, K. M. Stein, and B. B. Lerman, "Failure to decrease parasympathetic tone during upright tilt predicts a positive tilt-table test," *The American journal of cardiology,* vol. 75, pp. 591-595, 1995.

[9] G. Kochiadakis, P. Lees, E. Kanoupakis, N. Igoumenidis, E. Manios, and P. Vardas, "Spectral analysis of heart rate variability in the analysis of autonomic nervous system activity during tilt-table testing in patients with unexplained syncope," in *Computers in Cardiology 1997*, 1997, pp. 367-369.

[10] C. A. Morillo, G. J. Klein, D. L. Jones, and R. Yee, "Time and frequency domain analyses of heart rate variability during orthostatic stress in patients with neurally mediated syncope," *The American journal of cardiology,* vol. 74, pp. 1258-1262, 1994.

[11] A. Madrid, C. Moro, E. Marin-Huerta, L. Novo, J. Mestre, J. Lage*, et al.*, "[Usefulness of the RR variability in the diagnosis of neurogenic syncope]," *Revista espanola de cardiologia,* vol. 47, pp. 536-543, 1994.

[12] J. E. Naschitz, I. Rosner, M. Rozenbaum, M. Fields, H. Isseroff, J. P. Babich*, et al.*, "Patterns of cardiovascular reactivity in disease diagnosis," *QJM,* vol. 97, pp. 141-151, March 1, 2004 2004.

[13] Z. Mallat, E. Vicaut, A. Sangaré, J. Verschueren, G. Fontaine, and R. Frank, "Prediction of head-up tilt test result by analysis of early heart rate variations," *Circulation,* vol. 96, pp. 581-584, 1997.

[14] M. Sumiyoshi, Y. Nakata, Y. Mineda, T. Tokano, M. Yasuda, Y. Nakazato*, et al.*, "Does an early increase in heart rate during tilting predict the results of passive tilt testing?," *Pacing and Clinical Electrophysiology,* vol. 23, pp. 2046-2051, 2000.

[15] C. Kouakam, D. Lacroix, N. Zghal, R. Logier, D. Klug, P. Le Franc*, et al.*, "Inadequate sympathovagal balance in response to orthostatism in patients with unexplained syncope and a positive head up tilt test," *Heart,* vol. 82, pp. 312-318, 1999.

[16] G. A. Ruiz, C. MADOERY, F. ARNALDO, C. Menendez, and M. C. Tentori, "Frequency-Domain Analysis of Heart Rate Variability During Positive and Negative Head-Up Tilt Test: Importance of Age," *Pacing and Clinical Electrophysiology,* vol. 23, pp. 325-332, 2000.

[17] K. Efremov, D. Brisinda, A. Venuti, E. Iantorno, C. Cataldi, F. Fioravanti*, et al.*, "Heart rate variability analysis during head-up tilt test predicts nitroglycerine-induced syncope," *Open Heart,* vol. 1, June 1, 2014 2014.

[18] L. Mangin, A. Kobeissi, D. Lelouche, Y. D'Hérouville, P. Mansier, B. Swynghedauw*, et al.*, "Simultaneous Analysis of Heart Rate Variability and Myocardial Contractility During Head-Up Tilt in Patients with Vasovagal Syncope," *Journal of cardiovascular electrophysiology,* vol. 12, pp. 639-644, 2001.

[19] D. Schang, M. Feuilloy, G. Plantier, J.-O. Fortrat, and P. Nicolas, "Early prediction of unexplained syncope by support vector machines," *Physiological Measurement,* vol. 28, p. 185, 2007.

[20] E. Bellard, J. O. Fortrat, D. Schang, J. M. Dupuis, J. Victor, and G. Leftheriotis, "Changes in the transthoracic impedance signal predict the outcome of a 70 degrees head-up tilt test," *Clin Sci (Lond),* vol. 104, pp. 119-26, Feb 2003.

[21] C. Chun-An, C. Hsin, and C. Hung-Wen, "Early detection of vasovagal syncope in tilt-up test with hemodynamic and autonomic study," in *Computing in Cardiology, 2011*, 2011, pp. 529-532.

[22] N. Virag, R. Sutton, R. Vetter, T. Markowitz, and M. Erickson, "Prediction of vasovagal syncope from heart rate and blood pressure trend and variability: Experience in 1,155 patients," *Heart Rhythm,* vol. 4, pp. 1375-1382, 2007.

[23] R. Mereu, G. De Barbieri, T. Perrone, A. Mugellini, A. Di Toro, and L. Bernardi, "Heart rate/blood pressure ratio as predictor of neuromediated syncope," *International Journal of Cardiology,* vol. 167, pp. 1170-1175, 8/20/ 2013.

[24] E. Chung, G. Chen, B. Alexander, and M. Cannesson, "Non-invasive continuous blood pressure monitoring: a review of current applications," *Frontiers of Medicine,* vol. 7, pp. 91-101, 2013/03/01 2013.

[25] J. Muehlsteff, T. Correia, R. Couceiro, P. Carvalho, A. Ritz, C. Eickholt*, et al.*, "Detection of hemodynamic adaptations during impending syncope: Implementation of a robust algorithm based on pulse arrival time measurements only," *35th Annual Int. Conf. of the IEEE Eng. in Medicine and Biology Society, EMBC 2013,* vol. 2013, pp. 2291-4, 2013.

[26] C. Eickholt, T. Drexel, J. Muehlsteff, A. Ritz, M. Siekiera, K. Kirmanoglou*, et al.*, "Neurally mediated syncope prediction based on heart rate and pulse arrival time," *European Heart Journal,* vol. 34, August 1, 2013 2013.

[27] C. Meyer, G. Morren, J. Muehlsteff, C. Heiss, T. Lauer, P. Schauerte*, et al.*, "Predicting neurally mediated syncope based on pulse arrival time: algorithm development and preliminary results," *Journal of cardiovascular electrophysiology,* vol. 22, pp. 1042-1048, 2011.

[28] R. Couceiro, P. Carvalho, R. P. Paiva, J. Muehlsteff, J. Henriques, V. Schulze*, et al.*, "Characterization of surrogate parameters for blood pressure regulation in neurally-mediated syncope," in *35th Annual Int. Conf. of the IEEE Eng. in Medicine and Biology Society, EMBC 2013*, 2013, pp. 5381-5385.

[29] R. Couceiro, P. Carvalho, R. P. Paiva, J. Henriques, and J. Muehlsteff, "Detection of motion artifact patterns in photoplethysmographic signals based on time and period domain analysis," *Physiological Measurement,* vol. 35, p. 2369, 2014.

[30] C.-C. Chang and C.-J. Lin, "LIBSVM : a library for support vector machines. ACM Transactions on Intelligent Systems and Technology," vol. 2, pp. 27:1--27:27, 2011.

[31] J. a. T. Pan, W. J., "A real-time QRS detection algorithm.," *EEE Trans Biomed Eng,* pp. 230-236, 1985.

[32] R. Couceiro, P. Carvalho, R. Paiva, J. Henriques, M. Antunes, I. Quintal*, et al.*, "Multi-Gaussian fitting for the assessment of left ventricular ejection time from the Photoplethysmogram," in *34th Annual Int. Conf. of the IEEE Eng. in Medicine and Biology Society, EMBC 2012*, San Diego, 2012.

[33] Y. Sun, K. Chan, and S. Krishnan, "Characteristic wave detection in ECG signal using morphological transform," *BMC Cardiovascular Disorders,* vol. 5, p. 28, 2005.

[34] U. Rubins, "Finger and ear photoplethysmogram waveform analysis by fitting with Gaussians," *Medical and Biological Engineering and Computing,* vol. 46, pp. 1271-1276, 2008.

[35] M. Baruch, D. Warburton, S. Bredin, A. Cote, D. Gerdt, and C. Adkins, "Pulse Decomposition Analysis of the digital arterial pulse during hemorrhage simulation," *Nonlinear Biomedical Physics,* vol. 5, p. 1, 2011.

[36] R. A. Waltz, J. L. Morales, J. Nocedal, and D. Orban, "An interior algorithm for nonlinear optimization that combines line search and trust region steps," *Mathematical Programming,* vol. 107, pp. 391-408, 2006/07/01 2006.

[37] J. Muehlsteff, A. Ritz, T. Drexel, C. Eickholt, P. Carvalho, R. Couceiro*, et al.*, "Pulse Arrival Time as surrogate for systolic blood pressure changes during impending neurally mediated syncope," in *34th Annual Int. Conf. of the IEEE Eng. in Medicine and Biology Society, EMBC 2012*, 2012, pp. 4283-4286.

[38] C. Meyer, G. Morren, J. Muehlsteff, C. Heiss, T. Lauer, P. Schauerte*, et al.*, "Predicting neurally mediated syncope based on pulse arrival time: algorithm development and preliminary results," *J Cardiovasc Electrophysiol,* vol. 22, pp. 1042-8, Sep 2011.

[39] S. S. DeLoach and R. R. Townsend, "Vascular Stiffness: Its Measurement and Significance for Epidemiologic and Outcome Studies," *Clinical Journal of the American Society of Nephrology,* vol. 3, pp. 184-192, 2008.

[40] O. Salem, L. Yaning, and A. Mehaoua, "A lightweight anomaly detection framework for medical wireless sensor networks," in *Wireless Communications and Networking Conference (WCNC), 2013 IEEE*, 2013, pp. 4358-4363.

[41] R. Wang and K. Tang, "Feature Selection for Maximizing the Area Under the ROC Curve," in *Data Mining Workshops, 2009. ICDMW '09. IEEE International Conference on*, 2009, pp. 400-405.

[42] "Philips MP50," ed. www.philips.com.

[43] "Taskforce Monitor," ed. www.cnssystems.com.

[44] M. Brignole, F. Croci, C. Menozzi, A. Solano, P. Donateo, D. Oddone*, et al.*, "Isometric arm counter-pressure maneuvers to abort impending vasovagal syncope," *Journal of the American College of Cardiology,* vol. 40, pp. 2053-2059, 12/4/ 2002.

[45] H. Reiter, J. Muehlsteff, and A. Sipila, "Medical application and clinical validation for reliable and trustworthy physiological monitoring using functional textiles: experience from the HeartCycle and MyHeart project," in *33th Annual Int. Conf. of the IEEE Eng. in Medicine and Biology Society, EMBC 2011*, 2011, pp. 3270-3.

[46] J. Muehlsteff, P. Carvalho, J. Henriques, R. P. Paiva, and H. Reiter, "Cardiac status assessment with a multi-signal device for improved home-based congestive heart failure management," in *33th Annual Int. Conf. of the IEEE Eng. in Medicine and Biology Society, EMBC 2011*, 2011, pp. 876-9.

Chapter 7.
CONCLUSIONS AND FUTURE WORK

To face the high human and social costs in the current health care systems, the paradigm of health care is undergoing profound changes, with an increased emphasis in personalized health monitoring and preventive care. However, the current standard techniques for assessment of the cardiovascular function and assistance in diagnosis of cardiovascular diseases, either lack in portability, are expensive and/or require the presence of a trained technician. This problematic is particularly important in elderly populations, where the personal health systems can bring a huge step forward in the diagnosis and management of cardiovascular diseases and, consequently, prevent further complications. Therefore, it is essential to provide new methodologies for the evaluation of the cardiovascular health, in a non-invasive and continuous basis, capable of being applied to low cost and portable devices.

Several cardiovascular parameters have been presented in the literature to monitor the cardiovascular health of an individual based on the analysis of the electrocardiogram (ECG) and photoplethysmogram (PPG). However, the robust and accurate assessment of these parameters greatly depends on the used modalities, methods, and physiological and surrounding contexts. One good example is the photoplethysmogram, which is highly susceptible to noise and motion artifacts contaminations. Therefore, the initial concern of the present thesis was the extraction of a reliable metric capable of discriminating the uncorrupted sections of the photoplethysmogram. Consequently, we focused on the assessment of cardiac function surrogates and in the extraction of blood pressure and vascular tone surrogates. Finally, the extracted cardiovascular function surrogates were applied to the prediction of syncope events (and more specifically neurally mediated syncope), which is on of the main causes of unwanted falls in the elderly.

The first contribution of the present thesis was the development of an algorithm for the detection of motion artifacts in the photoplethysmogram. Although it is nearly ubiquitous in hospital settings and is widely used in anesthesia, surgical recovery and critical care, the photoplethysmogram can be highly prone to noise and motion artifacts, which represents a major obstacle in the assessment of valuable information. Despite the good results presented in the literature, none of the proposed motion artifacts detection methods was validated in patients with cardiovascular diseases. Moreover, it was still unclear what features best distinguish clean and corrupted PPG sections. Therefore, we proposed a new motion artifact detection method, which is based on the analysis of the time and period domain characteristics of the PPG. Several time and period domain features were assessed from the analysis of the PPG morphology and PPG period spectra. The best features were selected and used as inputs to a support vector machine (SVM) classification model. The results achieved by the proposed method show that the characteristics of period components of the PPG signal might be used as discriminative features for motion artifact detection. Moreover, the different performances of the proposed methods in the healthy and cardiovascular diseased patients suggest that the discrimination ability of the time and period

domain features depends on the physiological context, i.e., healthy or cardiovascular diseased. Finally, the proposed method is able to achieve a high accuracy regardless of the motion artifact source.

The second contribution of the present thesis was the development of a method for the assessment of cardiovascular surrogates based on the decomposition of the PPG pulse into its forward and reflection waves, using a Multi-Gaussian (MG) model formulation. The main methods for the extraction of cardiovascular surrogates proposed in the literature are based on a multi-derivative analysis of the PPG pulse, which is known to lack robustness in the presence of seriously damped signals. Consequently, the correct identification of the PPG components can be compromised. Therefore, we proposed the extraction of the left ventricular ejection time based on the analysis of the systolic components rather than the whole PPG pulse. Additionally, we were also able to extract surrogates of blood pressure and vascular tone from the analysis of the morphology of the systolic and diastolic PPG pulse components. The extracted parameters were compared with the reference values LVET, blood pressure and total peripheral resistance, in healthy and cardiovascular diseased patients. The proposed method for LVET assessment was able to achieve better results than the methods presented in the literature, despite not presenting the best results in the cardiovascular diseased population. Moreover, the good correlation between the extracted surrogates and the reference parameters suggests that these indexes can provide valuable information about blood pressure and vascular tone changes, especially in patients presenting hemodynamic instability.

The final contribution of the present thesis was the development of a novel algorithm for the prediction of neurally mediated syncope (NMS), employing cardiovascular parameters that characterize the chronotropic (HR), inotropic (left ventricular ejection time - LVET), vascular tone and blood pressure (PAT, stiffness index – SI – and reflection index - RI, respectively) changes underlying the mechanisms that trigger NMS. In order to get patient unspecific features, the extracted parameters were normalized regarding the patient orthostatic stable state. The best features were selected and used as inputs to a model that measures the distance to the stable state and a threshold-based approach was adopted to detect impending syncope. The results achieved by the proposed method evidences the importance of the combined analysis of multiple cardiovascular parameters in the prediction of NMS. Additionally, the good prediction time and the low false positive rate achieved by the proposed method are good indicators of the method robustness, which is a key aspect in its translation to ambulatory and p-health settings.

In the future, the proposed NMS prediction method will be validated in a larger dataset also including signals collected by a wearable multi-sensor device developed within the HeartCycle project, called Sensatron.

Furthermore, we will focus on the extraction of features that characterize the deregulation of the autonomic nervous system mechanisms during the development of NMS. Although it has been the focus of intensive research, we believe that the inclusion of features related to the autonomic

modulation will bring further improvments in the prediction capability of the proposed method. Therefore, we will start by applying frequency domain techniques to the analysis of the heart rate variability, such as the short time Fourier transform. Secondly, we will evaluate the ability of the extracted blood pressure surrogates to assess the baroreflex sensitivity (BRS). Despite the good results presented in the present thesis, the extracted blood pressure surrogates still exhibit some uncertainty (specially in seriously damped pulses), which may limit their application in the BRS assessment using time domain methods. Therefore, the use of frequency domain techniques might be the solution in the application of these surrogates to the assessment of BRS.

Moreover, it would also be interesting to apply the developed methods to the arterial blood pressure waveform, since this waveform is less prone to artifacts and is much richer in what concerns to the morphological features. Thus, it would be expected to reduce the uncertainty of the extracted parameters and, therefore, achieve better results. Moreover, the use of this waveform could enable the extraction of a wider range of cardiovascular trends such as cardiac output changes.